The determination of trace elements in complex matrices by electrochemical techniques

by

Caren Billing

Submitted in partial fulfillment of the requirements for the degree

MAGISTER SCIENTIAE

In the Faculty of Science
University of Pretoria
Pretoria
October 2000

The determination of trace elements in complex matrices by electrochemical techniques

by

Caren Billing

Supervisors: Prof Jacobus F. van Staden
Department of Chemistry
University of Pretoria
Dr Dick R. Groot
Analytical Science Division
Mintek

Degree: Magister Scientiae

SYNOPSIS

Some problems in the determination of trace impurities in complex matrices by stripping voltammetry was investigated. Two separate analyses were studied, namely the determination of cobalt in a zinc electrolyte and the determination of arsenic in high purity gold. In both cases matrix exchange was employed, thus flow systems were designed which included an on-line deoxygenation system. In the former case, a flow cell containing a hanging mercury drop electrode with perpendicular mercury and solution flow was designed. Cobalt was complexed by dimethylglyoxime (DMG) and determined by adsorptive stripping voltammetry. Interference from zinc was removed by chelating it with citrate. In the latter case, a wall-jet cell was used with a gold film plated onto a glassy carbon substrate as the working electrode. Arsenic was determined by anodic stripping voltammetry. Interference from the large excess of gold present was prevented by forming the kinetically inert gold (I) complex. The pH of the solution was

adjusted to 3 to prevent electrode passivation, while avoiding decomposition of the gold (I) cyanide complex. However, copper was found to be a major interference in this analysis. This project demonstrated that electroanalytical techniques could be used for the determination of trace elements in complex matrices.

Die bepaling van spoor elemente in komplekse monsters met elektrochemiese tegnieke

deur

Caren Billing

Leiers: Prof Jacobus F. van Staden
Departement van Chemie
Universiteit van Pretoria
Dr Dick R. Groot
Analitiese Wetenskap Afdeling
Mintek

Graad: Magister Scientiae

SAMEVATTING

Enkele probleme met die bepaling van spoor onsuiwerhede in komplekse monsters is met stropingsvoltammetrie ondersoek. Twee verskillende ontledings is bestudeer; naamlik, die bepaling van kobalt in 'n sink elektroliet en die bepaling van arseen in hoë suiwerheid goud. In albei gevalle is matrysuitruiling gebruik, waarvoor vloeisisteme ontwerp is wat ook aanlyn-suurstofonttrekking ingesluit het. Eerstens is 'n vloeisel met 'n hangende kwikdruppel elektrode ontwerp waar die kwik- en oplossingvloei loodreg op mekaar is. Kobalt is met dimetielglioksiem (DMG) gekomplekseer en bepaal deur middel van adsorptiewe stropingsvoltammetrie. Die steuring van sink is oorkom deur die sinksitraatchelaat te vorm. Tweedens is 'n muurspuitsel gebruik waar die werkende elektrode 'n goudfilm glasagtige koolstof elektrode was. In die bepaling van arseen met anodiese stropingsvoltammetrie is sianied gebruik om die goud te komplekseer as die goud(I)sianiedkompleks. Steuring deur die groot oormaat goud is voorkom deur die

vorming van die kineties inerte goud(I)sianiedkompleks. Die pH van die oplossing was 3 om passivering van die elektrode te verhoed, terwyl dit terselfdertyd voorkom dat die goud(I)sianiedkompleks ontbind. Die projek het aangetoon dat koper erg steur in hierdie bepaling. Dit bewys dat elektroanalitiese tegnieke vir die bepaling van spoor elemente in komplekse monsters gebruik kan word.

ACKNOWLEDGEMENTS

I thank Mintek for providing me with the opportunity to do an MSc and for providing the resources and the support that was required.

In particular, I thank Dr Dick Groot for all his assistance and insight, and for persevering with me through all the highs and the lows.

I thank Prof. Koos van Staden for affording me the opportunity to do this MSc under his supervision and for his patience during the times when work was going slow due to other work pressures.

I thank my family and friends for all their support and encouragement.

And lastly, but certainly not least, I thank my husband Dave for all the time he spent encouraging me, advising me and listening to me. Thank you for always being there, for making the meals and helping me where you could during those nights and weekends spent in front of the computer.

CONTENTS

LIST OF ABBREVIATIONS

ac	alternating current
AdSV	adsorptive stripping voltammetry
ASV	anodic stripping voltammetry
BSWV	Barker square wave voltammetry
CSV	cathodic stripping voltammetry
CV	cyclic voltammetry
DMG	dimethylglyoxime
DPSV	differential pulse stripping voltammetry
DPV	differential pulse voltammetry
GCE	glassy carbon electrode
HMDE	hanging mercury drop electrode
LSSV	linear sweep stripping voltammetry
LSV	linear sweep voltammetry
MFE	mercury film electrode
NPV	normal pulse voltammetry
OSWV	Osteryoung square wave voltammetry
PSA	potentiometric stripping analysis
SMDE	static mercury drop electrode
SWV	square wave voltammetry
TLD	thin layer detector
TMFE	thin film mercury electrode
WJC	wall-jet cell
WJE	wall-jet electrode

CHAPTER 1

INTRODUCTION

The need for trace analyses in complex matrices is becoming more apparent. There are, however, many difficulties surrounding this type of analysis. For example, solutions with trace impurities in a matrix solution that has a high salt content or a high concentration of total dissolved solids present a problem when analysing by spectroscopic techniques. In contrast, the high salt content is generally beneficial in improving the conductivity of the solution when using an electrochemical technique. This technique also provides the sensitivity needed and can be selective depending on the background electrolyte used. This project was aimed at finding whether an electrochemical technique would be suitable to solve this problem. In addition, electrochemical techniques offer the ability to do speciation, which spectroscopic techniques are not always suitable to do.

The peak potentials of a number of metals are close together, but it is often relatively easy to carry out the determination of several metals in one run, if they are present in similar concentrations. It is, however, more complicated to determine a trace amount in the presence of a large excess of an interfering substance. There are many different kinds of interferences that need to be recognised in these situations. Surface-active agents could adsorb onto the electrode surface which could poison the electrode. Substances could react with the electrode material. Two substances could be deposited together at a given potential and influence each other during the stripping process, for example, their peaks could overlap. The analyte could be deposited while another substance that is present in excess, which stays in solution, undergoes a simultaneous electrode reaction. During the stripping process, the substance in the solution undergoes the reverse electrode reaction that may interfere owing to the appearance of a wave or a broad peak in the vicinity of the analyte peak [1].

The selectivity of an electrochemical analysis can be improved in a number of ways. A preliminary separation could take place, such as a solvent extraction, coprecipitation, volatilisation, chromatographic techniques, electrophoresis and so on. However, this is not preferable as it requires a significantly longer analysing time, more contamination could occur and it is often not suited to trace determination. Electrochemistry has a "built-in" preconcentration step, namely pre-electrolysis, which is more suitable. The pre-electrolysis conditions, the stripping technique and the choice of the electrode material could all improve selectivity. It also enhances the sensitivity greatly.

Stripping analysis consists of two main steps, namely the preconcentration step and the stripping step. In the preconcentration step, the analyte is accumulated onto or into the electrode. In the stripping step, the accumulated material is oxidised or reduced back into solution. The response recorded in the latter step is proportional to the amount of accumulated analyte which, in turn, is proportional to the bulk concentration. There are various stripping techniques such as anodic stripping voltammetry (ASV), cathodic stripping voltammetry (CSV), potentiometric stripping analysis (PSA), adsorptive stripping voltammetry (AdSV) and so on [2]. Only ASV and AdSV will be looked at in detail here as they were the techniques used in this project.

ASV entails the reduction of a metal ion to the metal during the preconcentration step. This is achieved by applying a potential, that is more cathodic than the standard potential of the least easily reduced metal to be analysed, for a specified time period. A metallic layer forms on the surface of the electrode or an amalgam is formed when a mercury electrode is used. This step generally involves forced convection to improve the mass transport of the analyte to the surface of the electrode. The convection is stopped and a rest period of a couple of seconds is implemented to ensure that the stripping step occurs in a quiescent solution and to establish a uniform concentration within the mercury if a mercury electrode is used. A positive-going potential scan is then applied and the accumulated species are then reoxidised. The metals are stripped from the electrode in an order that is a function of their standard potential. This gives

rise to anodic peak currents which are measured. The concentration of the metal can then be deduced from the heights (or areas) of the peaks produced [2].

The concept for AdSV is very much the same as that for ASV. In the case of a metal determination, a metal chelate is formed and this is adsorbed onto the surface of the electrode at a particular potential for a specified time period. Stripping is achieved by a negative-going potential scan and reduction occurs, either through the metal or the ligand. The current response is proportional to the surface concentration of the analyte, which is proportional to the bulk concentration in solution. Many other surface-active substances can be analysed in this way [2].

Complexing agents provide various ways of improving selectivity of the stripping methods. A suitable complexing agent could shift the deposition potential of an interfering metal so that it will not deposit at the electrode, or move the stripping peaks further apart. The analyte could also be complexed, resulting in an adsorption of this complex at the electrode. It is necessary to know the electrode reactions of the complexing agents themselves under the conditions of the determination, to avoid possible interferences.

Pre-electrolysis together with matrix exchange is a powerful way to improve the selectivity. After pre-electrolysis from the sample solution, the stripping process is carried out in another electrolyte that is free of interfering species. The best way to perform a matrix exchange is by using a flow system. In this manner the deposit is not exposed to air when the solution is changed and the deposit does not undergo mechanical forces and possible losses when the electrode is removed from the one solution and inserted into another. An electrochemical detector can readily be inserted into the conduits of a flow system and thus on-line analysis is also made possible. Other advantages of a flow system include convective mass transport, automation, increased precision, reduced analysis time and reduced contamination.

In these trace analyses, it is not only the selectivity that is an issue, but also the sensitivity. Generally some form of enrichment of the analyte is required. Electrolytic accumulation is a simple and convenient way to both isolate and preconcentrate the component of interest. This can be done in a number of ways, for example the deposition of the analyte on the surface or into the electrode, the adsorption of a complex onto the surface of the electrode, the use of modified electrodes and so on.

Two different matrices were looked at in the project, namely a zinc electrolyte and high purity gold. The impurities analysed for were cobalt and arsenic respectively.

1.1) DETERMINATION OF COBALT IN ZINC ELECTROLYTES

There are several grades of zinc on the market, the purest of which is produced by the electrolytic process [3]. The main procedures in producing zinc involve mining and concentrating the ore. This is then roasted to form zinc oxide which is dissolved in dilute sulphuric acid. The solution is purified to remove unwanted impurities and electrolysis is carried out on this solution. It is at this point where impurities present even in very small quantities could have extremely undesirable effects. Once depleted, the zinc sulphate solution and the generated sulphuric acid are returned to the leaching step. This cyclic circuit is susceptible to the accumulation of impurities [3,4].

Elements that could have a deleterious effect on zinc electrowinning and that are generally present in significant quantities are iron, cobalt, nickel, copper, arsenic, antimony, germanium, tin, selenium, tellurium, cadmium, silver, lead, chlorine, fluorine and manganese [3,5-8]. The type and quantity of impurities present would depend on the location of the ore body. Some of the problems experienced due to the presence of these impurities are: reduced current efficiencies, a poor deposit morphology, the co-deposition with zinc, the redissolution of deposited zinc, the lowering of the hydrogen over-voltage or the zinc deposit could adhere to the cathode [3,5,9,10]. Elements such as sodium, potassium, calcium and magnesium may be present in large quantities

without having detrimental effects [3]. It is therefore important to be able to analyse the electrolyte before the electrolysis step to prevent any of the above mentioned problems.

Cobalt as an impurity was particularly looked at in this study. The presence of cobalt causes the formation of round holes in the zinc deposit as a result of redissolution of zinc [3,9]. This redissolution is caused by an increased amount of hydrogen evolution due to cobalt present. [11] It has also been reported that it decreases the current efficiency [12]. Cobalt can be tolerated to about 10 $mg.l^{-1}$ in the absence of other impurities, but its harmful effects are increased by the presence of other elements such as germanium [3]. It is therefore estimated that a maximum of 0.3 $mg.l^{-1}$ cobalt is acceptable [12]. In theory cobalt should be removed by the addition of zinc dust, but in practice it does not remove sufficient amounts. A number of other additives could be used for cobalt removal, such as potassium antimony tartrate, antimony trioxide, Nitroso-Beta-Naphthol, hot copper-arsenic-zinc dust or an aqueous solution of sodium ethyl xanthate [3].

In this project, cobalt was determined as its DMG (dimethylglyoxime) complex at a hanging mercury drop electrode (HMDE) and hence AdSV was used. This would curb problems experienced with cobalt at a mercury electrode such as the irreversibility of the redox process and the poor sensitivity of stripping methods due to the low solubility of cobalt in mercury [12-14]. This would also give some selectivity as the reduction potentials of cobalt and zinc are similar.

The work by Mrzljak *et al.* [12] was used as a basis for this part of the project as they also analysed for cobalt in a zinc electrolyte. This was to ensure that the flow system designed for this project was working well and this was best done using a method that had been proven to work previously. The project could then be extended to unknown scenarios. Their work takes many things into account. The cobalt sensitivity was enhanced by forming the DMG complex. The interference from the extremely high zinc concentrations present were reduced in two ways, namely, by complexing the zinc with

sodium citrate which moves the zinc reduction peak to more negative potentials and by utilising a matrix exchange method where stripping occurs in a comparatively uncontaminated solution. [12]

Mrzljak *et al.* [12] used a bottom-drain cell displayed in figure 1.1. The zinc electrolyte was first diluted six times with a supporting electrolyte. The sample was then injected directly over the HMDE from the flow adapter and during this time the analyte was collected at the working electrode that was held at a fixed potential. Due to the greater density of the sample versus the stripping electrolyte contained in the cell, the sample sank to the bottom of the cell and stripping occurred in a relatively uncontaminated solution, thus reducing zinc interference. The contaminated stripping electrolyte was then drained and replaced by fresh electrolyte [12]. This cell design restricted its use to samples with fairly high specific gravities, whereas the cell designed for this project was aimed at producing a cell that would be more versatile (refer to chapter 3).

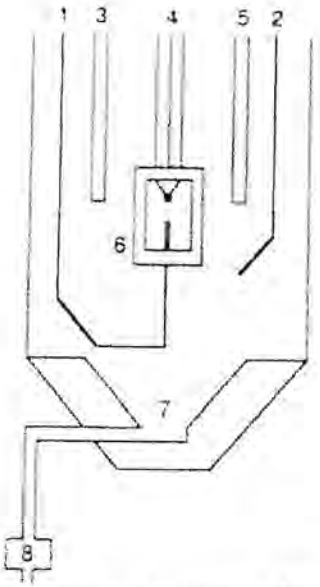

Figure 1.1: Schematic diagram of the bottom-drain cell used by Mrzljak *et al* [12]. (1) Sample inlet line; (2) nitrogen purge line; (3) reference electrode; (4) Metrohm HMDE; (5) auxiliary electrode; (6) PAR 310 flow adapter; (7) sample-electrolyte drain to waste; (8) control valve

Included in the flow system was a deoxygenation system. This was to remove dissolved oxygen present in solution which interferes in the application of electroanalytical techniques. A semi-permeable membrane set-up was used due to its efficiency in oxygen removal and its ability to be used in flow systems (refer to chapter 4).

1.2) THE DETERMINATION OF ARSENIC IN HIGH PURITY GOLD

It is necessary to be able to determine the amount of impurities in gold in order to assess the value, to check its physical properties for other uses, for example in medicine and in microelectronics, and to establish its point of origin. The typical content of trace impurities in high purity gold is represented in table 1.1 [15].

Table 1.1: Typical content of trace impurities in high purity gold [15]

Element	**Concentration / $\mu g.g^{-1}$**	**Element**	**Concentration / $\mu g.g^{-1}$**
Cu	0.5	Zn	0.5
Fe	0.6	As	0.24
Pb	1.2	Sb	0.12
Ni	0.6	Sn	0.05
Co	0.015	Bi	0.06
Mn	0.019	Al	6.0
Cd	0.1	Se	<0.01
Cr	0.5	Te	<0.01
Pd	1.0	V	<0.01
Rh	0.5	Pt	<0.01

The minerals arsenopyrite ($FeS_2.FeAs_2$), realgar (As_2S_2) and orpiment (As_2S_3) are associated with some gold ores [21]. Since arsenic is slightly soluble in gold forming an alloy, it is often found as an impurity in gold.

Work has been done by several authors [15-20] in this regard by different techniques and mechanisms. E. Ivanova *et al.* [15-18] used flame AAS and ETAAS to determine the impurities in high purity gold. They used different sample preparations to remove the matrix element, such as sorption onto a strong-base anion exchanger [16]; the use of chelating sorbents of the pyrazolone type [17]; solvent extraction with methylethylketone/chloroform [15]; and the reduction of gold to its elemental state by hydrazine hydrate [18]. Karadjova *et al.* [19] also looked at the reduction of gold to its elemental state by various organic compounds, namely, hydrazine hydrate, hydroquinone, ascorbic acid and oxalic acid. They found that oxalic acid performed the best as there was little coprecipitation of the trace elements to be determined. ICP-AES has been used to determine the impurities in gold [19]. The spontaneous reduction of gold in the nebuliser system caused clogging of the system and led to strong memory effects. ICP-MS was also employed [19,20] and it was found that there were several spectral, matrix and molecular ion interferences. These include producing the interfering polyatomic $^{49}Ar^{35}Cl^{-}$ on monoisotropic $^{75}As^{+}$, gold suppressing the analyte signal by its space-charge effect and the total dissolved solids had to be less than 0.5% (m/m) to prevent deposition of material on the skimmer cones to avoid drift and loss of sensitivity [23]. However, detection limits were still reported at 1 $\mu g.g^{-1}$ for most impurities except for arsenic and antimony, for which the limit of detection was 5 $\mu g.g^{-1}$.

Arsenic has been determined in many other matrices by various methods and techniques. Spectrophotometric (colourometric) methods are widely used for arsenic determination due to the simplicity and low cost. However they have limited use because of the poor sensitivity. Techniques that have been employed for the sensitive determination of arsenic include: hydride generation atomic absorption spectrometry (HG-AAS) [22-26], flame atomic absorption spectrometry (FAAS) [27], hydride generation inductively coupled plasma atomic emission spectrometry (HG-ICP-AES) [28], high performance liquid chromatography hydride generation atomic fluorescence spectrometry (HPLC-HG-AFS) [29], capillary electrophoresis (CE) [30], potentiometric stripping analysis (PSA) [31,32] and voltammetry [33-36]. Ways to separate the arsenic

from interferences or to preconcentrate the arsenic were also studied [22,37,38], but these methods were tedious, time consuming and could lead to contamination.

Voltammetry was used to detect arsenic (III) in a gold sample in this project. A gold film electrode was used which was formed by depositing a gold film onto a glassy carbon electrode. A preparation procedure for this electrode was developed in order to produce a uniform, non-porous film (refer to chapter 2).

The gold in the sample was complexed with cyanide to form the extremely stable aurous cyanide complex ($Au(CN)_2^-$) which has a stability constant of $2x10^{38}$ [21]. Due to the slow kinetics of reduction for this complex, the deposition potential for the gold is shifted in a negative direction. This was done to prevent the gold from plating together with the arsenic onto the electrode. The ratio of the gold and arsenic concentrations in the sample is of the order of $4x10^6$. Due to this large difference, the method would be very insensitive if the gold and arsenic were plated simultaneously, as it would be predominantly gold accumulated on the electrode surface. The formation of the gold (I) cyanide complex would involve dissolving the gold sample in an alkaline cyanide solution in the presence of oxygen.

Matrix exchange was performed to prevent the passivation of the gold film electrode and also to improve the sensitivity of the detection. A wall-jet cell (WJC) was employed for this purpose (refer to chapter 3). In a WJC, the flow of a jet of fluid strikes the plane electrode perpendicularly and flows radially over its surface [39-44]. The same deoxygenation system as described previously was used, but solutions needed to be sparged with nitrogen beforehand to achieve the necessary extent of deoxygenation.

1.3) REFERENCES

1) A.J. Bard and L.R. Faulkner, Electrochemical Methods - Fundamentals and Applications, John Wiley and Sons, 1980

2) P.T Kissinger and W.R. Heineman, Laboratory Techniques in Electroanalytical Chemistry, 2nd Edition, Marcel Dekker Inc., New York, 1996
3) G.T. Wever, JOM, 11 (1959) 130
4) J.A. Gonzalez-Dominguez and R.W. Lew, JOM, 47 (1995) 34
5) M. Karavasteva, Hydromet., 35 (1994) 391
6) M. Geissler and R. Da Maia, Fresnius Z. Anal. Chem., 330 (1988) 624
7) E.S. Pilkington, C. Weeks and A.M. Bond, Anal. Chem., 48 (1976) 1665
8) A.M. Bond, R.W. Knight and O.M.G. Newman, Anal. Chem., 60 (1988) 2445
9) L. Muresan, G. Maurin, L. Oniciu and D. Gaga, Hydromet., 43 (1996) 345
10) A.M. Bond, B.V. Pfund and O.M.G. Newman, Anal. Chim. Acta, 277 (1993) 145
11) C. Cachet, C. Le Pape-Rerolle and R. Wiart, J. Appl. Electrochem., 29 (1999) 813
12) R.I. Mrzljak, A.M. Bond, T.J. Cardwell, R.W. Cattrall, R.W. Knight, O.M.G. Newman, B.R. Champion, J. Hey and A. Bobrowski, Anal. Chim. Acta, 281 (1993) 281
13) B. Pihlar, P. Valenta and H.W. Nurnberg, Fresenius Z. Anal. Chem., 307 (1981) 337
14) S.B. Adeloju, A.M. Bond and M.H. Briggs, Anal. Chim. Acta, 164 (1984) 181
15) E. Ivanova, N. Jordanov, I. Havesoz, M. Stoimenova and S. Kadieva, Fresenius J. Anal. Chem., 336 (1990) 501
16) E. Ivanova and H. Berndt, Fresenius J. Anal. Chem., 340 (1991) 419
17) E. Ivanova, O. Todorova and M. Stoimenova, Fresenius J. Anal. Chem., 344 (1992) 316
18) E. Ivanova, I. Havesoz, H. Berndt and G. Schaldach, Fresenius J. Anal. Chem., 336 (1990) 320
19) A. Karadjova, S. Arpadjan and L. Jordanova, Fresenius J. Anal. Chem., 367 (2000) 146
20) S.M. Graham and R.V.D. Robert, Talanta, 41 (1994)1369
21) Gold metallurgy in South Africa, Chamber of Mines of SA, Johannesburg, 1972
22) T. Kubota, T. Yamaguchi and T. Okutani, Talanta, 46 (1998) 1311
23) P. Becotte-Haigh, J.F. Tyson, E. Denoyer and M.W. Hinds, Spectrochim. Acta Part B, 51 (1996) 1823

24) R.I. Ellis, N.G. Sundin, J.F. Tyson, S.A. McIntosh, C.P. Hanna and G. Carnrick, Analyst, 123 (1998) 1697
25) J. Stummeyer, B. Harazim and T. Wippermann, Fresenius J. Anal. Chem., 354 (1996) 344
26) S. Karthikeyan, T. Prasada Rao and C.P.S. Iyer, Talanta, 49 (1999) 523
27) A.R.K. Dapaah and A. Ayame, Anal. Chim. Acta, 360 (1998) 43
28) B. Jamoussi, M. Zafzouf and B. Ben Hassine, Fresenius J. Anal. Chem., 356 (1996) 331
29) Z. Slejkovec, J.T. van Elteren and A.R. Byrne, Talanta, 49 (1999) 619
30) E. P. Gil, P. Ostapczuk and H. Emons, Anal. Chim. Acta, 389 (1999) 9
31) J.H. Aldstadt and A.F. Martin, Analyst, 121 (1996) 1387
32) S.B. Adeloju, T.M. Young, D. Jagner and G.E. Batley, Anal. Chim. Acta, 381 (1999) 207
33) H. Li and R.B. Smart, Anal. Chim. Acta, 325 (1996) 25
34) G. Henze, W. Wagner and S. Sander, Fresenius J. Anal. Chem., 358 (1997) 741
35) D. Sancho, M. Vega, L. Deban, R. Pardo and G. Gonzalez, Analyst, 123 (1998) 743
36) P.H. Davis, G.R. Dulude, R.M. Griifin, W.R. Matson and E.W. Zink, Anal. Chem., 50 (1978) 137
37) I. Eguiarte, R. M. Alonso and R.M. Jimenez, Analyst, 121 (1996) 1835
38) W. Wisniewski, Hydromet., 46 (1997) 235
39) A.J. Bard, Electroanalytical Chemistry, Volume 16, Marcel Dekker Inc., 1989
40) W.J. Albery and C.M.A. Brett, J. Electroanal. Chem., 148 (1983) 211
41) W.J. Albery and C.M.A. Brett, J. Electroanal. Chem., 148 (1983) 201
42) J. Wang and B.A. Freiha, Anal. Chem., 57 (1985) 1776
43) R.G. Compton, A.C. Fisher, M.H. Latham, R.G. Wellington, C.M.A. Brett and A.M.C.F. Oliveira Brett, J. Appl. Electrochem., 23 (1993) 98
44) P. Laevers, A. Hubin, H. Terryn and J. Vereecken, J. Appl. Electrochem., 25 (1995) 1017

CHAPTER 2

ELECTRODES

A three-electrode system was used in the various set-ups, in other words they had a working electrode, an auxiliary electrode and a reference electrode. This leads to compensated and uncompensated resistance. The uncompensated iR drop is basically the resistance of the working electrode itself and the solution resistance between the working electrode and the reference electrode [1,2].

2.1) WORKING ELECTRODES

The main properties required by a working electrode, in order to give high accuracy, reproducibly, sensitivity and low detection limits, are:

- electrochemical inertness over a broad potential interval, [3]
- high oxygen and hydrogen overpotential, [3]
- stability for infinite time periods, [1,4]
- good signal-to-noise ratios, i.e. the residual current must be low but the current response to electroactive species must be high, [4]
- low ohmic resistance [3] and
- the possibility of easy and sufficient surface regeneration. [3]

Needless to say, such an electrode does not exist, thus choosing a suitable working electrode is a compromise to best fit the experiment.

2.1.1) Mercury Electrodes for the Determination of Cobalt

2.1.1.1) Theory

It has been shown that cobalt(II) is potentiostatically adsorbed onto a mercury electrode as its DMG complex [5]. The advantage of using a mercury electrode is that it has a high hydrogen overpotential [4,6]. The down side is the toxicity of mercury and the limited potential range for anodic reactions due to mercury oxidation from approximately 0.4 V [7]. There is also strong interference from oxygen [8,9] and

the electrode can easily be fouled when exposed to complex samples [10]. This proved to be the most feasible electrode for these studies and its accessible potential range was as required, but some deoxygenation would be necessary.

When comparing the HMDE and the thin film mercury electrode (TFME) the main difference is that the HMDE has a fresh, smooth surface for each analysis, thus leading to very reproducible results, and there is no need for polishing or reactivation. The HMDE also has a linear response over a wide range of concentrations, without exhibiting saturation or interference effects [11]. The double layer charging current is, however, high due to the large surface area of a mercury drop [4]. A TFME is more sensitive [12] and gives better resolution than a HMDE as peak widths are narrower [13]. However, the experimental complexity and time is increased and there are problems maintaining a constant active surface area [9]. It is also more difficult to obtain a reproducible and stable electrode surface [14]. The HMDE produces broad stripping peaks as the metal slowly diffuses from the interior to the surface of the drop. This can be overcome by using high frequency techniques, such as ac or pulse techniques, which give narrower stripping peaks because it is only the metal on the surface of the drop that is looked at [12]. In the case of AdSV, adsorption on the analyte only takes place on the surface of the electrode. In flow cells the TFME is easier to manage as the HMDE produces vibration or turbulence at high flow rates, which leads to poor performance [4,9,10,15].

Considering the pros and cons of the HMDE and the TFME, it was decided to utilise the HMDE due to its ease of use and readily renewable surface, especially when analysing the complex zinc electrolyte, hence avoiding many surface related problems. Using differential pulse stripping voltammetry could enhance the sensitivity. The major problems that had to be overcome was to design a stable flow system using a HMDE and provide on-line deoxygenation.

2.1.1.2) Experimental

An EG&G Princeton Applied Research Model 303 Static Mercury Drop Electrode (SMDE) (EG&G, New Jersey, USA) was used as shown in figure 2.1. The BAS 100B/W Electrochemical Workstation (Bioanalytical Systems, West Lafayette, USA) remotely controlled it.

Figure 2.1: EG&G Princeton Applied Research Model 303 Static Mercury Drop Electrode

The area of the mercury drop could be calculated from the mass of the drops, assuming a spherical shape. This was done by Peterson [7] for the PARC SMDE and the results he found are shown in table 2.1. The drop mass was an average of 20 determinations and the areas calculated represent typical areas for these electrodes.

Table 2.1: The electrode areas calculated for various drop sizes for the PARC SMDE [7]

Drop size	**Drop mass / mg**	**Drop area / cm^2 x 10^2**
Small	1.2	0.96
Medium	2.5	1.56
Large	5.4	2.61

A schematic diagram of the mechanical assembly of the SMDE is shown below in figure 2.2 [16]. The mercury flows from the reservoir through a vertical hole into the top of the solenoid body and down around the valve stem. The compression spring continuously exerts a downward force on the retaining ring so that the polyurethane tip at the end of the valve stem seals the top end of the capillary. When the solenoid is activated, the valve stem is lifted and mercury can then flow down the capillary. The drop forms quickly to the required size, which is controlled by the duration the valve is lifted, and then remains that size until it is dislodged. The metallic parts that are in contact with the mercury are made of stainless steel to prevent contamination and the non-metallic materials do not react with mercury [16].

The SMDE needed some maintenance before it could be used as it was standing for a number of years. The old mercury was drained and the whole system was cleaned because much of the mercury had oxidised. The reservoir was filled with clean triply distilled mercury. (In all cases the mercury was collected and disposed of in the appropriate manner.) The polyurethane seal on the tip of the valve stem was also remade as it had become hard over the years and was indented by the capillary. This was moulded from an epoxy resin (Pratley) glue because it could adhere to the tip of the valve stem and also had a similar pliability to the polyurethane tip, hence it would make a good seal with the top of the capillary. A new capillary was carefully installed so that there was no air trapped in it. The capillaries had a bore of approximately 0.15 mm. A new glass sleeve with a Vycor frit for the Ag/AgCl reference electrode was filled with fresh saturated silver chloride solution, ensuring that there were no trapped air bubbles, and was also put in place. This reference electrode has a potential no more than 50mV more positive than the standard calomel electrode [16] and was only used in the cup-cell arrangement.

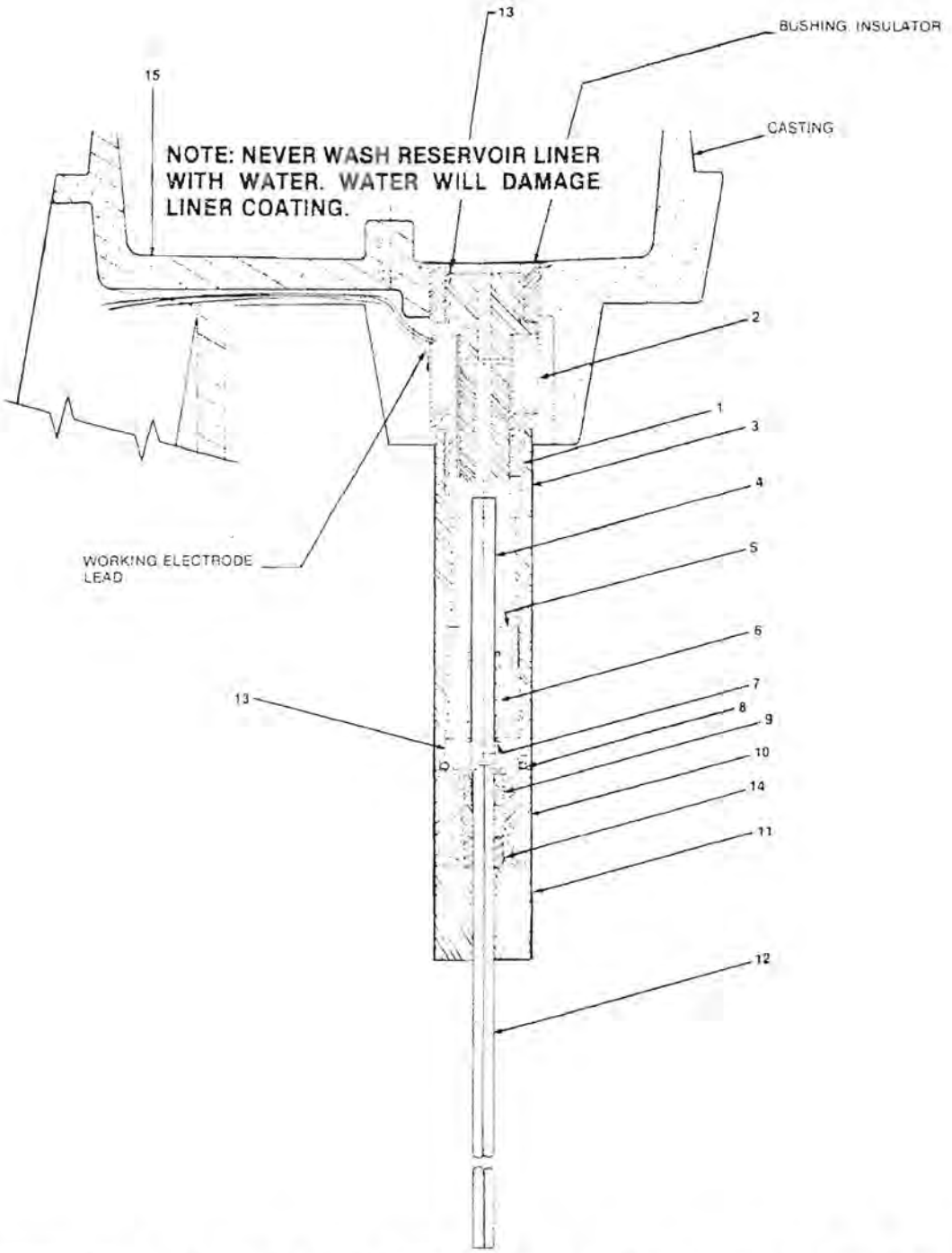

Figure 2.2: Schematic diagram of the mechanical assembly of the SMDE. The labels are as follows: (2) solenoid body, (3) valve body, (4) valve stem assembly, (5) valve guide bushing, (6) compression spring, (7) retaining ring, (8) O-ring, (9) capillary seal, (10) valve seat, (11) capillary nut, (12) capillary assembly, (14) ferrule support and (15) reservoir liner.

On occasion, the capillaries were replaced when the drops would not adhere to the tip of the capillary. This was probably due to solution creeping up the mercury capillary resulting in a narrower neck which was unable to hold the weight of the drop [6]. The capillary was cleaned by aspirating 10% (v/v) hydrofluoric acid through it for about 15 seconds, followed by copious amounts of deionised water. A siliconising solution contained 5% (v/v) dichlorodimethylsilane in carbon tetrachloride. It was aspirated halfway up the bore of the capillary and allowed to stand for an hour. The solution was removed by aspiration and the capillaries were then dried in an oven at 65°C overnight [16].

The SMDE was used in the HMDE mode. At the start of each run the drop knocker is activated, the old mercury drop is dislodged off the end of the capillary and a new drop is formed. A small or medium drop size was generally used. A large mercury drop led to mechanical instability in the flow cell and it is also reported that the greater the working electrode's surface area, the greater the extent of noise [1].

2.1.2) Thin Gold Film Electrodes for the Determination of Arsenic

2.1.2.1) Theory

Several electrode materials have been used for the determination of arsenic by stripping techniques. These include the HMDE with the aid of Cu(II) or Se(IV) to preconcentrate the As(III) by way of forming intermetallic compounds on the electrode and the codeposition with copper on a platinum electrode [19]. But the most suitable electrode material has been found to be gold, whether it be a solid gold disk or a thin film gold electrode [19-28]. The use of a mercury electrode on its own was unsuccessful as arsenic is sparingly soluble in mercury [25] and the arsenic oxidation peak appeared as a shoulder on the mercury oxidation wave which was of little analytical use [19,22]. Silver was also found to be unsuitable due to the arsenic peak emerging as a shoulder [22]. Arsenic had been determined at a platinum electrode, but gold was found to be superior [20,22]. Gold has a higher hydrogen overpotential than platinum, so interference from hydrogen was reduced. Gold electrodes also display better reversibility of the electrode reactions which results in higher and sharper oxidation peaks for arsenic [19,22].

The problem with using solid electrodes, such as gold, is that the electrode response is strongly dependent on the past history, pretreatment and oxide film formation [19,22]. A huge problem is the lack of understanding of the true electrode surface conditions and their effect on the electrode process [29], as well as the difficulty to reproduce the electrode surface [30]. It is important that the electrode surface is clean and that deleterious effects such as adsorption, electropolymerisation, fouling and poisoning be avoided [29,31]. The accumulation of foreign material on the electrode results in reduced electrode activity. Methods have been devised to rejuvenate the working electrode activity, for example, chemical treatments, potential excursions and mechanical polishing [29,32,33]. Mechanical polishing has been shown to temporarily alter the electrode response such that an equilibration period is necessary to stabilise it [29]. Electrochemical pretreatment of the electrode is very convenient and it produces electrode stability and a decrease in the extent of overpotential [33].

In many respects the thin gold film and the thin mercury film behave in much the same manner. These are usually plated on a glassy carbon electrode (GCE) substrate. This is due to glassy carbon having low background currents over a wide potential range, a high hydrogen overpotential, low porosity, extreme hardness and high chemical inertness [31]. Glassy carbon is a gas-impermeable carbon material made from phenolic resins by heating it in an inert atmosphere. Different conditions give slightly different properties of the glassy carbon, therefore it is difficult to compare results for different electrodes. The microstructures of different electrodes vary significantly, even when they are cut from the same rod. They exhibit randomly scattered surface defects in the form of very small craters, ruts and pits which cannot be removed by polishing. It has been shown that the smooth areas consist of pure carbon whereas metals (for example Fe, Mg, Al, Si, V, Ni, and Cr) can be found in the micropores [31]. Other substrates that have been used are impregnated graphite [34], pyrolytic graphite[19], platinum [32] and solid gold [34]. It is important that the effects observed are not due to reactions with the substrate material; thus the film should not be porous or have imperfections [32].
The GCE surface had to be treated as any solid electrode to ensure reproducibility and a low background current [34,35]. The performance of a gold film on a GCE was

markedly affected by the condition of the GCE surface prior to gold deposition and by the amount of gold that was deposited [30]. Mercury plates onto the active sites on the GCE, leaving the less active sites uncovered. It appears that gold deposits in a similar manner. As the extent of oxidation on the GCE expanded, the number of active sites were reduced and the gold tended to deposit in larger particles at fewer sites, so that the specific surface available for analyte deposition is decreased [30]. Contrary to expectation, surfaces with greater roughness and irregularities gave more reproducible results for mercury films [31]. This is probably due to a larger number of active sites on the electrode surface and it would be expected that the gold film behave in a similar way. This also yielded a more mechanically stable film. It was shown that merely wiping the used gold film from the GCE surface with a tissue before replating a new film was insufficient as the sensitivity between analyses dropped more rapidly [30]. More rigorous methods such as potential cycling or polishing were necessary [19,26,27,30-36].

A thin film shows gradual deterioration due to mechanical stresses, the deposition and/or adsorption of contaminants and so on [37]. Usually a single gold film could be used for a number of determinations [25,26,30], but at times deterioration between analyses is too great [19]. It was found that if electrolytes contained high concentrations of chloride, the gold film would degrade quickly. This was because of the $AuCl_4^-$ complex formation, which resulted in the gold film being dissolved. A make-up procedure was run between analyses where a small amount of gold was plated again. The presence of impurities also had a profound effect on the behaviour of the gold film electrode [19].

In a flow cell, the film thickness should be less than the diffusion layer thickness. This is easily satisfied in a wall-jet cell where the diffusion layer thickness is of the order of 10 μm for flow rates between 1-4 $ml.min^{-1}$ [35]. The thickness of the film can be calculated if it can be approximated that the atoms are uniformly deposited. This is done by measuring the limiting current (i_{lim}) when the film is stripped from the substrate and applying the following equation [35]:

$$\ell = \frac{i_{lim} M}{nF\pi R^2 \rho}$$

where M is the atomic mass of gold (in the case of a gold film), n is the number of electrons, F is Faraday's constant, R is the radius of the electrode and ρ is the density of gold. A film has been deposited at a wall-jet electrode [38], but it has also been shown that a mercury film was partly removed by the impinging solution [31]. It is thus important that the film is mechanically stable in a hydrodynamic cell.

2.1.2.2) Experimental

A number of different substrate preparation and gold plating regimes were adopted by various authors [19,25-27,30,33,34,36]. This work encompassed plating a gold film onto a glassy carbon substrate to produce a uniform, lustrous film.

The plating solution used for the formation of the gold film electrode was a 50 $mg.l^{-1}$ gold (III) solution in 5% (v/v) sulphuric acid. This was obtained by dissolving 99.99% gold in aqua regia to produce a 10 $g.l^{-1}$ gold solution. It was then diluted and the appropriate amount of sulphuric acid was added.

The film was not plated in the flow cell mainly owing to three reasons which are discussed below. It was previously shown that plating in a stationary solution produced a lustrous gold surface, whereas if plating took place in a hydrodynamic solution the film was more like a brown powder [19,25]. The whole electrode surface is not equally accessible in a wall-jet cell which could affect the evenness of the film. Due to the cost of the plating solution, it could be reused if plated from a vial. However, the electrode is not exposed to air when plated in the flow cell. Gold is not affected by oxygen at any temperature, whether moisture is present or not [21]. Thus the exposure of the gold film electrode to air for very short periods should not have detrimental effects. In the case of mercury films, it was reported that the removal of the electrode after plating occurred produced a patchy texture because the mercury droplets coalesced [31]. This was not observed with the gold film that was plated.

Plating took place in the BAS C2 Cell Stand (Bioanalytical Systems, West Lafayette, USA). The vial was filled with 8 ml of gold plating solution. The working electrode was a 3 mm diameter GCE, the reference electrode was a RE-5 silver/silver chloride electrode and the counter electrode was a platinum wire, all supplied by BAS. The solution was sparged with nitrogen for 5 minutes before plating commenced and a

nitrogen blanket was maintained above the surface of the solution during plating. It was discovered that lifting and reinserting the GCE in and out of the solution about three times after sparging removed any bubbles that were lodged on the electrode surface. If the nitrogen bubbles were not removed, the gold film that was plated had holes in it where the bubbles were situated.

Initially the GCE was polished with 1 μm alumina. This was done as specified in the BAS electrode polishing and care pamphlet [17]. A microcloth was stuck to a glass block and the cloth was wetted with some water. Some alumina paste was added to the surface of the cloth and the electrode was polished by placing it perpendicular to the glass block and moving it in the shape of a figure-8. This was done without applying excessive pressure. After a short period the electrode was rotated 120° and the figure-8 motion was continued for the same length of time. This was repeated once more to ensure an evenly polished surface. The electrode was then rinsed in water and ultrasonicated for 2 minutes in water to remove any residual alumina or abraded glassy carbon particles. It was then rinsed successively in water, 1 mol.l^{-1} nitric acid and finally water again.

Deposition of the gold film took place as suggested by Sun *et al.* [19] at –200 mV for 4 minutes in a quiescent solution. The reproducibility of the film was tested by analysing an arsenic (III) solution in 20% (v/v) hydrochloric acid. It was also suggested [19] that a "make-up" plating run be done between analyses to restore the gold film. This was done in the deoxygenated plating solution at +500 mV for 10 s, once again ensuring that there were no bubbles on the electrode surface.

The first tests performed in a vial (not the flow cell) showed erratic results as depicted in figure 2.3. A 5 mg.l^{-1} arsenic (III) solution was tested at various deposition times in a stirred or quiescent solution. The solution was first sparged with nitrogen for 5 minutes. The deposition potential was –300 mV and the final potential was 100 mV. DPSV was done with a scan rate of 50 mV.s^{-1}, a pulse height of 50 mV, a pulse width of 50 ms, a pulse period of 200 ms and a sample width of 20 ms. Stirring took place at a setting of 5 on the C2 Cell Stand and a 15 s quiet time was employed. It can be seen that the longer arsenic accumulation times showed a greater general increasing trend in the peak current. This was probably due to the arsenic not being totally

stripped off the electrode during the stripping step and hence there was some accumulation at the electrode. For the shorter deposition times, results were more reproducible when no stirring occurred during the accumulation step. This could be due to two phenomena, namely the increased noise during stirring and thus during the plating step, and the increase in mass transport led to a greater amount of arsenic being deposited and once again the stripping step may not have removed it all.

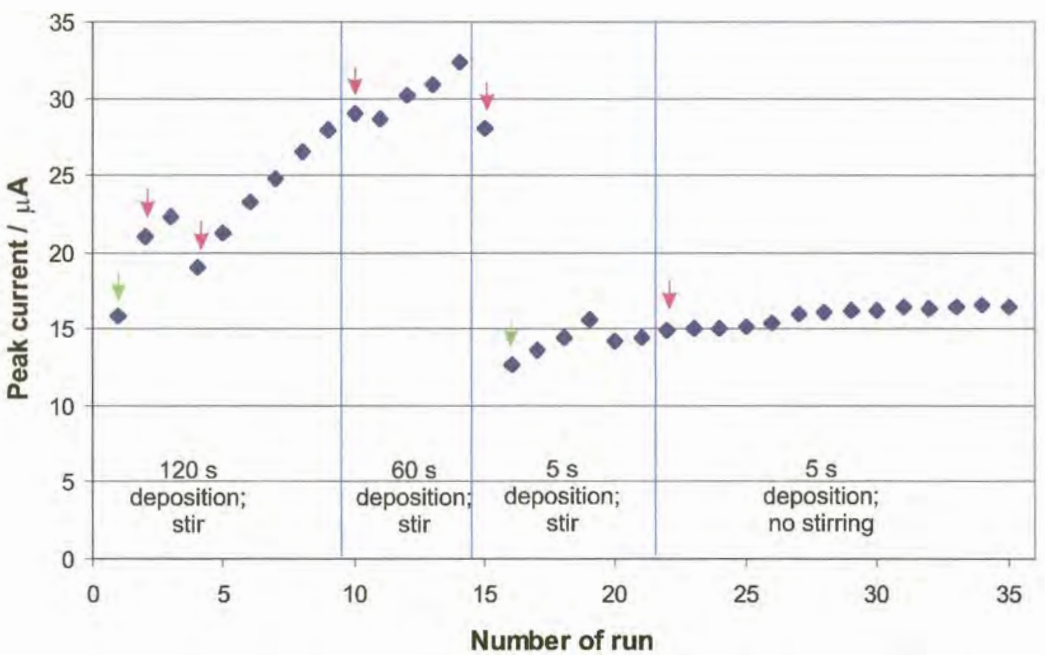

Figure 2.3: Testing the reproducibility of the gold film electrode. The green arrows represent plating the gold film before the analysis and the pink arrows represent doing a make-up plating run before the analysis.

The gold film electrode was stored in a deoxygenated solution of 0.1 mol.l^{-1} sulphuric acid overnight. Once again the peak currents were measured, as before, in arsenic (III) solutions. It was found that after sparging the arsenic solutions, lifting and reimmersing the working electrode in and out of the solution gave more reproducible results. The results in figure 2.4 show the peak currents for different concentrations of arsenic (III) solutions applying a deposition time of 5 s to quiescent solutions. The RSD is less than 5% for all concentrations which is acceptable. The correlation coefficient for the calibration was 0.9938, as shown in figure 2.5. This graph implied that when no arsenic was present, the peak height should be –6.9 μA. This would be

impossible, hence the integrity of the results were questioned. Positive results were that the peak currents for the 2 mg.l^{-1} arsenic solution were reproducible, whether a make-up plating run was done before the determination or not. It also showed that storing the gold film electrode in the deoxygenated sulphuric acid solution seemed to stabilise the electrode. When the gold film was looked at, it was more of a brown powdery coating with a relatively high resistance.

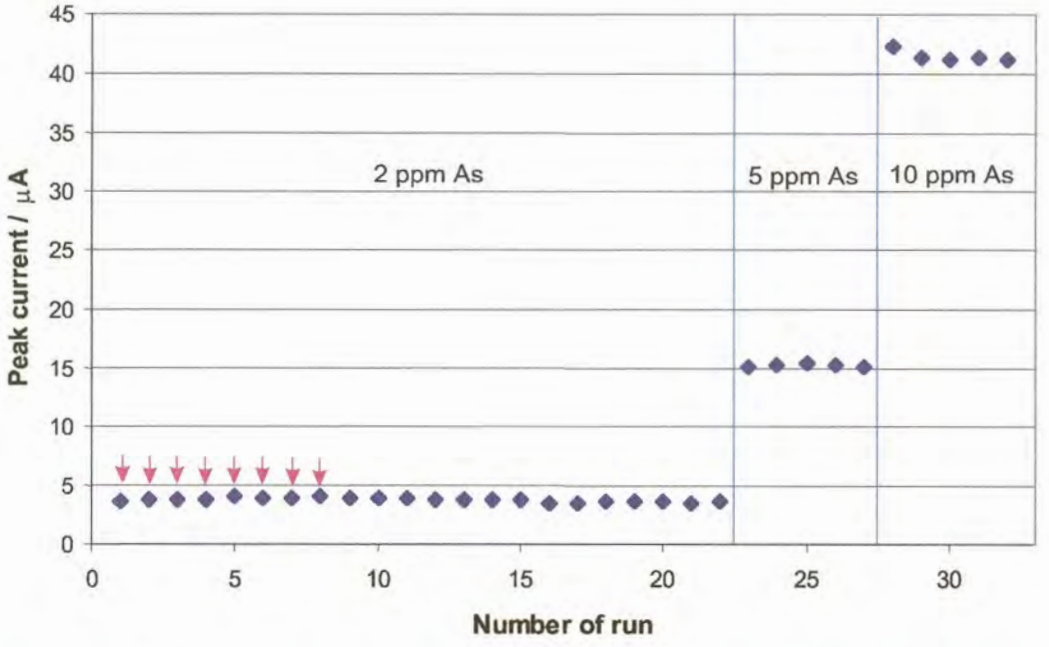

Figure 2.4: Testing the reproducibility of the gold film electrode at various arsenic (III) concentrations. The pink arrows represent a make-up plating run before the analysis.

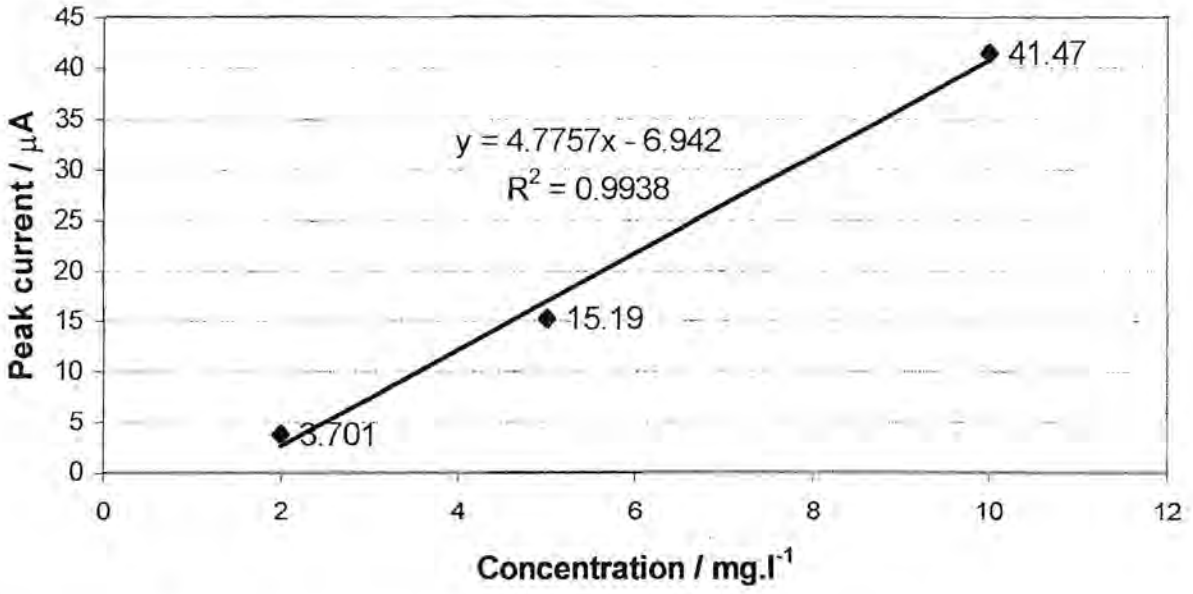

Figure 2.5: The graph of peak current versus arsenic (III) concentration

It was decided to reconsider the plating potential for the gold film. A cyclic voltammogram was obtained at the GCE in the gold plating solution. This is displayed in figure 2.6. The potential at which the gold was being plated (-200 mV) was in the diffusion-controlled region. It was decided to try and plate the gold film in the activation-controlled potential region. Thus plating occurred at potentials from 730 to 790 mV in quiescent solutions. This did not produce the film properties required. Plating in stirred solutions was also attempted as this kept conditions further away from diffusion-control, but with no success.

When the gold film was studied under a microscope at about 40 times magnification, the film was very irregular and there were white crystalline deposits on the surface, as illustrated in figure 2.7. The uneven film could be due to the electrode not being totally perpendicular during plating, or that the whole electrode surface was not uniformly activated. The white crystalline material was thought to be residual alumina from the polishing step. After the electrode was polished with 1 µm alumina, rinsed and ultrasonicated twice, the material was still there. It appeared as though it was embedded in the GCE. The electrode was then successively polished with 9 µm, 3 µm and 1 µm diamond paste with rinsing and ultrasonicating between the

different size abrasives. Lastly the electrode was polished with 1 μm alumina. The white material was removed.

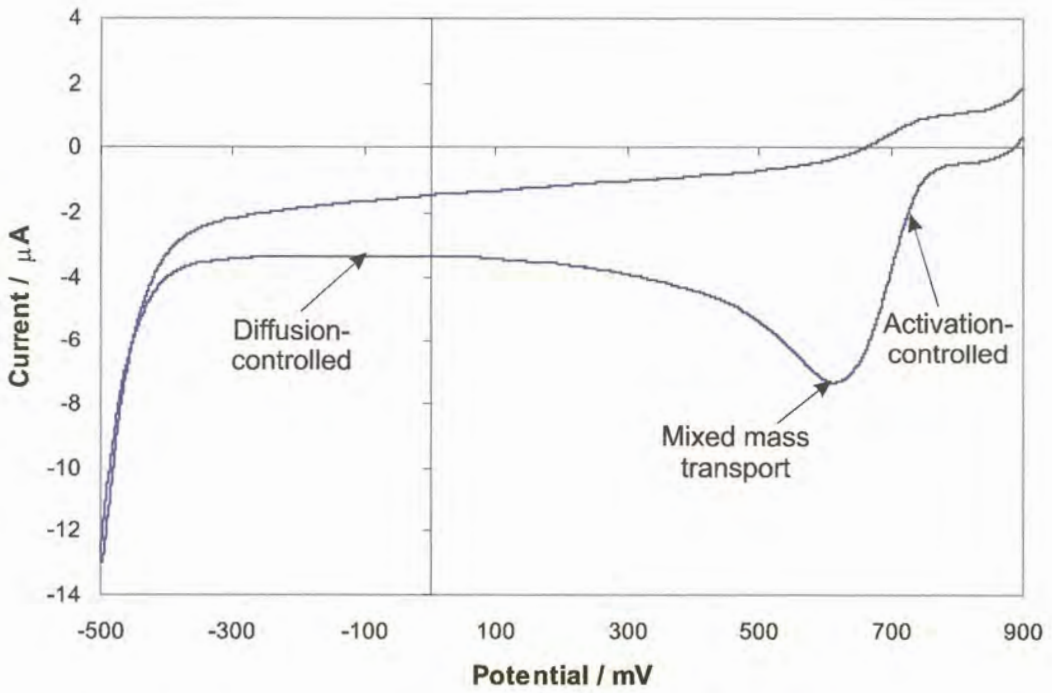

Figure 2.6: Cyclic voltammogram of the gold plating solution

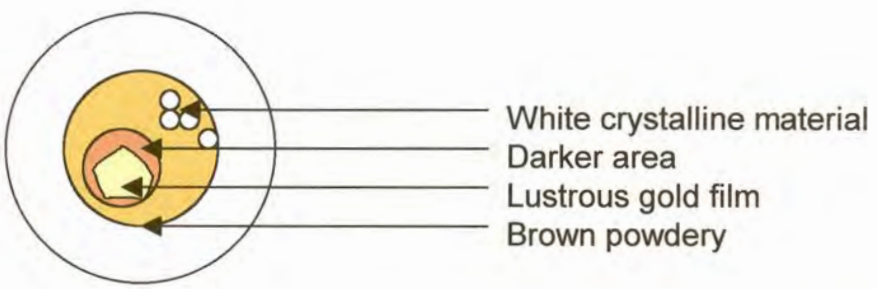

Figure 2.7: Gold film on the glassy carbon substrate at approximately 40 times magnification

After this rigorous polishing of the GCE, plating at –200 mV, as before, produced a lustrous dense gold film with a low resistance and doing a make-up run just after the plating of the film improved the reproducibility. Plating at 760 mV still produced a brownish deposit. It thus seems best to plate in the diffusion controlled region.

At a later stage during the project, it was found that the polishing procedure adopted did not sufficiently regenerate the GCE surface. An electrochemical treatment of the GCE was then investigated. It was found that applying a step function with a sample width of 250 ms between –700 mV and 700 mV for 1000 cycles in the gold plating solution produced the best results. The gold film was then plated as before.

2.1.2.3) Results

In order to produce a dense lustrous uniform gold film on a glassy carbon substrate, the developed procedure was summarised in point form below.

1) The GCE was polished with 1 μm alumina, rinsed with water and then ultrasonicated in water for about a minute. The electrode was then rinsed successively in water, 1 mol.l^{-1} nitric acid and water again.
2) If the deposited film was not uniform, a more rigorous polishing program was established. It included polishing successively with 9 μm, 3 μm and 1 μm diamond paste, with rinsing and ultrasonicating between the different size abrasives. Lastly the electrode was polished with 1 μm alumina as described above.
3) The plating solution for the gold film electrode was a 50 mg.l^{-1} gold solution in 5% (v/v) sulphuric acid. This was obtained by dissolving 99.99% gold in aqua regia to produce a 10 g.l^{-1} gold solution. It was then diluted and the appropriate amount of sulphuric acid was added.
4) Plating took place in a vial that was filled with 8 ml of gold plating solution. The solution was sparged with nitrogen for 5 minutes before plating commenced and a nitrogen blanket was maintained above the surface of the solution during plating. The GCE was lifted and reinserted in and out of the solution about three times after sparging to remove any bubbles lodged on the electrode surface.
5) The gold film was plated at –200 mV for 4 minutes in a stationary solution.
6) A gold make-up plating run was done straight after plating and when the electrode was starting to loose sensitivity. This was done similarly to the plating step, but a potential of 500 mV was applied for 5 s.
7) The plated electrode could be stored in a deoxygenated solution of 0.1 mol.l^{-1} sulphuric acid overnight. It was best to do a make-up run before starting analyses.

8) As the sensitivity of the gold film electrode does degrade with use, it may be useful to periodically include a check standard to assess the situation.
9) When the polishing procedure was not sufficient to regenerate the GCE surface, an electrochemical treatment was utilised. Applying a step function of sample width 250 ms between –700 mV and 700 mV `for 1000 cycles in the gold plating solution yielded the best results. The gold film was then plated as before.

2.2) REFERENCE ELECTRODES

The BAS RE-5 (MF-2063) Ag/AgCl reference electrodes were used in this work. An electrode is 7.5 cm long with an outer diameter of 6 mm. It has a Vycor tip and is filled with a 3 mol.l^{-1} NaCl solution saturated with AgCl. The viability of the reference electrodes were tested as suggested by the BAS Electrode Polishing and Care leaflet [17]. This was done due to the reported difficulties reference electrodes experience in solutions of high ionic strength [18]. The reference electrode in question, together with another reference electrode of the same type, was inserted into a beaker containing 3 mol.l^{-1} NaCl. They were then connected to a voltmeter and the potential difference was read. Ideally for electrodes of the same kind the potential difference should be zero, but there is some variation in practice. An acceptable reading is given as 0 $\pm$ 20 mV [17]. If there is a discrepancy, the electrodes could be compared to a third electrode to see which electrode is bad. Three of these electrodes were purchased simultaneously and were used in approximately two week cycles to maximise their lifetime.

2.3) AUXILIARY ELECTRODES

Platinum wire electrodes were used as the auxiliary electrodes in this work. The function of the auxiliary electrode is to allow current to flow through the electrolyte without influencing the measurement at the working electrode. Platinum is regularly used due to its low resistance and inert character.

2.4) REFERENCES

1) A.J. Bard, Electroanalytical Chemistry, Volume 16, Marcel Dekker Inc., 1989

2) P.T Kissinger and W.R. Heineman, Laboratory Techniques in Electroanalytical Chemistry, 2nd Edition, Marcel Dekker Inc., New York, 1996
3) Kh.Z. Brainina, Anal. Chim. Acta, 305 (1995) 146
4) D.C. Johnson, S.G. Weber, A.M. Bond, R.M. Wightman, R.E. Shoup and I.S. Krull, Anal. Chim. Acta, 180 (1986) 187
5) H. Eskilsson, C. Haraldsson and D. Jagner, Anal. Chim. Acta, 175 (1985) 79
6) I.G.R. Gutz, L Angnes and J.J. Pedrotti, Anal. Chem., 65 (1993) 500
7) W.M. Peterson, Reference unknown
8) J.J. Pedrotti, L. Angnes and I.G.R. Gutz, Anal. Chim. Acta, 298 (1994) 393
9) A.M. Bond, H.A. Hudson and P.A. van den Bosch, Anal. Chim. Acta, 127 (1981) 121
10) H.G. Jayaratna, C.S. Bruntlett and P.T. Kissinger, Anal. Chim. Acta, 332 (1996) 165
11) E.S. Pilkington, C. Weeks and A.M. Bond, Anal. Chem., 48 (1976) 1665
12) M. Florence, Analyst, 111 (1986) 489
13) A.M. Bond, Modern Polarographic Methods in Analytical Chemistry, Marcel Dekker Inc., 1980
14) A.Economou and P.R. Fielden, Trends in Anal. Chem., 16 (1997) 286
15) R.J. Rucki, Talanta, 27 (1980) 147
16) Model 303 Static Mercury Drop Electrode, Operating and Service Manual, 1978
17) BAS LCEC and EC Accessories, A-1302, Electrode Polishing and Care
18) A.M. Bond, H.A. Hudson, D.L. Luscombe, K.L. Timms and F.L. Walter, Anal. Chim Acta, 200 (1987) 213
19) Y.-C. Sun, J. Mierzwa and M.-H. Yang, Talanta, 44 (1997) 1379
20) P.Grundler and G.-U. Flechsig, Electrochim. Acta, 43 (1998) 3451
21) J.H. Aldstadt and A.F. Martin, Analyst, 121 (1996) 1387
22) G. Forsberg, J.W. O'Laughlin and R.G. Megargle, Anal. Chem., 47 (1975) 1586
23) M. Kopanica and L. Novotny, Anal. Chim. Acta, 368 (1998) 211
24) F.G. Bodewig, P. Valenta and H.W. Nurnberg, Fresenius J. Anal. Chem., 311 (1982) 187
25) P.H. Davis, G.R. Dulude, R.M. Griffin, W.R. Matson and E.W. Zink, Anal. Chem., 50 (1978) 137
26) T.W. Hamilton, J. Ellis and T.M. Florence, Anal. Chim. Acta, 119 (1980) 225
27) D. Jagner, M. Josefson and S. Westerlund, Anal. Chem., 53 (1981) 2144

28) J. Wang and B. Greene, J. Electroanal. Chem., 154 (1983) 261
29) A. Inoue, R.L. Earley, M.W. Lehmann and L.E. Welch, Talanta, 46 (1998) 1507
30) T.W. Hamilton, J. Ellis and T.M. Florence, Anal. Chim. Acta, 110 (1979) 87
31) W. Frenzel, Anal. Chim. Acta, 273 (1992) 123
32) F. Baumann and I. Shain, Anal. Chem., 29 (1957) 303
33) J. Wang and L.D. Hutchins, Anal. Chim. Acta, 167 (1985) 325
34) M. Korolczuk, Fresenius J. Anal. Chem., 357 (1997) 389
35) H. Gunasingham, K.P. Ang and C.C. Ngo, Anal. Chem., 57 (1985) 505
36) P.J. O'Connell, C.K. O'Sullivan and G.G. Guilbault, Anal. Chim. Acta, 373 (1998) 261
37) J. Wang and M. Ariel, J. Electroanal. Chem., 83 (1977) 217
38) M.M.P.M. Neto, M.M.G.S. Rocha and C.M.A. Brett, Talanta, 41 (1994) 1597
39) M.C. Sneed, J.L. Maynard and R.C. Brasted, Comprehensive Inorganic Chemistry II, D. von Nostrand Company, 1954

CHAPTER 3

FLOW CELLS

3.1) THEORY

There are a number of requirements that need to be met in order for an electrochemical detector to be reliable. The hydrodynamics through the flow cell needs to be reproducible. It need not be well-defined for analytical applications, but this does assist in the optimisation of parameters [1]. The dead volume, which is not necessarily the geometric volume, needs to be minimised [1]. The electrochemical cell should be easy to handle and maintain. The working electrode should be able to be removed in order to clean it. The electrode placement within the cell is also important. The electrodes need to be placed close together to reduce cell resistance and the counter electrode should be placed downstream from the working electrode to prevent reaction products from the counter electrode from interfering with the detection [1,2]. The reference electrode must be stable. The silver/silver chloride and calomel electrodes are the most frequently used reference electrodes in flow systems. The disadvantage with these electrodes is that a filling solution is used and it must be maintained at a constant concentration without cross-contamination from the bulk solution [1]. This problem can be overcome by using a salt bridge. In theory, an increase in the size of the working electrode surface should lead to an increased analytical signal. This does however also lead to an increase in noise and, in the case of a SMDE, the drop becomes physically unstable [3]. Hence a compromise pertaining to the electrode size needs to be reached.

3.2) FLOW CELL FOR A HMDE

An important aspect that should be borne in mind when designing a flow cell for a mercury drop electrode is that the flow through the cell must be laminar in order to minimise any effects from turbulence [4].

Many different flow cells were designed for the use of a HMDE. They considered factors such as laminar flow, mercury drop stability, removal of mercury waste from the cell and so on. These included simple designs, for example, that by Bond *et al.* in figure 3.1 [4], to more complex cells such as that by Alpizar *et al.* in figure 3.2 [3].

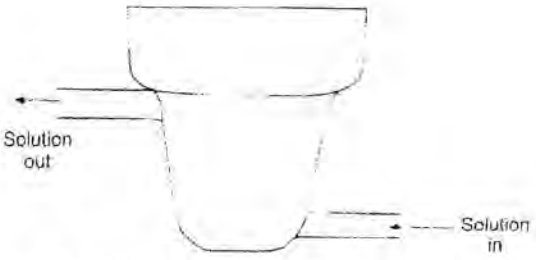

Figure 3.1: Flow cell with a volume of 30 ml to fit on a PARC Model 303 SMDE

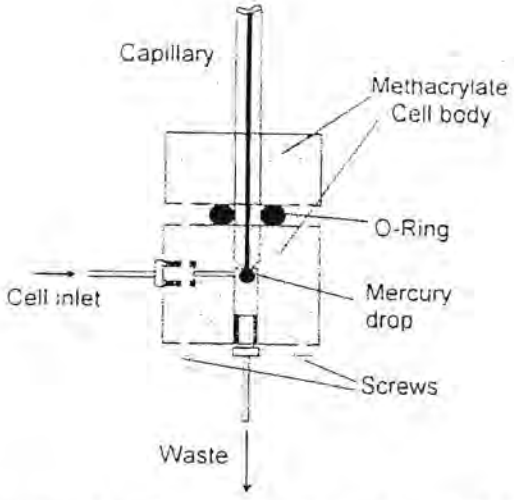

Figure 3.2: Flow cell with an Amel SMDE

Hanekamp *et al.* [2] looked at three types of mercury drop flow systems, namely:

1) parallel mercury and fluid flow

2) opposite mercury and fluid flow, and

3) mercury flow perpendicular to fluid flow.

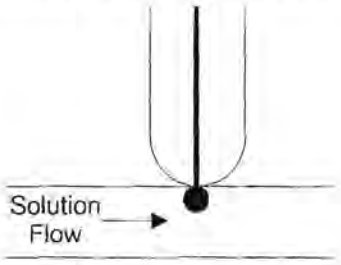

It was found that higher currents were obtained for opposite solution and mercury flow directions than for that in parallel directions, but the highest currents were obtained when the flow directions were perpendicular [2]. Hence the flow cell designed in this work had a perpendicular flow configuration. The mercury drop, which protruded into a horizontally flowing stream, was subjected to lateral forces that tended to displace it in the flow direction. This necessitated high flow rates to be avoided or else the mercury drop became unstable [4-6]. The reproducibility also decreases and the amount of noise increases at high flow rates, probably due to the mechanical instability of the mercury drop [4,5]. Saur *et al.* [7] found that the use of larger mercury drops increased the peak current to a greater extent in a flow cell with perpendicular flow than in a normal cup cell. This was due to the decrease of the

free channel cross-section which results in a locally increased flow speed. However, the use of larger mercury drops also leads to instability and irreproducibility. Thus a compromise between stability and sensitivity needs to be reached.

Stagnant areas of solution between the mercury drop and the capillary must be avoided. In figure 3.3 the stagnant areas are indicated in red [7]. It can be seen that perpendicular flow directions produce better results.

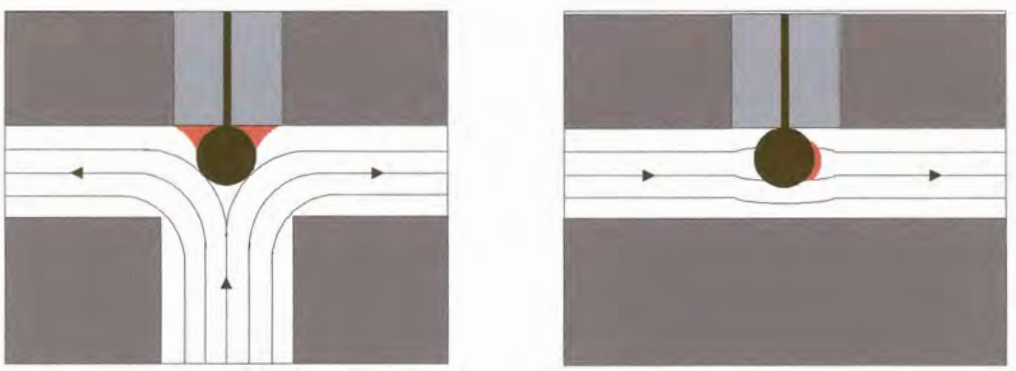

Figure 3.3: Flow geometry at a HMDE with a) opposite flow and b) perpendicular flow. The arrows and contours indicate the flow of the solution. The red areas indicate the stagnant areas.

3.2.1) Flow Cell for the SMDE for the Determination of Cobalt

The flow cell designed for this work is illustrated in figure 3.4. The flow cell is made from a polymethylmethacrylate (Perspex) cylinder as it is inert to the solutions used and in order to see what is happening inside during an analysis. There are spaces for the mercury capillary, a platinum wire for the auxiliary electrode and a BAS reference electrode. The reference electrode is placed after the working electrode to prevent any bleeding from interfering and it is also outside the electrical field between the working and counter electrodes [7].

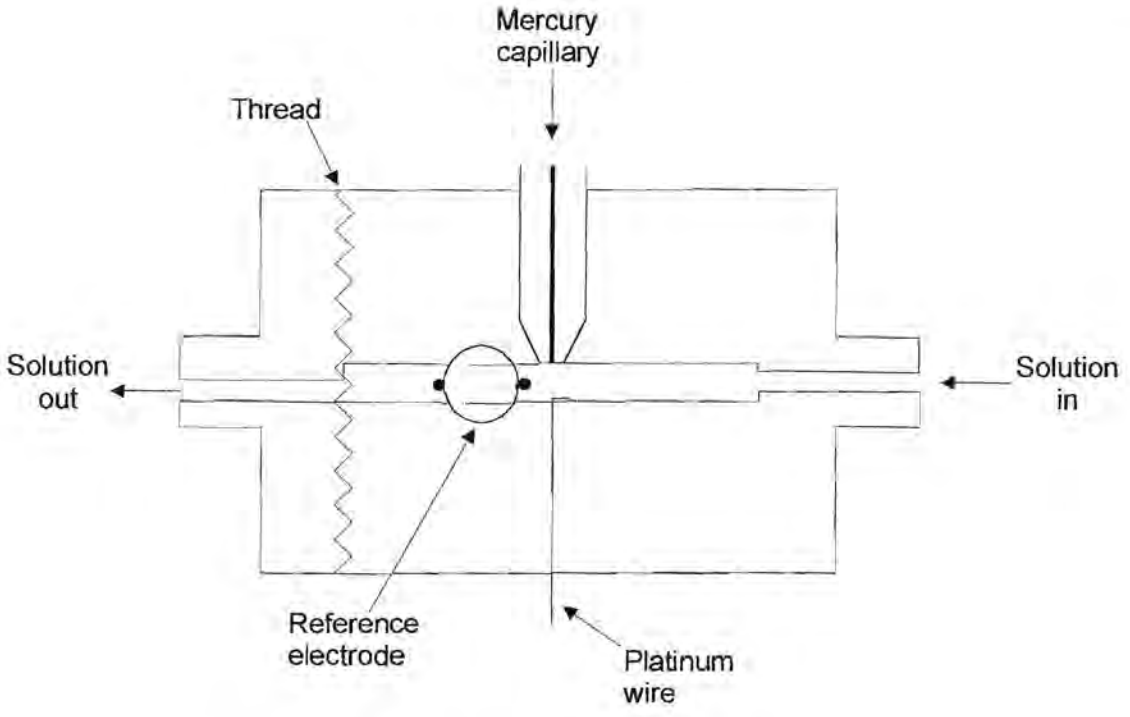

Figure 3.4: Flow cell for the SMDE

The platinum wire was sealed into place using an epoxy resin. This was later modified by soldering the platinum wire onto a brass screw and it was the screw to which a crocodile clip was then fastened (see figure 3.5). Both the platinum wire and the screw were sealed into place with epoxy resin.

The position of the platinum wire in the flow cell was also adjusted. Initially it was positioned just below the mercury drop in order to minimise the iR drop between these electrodes [8,9], but after a short time of use, the mercury formed an amalgam with the platinum and the mercury was not washed out of the flow cell. Instead it built up over the platinum until it merged with the mercury drop being dispensed from the capillary. It is generally specified that the counter electrode be place after the working electrode in the direction of flow in the cell so that the products generated at this electrode are not detected by the working electrode [8,10]. This may, however, have had a similar result. A few runs were done with a platinum wire situated before and after the working electrode in the zinc electrolyte that was to be analysed and no difference in the results were found.

The capillary was also initially sealed in place using silicone sealant, but later an o-ring was inserted to hold it firmly in place. The reference electrode was also held in place with two o-rings. In both cases, slight variations in size of the capillaries and reference electrodes necessitated that they be covered with some Teflon tape first to provide a good seal.

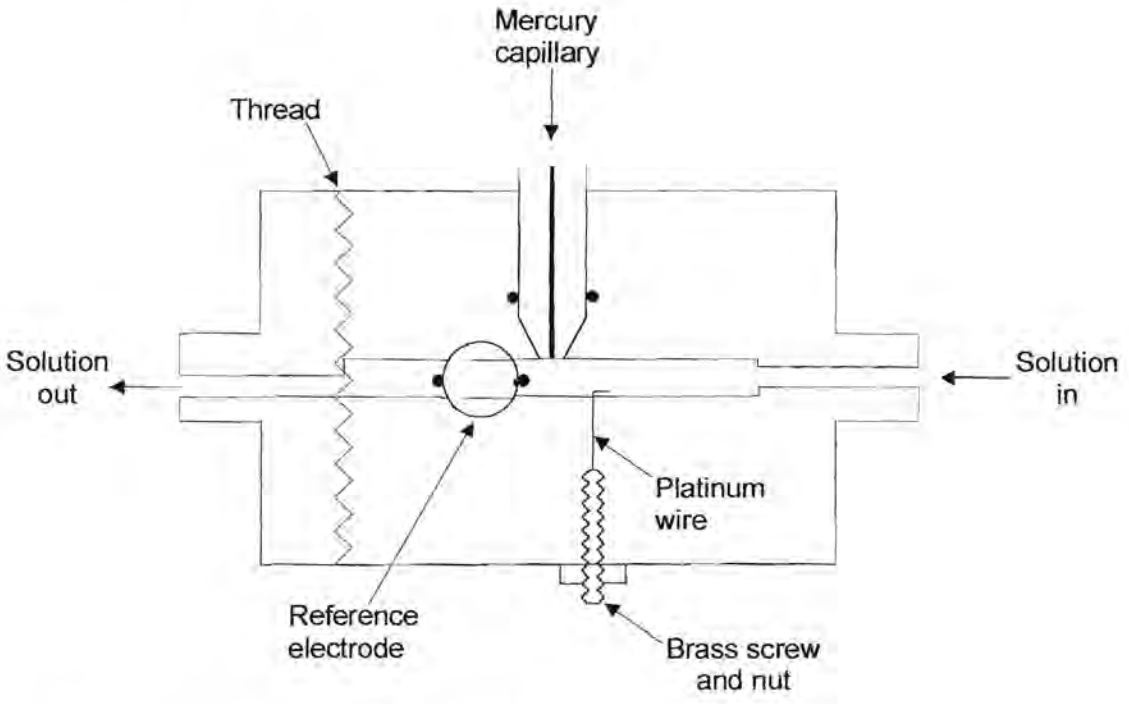

Figure 3.5: Modified flow cell for the SMDE

The dimensions of the flow cell are shown in figure 3.6. The diameter of the inlet is similar to that of the tubing through which the solution passed before it entered the flow cell. This was chosen so that the turbulence in flowing from the tubing to the flow cell would be minimal and also to assist in the joining of the tubing to the cell. The inner diameter is then increased so that there would be enough space for the solution to flow around the mercury drop hanging from the end of the capillary, but making sure that the amount of dead space is kept to a minimum. The cross-sectional area also needs to be kept small in order to increase the mean linear solution velocity [2,7]. Once again it was tried to minimise the turbulence by placing the entrance into the wider channel in the centre. Additionally, the most suitable flow rate would have to be determined to produce laminar flow for this particular cell. The exit from this channel is narrowed again to apply a back-pressure and is situated at

the bottom of the wide channel so that the used mercury drops could be easily washed out of the cell into waste. The outer diameter of the inlet is 5 mm in order to allow the tubing that was used in the deoxygenation system (see chapter 4) to fit tightly over it.

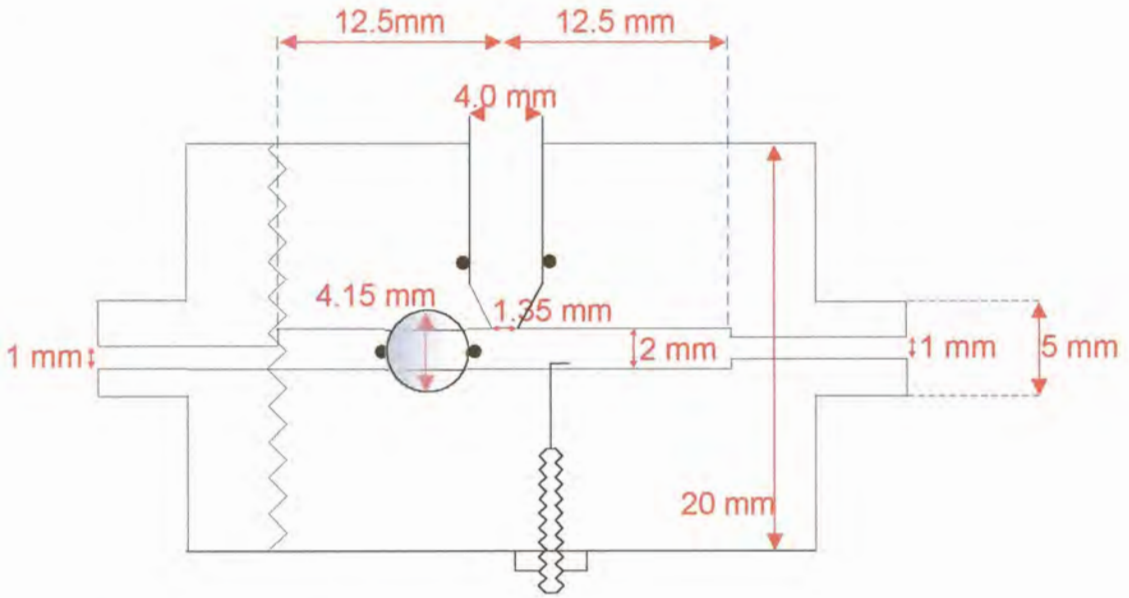

Figure 3.6: Flow cell dimensions

The end of the flow cell could be screwed off at the point indicated by the thread in figure 3.5. This was to allow the manufacturer to make a wide channel between the narrower inlet and outlet. This also assisted in inserting a wire to bend the platinum wire counter electrode flat against the side of the channel, so as not to obscure the path of the solution. When a significant back-pressure was applied, the cell started leaking at the thread, so a gasket made from a thick plastic sheet was inserted.

Another problem was that the drop knocker could not shake the capillary sufficiently to dislodge the mercury drop when it was in position in the flow cell. It was found that allowing an air bubble to pass through the cell dislodged the drop and carried it out into waste. Introducing air into the system would diminish previous deoxygenation as the oxygen would diffuse into the solution, so nitrogen was used instead.

This cell was used as part of the flow system described in chapter 5 for the determination of cobalt in a zinc electrolyte. The characteristics of the flow cell were also investigated in that chapter.

3.3) WALL-JET CELLS

A wall-jet is described as the flow of a jet of fluid that strikes a plane perpendicularly and flows radially over its surface [1,11-15]. It was noted that the velocity of the fluid in the direction normal to the electrode is towards the electrode at large distances from the electrode, but the flow is away from the electrode close to the electrode. The flow is zero along the surface given by:

$$\eta = 0.51\,k\left(\frac{V}{\nu}\right)^{3/4} a^{-1/2} r^{-5/4} z = 3.96$$

where V is the volume flow rate through the inlet, ν is the kinematic viscosity, a is the nozzle diameter, r is the radial distance, z is the distance normal to the electrode and k is equal to 0.86 [1,11,16]. This is illustrated in figures 3.7 and 3.8.

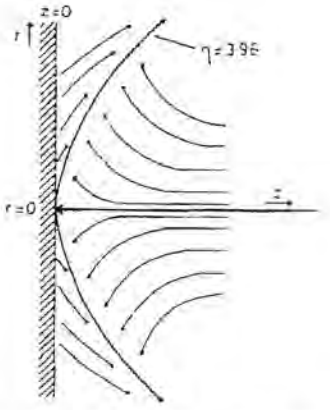

Figure 3.7: Velocity flow profiles at the wall-jet electrode (WJE) where r is the electrode radius, z is the direction normal to the electrode and η is the stagnant region [1]

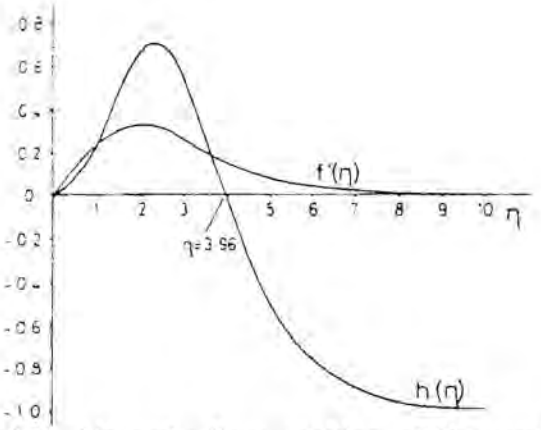

Figure 3.8: Velocity flow profiles at the wall-jet electrode (WJE) where f'(η) is the radial velocity profile and h(η) is the velocity profile normal to the electrode surface. η=3.96 is the stagnant region [1]

Laevers *et al.* [15] subdivided the flow pattern into 4 hydrodynamic regions, namely, the potential core, the free-jet region, the stagnation zone and the wall-jet region. These are depicted in figure 3.9. As solution flows from the submerged nozzle, the solution in the jet exchanges momentum with the surrounding fluid to create a free-jet. This forms a conical potential core which varies from 4 to 8 nozzle diameters in length, depending on the shape of the nozzle. Due to intensive momentum exchange, the jet broadens as it gets close to the electrode, up to a limiting distance of 1.2 to 2.2 nozzle diameters from the electrode surface, which is then the start of the stagnation zone. In the stagnation zone the flow is deflected by the electrode surface, its axial velocity is decelerated and transformed to an acceleration parallel to the surface. Due to the exchange of momentum with the quiescent surrounding fluid, the accelerating flow transforms into a decelerating wall-jet. The velocity parallel to the electrode surface reaches a maximum 0.6 to 1.4 nozzle diameters from the stagnation point, where the stagnation zone transforms into the wall-jet region. In the wall-jet region, the flow is influenced by both the quiescent surrounding fluid and the electrode surface [15].

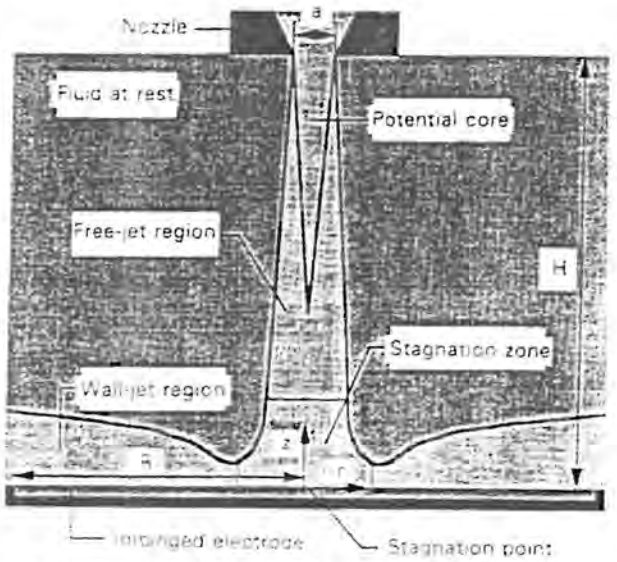

Figure 3.9: The flow pattern in a WJE [15]

This flow pattern clearly shows that the WJE is not uniformly accessible as the rate of mass transport is higher towards the centre of the electrode than at the edge [1,14,15]. Only fresh solution from the jet reaches the electrode surface, not the dead solution in the cell chamber. Therefore it is not necessary to flush out the cell compartment between analyses [11,16,17].

The mass transport of electroactive species (*i*) to the impinged surface of the WJE can be described by the convective diffusion equation:

$$\frac{\partial C_i}{\partial t} = D_i \frac{\partial^2 C_i}{\partial z^2} - v_r \frac{\partial C_i}{\partial r} - v_z \frac{\partial C_i}{\partial z}$$

where r and z are the distances along and normal to the electrode in cylindrical pole coordinates with the origin at the intersection of the jet axis and the electrode surface, v_r and v_z are the corresponding velocity components and D_i is the diffusion coefficient of *i* [18]. Two assumptions were made to reach this equation, namely that homogeneous reactions producing or consuming *i* do not occur and radial diffusion is omitted. Radial diffusion effects only become important where the solution is most stagnant which occurs at the outer radius of the electrode. However, in this region the radial concentration gradients are small, thus the effect of radial diffusion on concentration changes can be neglected [18].

The limiting current can be calculated by:

$$i_{lim} = 1.38nFCD^{2/3}\nu^{-5/12}V^{3/4}a^{-1/2}R^{3/4}$$

where n is the number of electrons, F is Faraday's constant, C is concentration, D is the diffusion coefficient, ν is the kinematic viscosity, V is the flow rate, a is the nozzle diameter and R is the electrode radius [15,16,19]. Although the equation does not include a term for the separation between the inlet nozzle and the electrode surface, it is assumed that the jet does not break up before it impinges in the electrode [1,15,19].

When a fluid flows over the electrode surface, a very thin layer is formed at the surface where the velocity gradient normal to the surface is very large. This layer is called the boundary layer [1,20]. The boundary layer thickness for the WJE is calculated as follows:

$$\delta_{bl} = 5.8\pi^{3/4}a^{1/2}\nu^{3/4}x^{5/4}V^{-3/4}$$

where a is the inlet diameter, ν is the kinematic viscosity, x is the electrode radius and V is the flow rate [19,21]. From this it can be deduced that the boundary layer thickness increases rapidly from the centre of the electrode to the outer edge and that it decreases rapidly as the flow rate increases.

The diffusion layer thickness is calculated by:

$$\delta_{dl} = 5.8k_2\pi^{3/4}D^{1/3}a^{1/2}\nu^{5/12}x^{5/4}V^{-3/4}$$

where $k_2 = 0.17$. It is estimated that the diffusion layer is 2% of the hydrodynamic boundary layer thickness [16,19].

When considering the design of a wall-jet cell (WJC), there are a number of factors to take into consideration. Some of these are listed below.

1) In order to maintain true wall-jet behaviour, there should be no interference with the development of the boundary layer in a WJC, therefore the nozzle body, the back wall, the counter electrode and the reference electrode should not be located close to the working electrode [1,16]. The bulk volume of the cell should also be large [16]
2) The jet formed should be stable, preferably with laminar flow characteristics [16].

3) The proportionality between the limiting current and the flow rate is obeyed only when the inlet-electrode separation is greater than a certain value which is governed by several factors such as electrode diameter, solution flow rate, solution viscosity and the geometry of the nozzle body [19].
4) Laevers *et al.* [15] found that for true wall-jet behaviour the following relationship between the nozzle diameter (a) and the nozzle-electrode separation (H) should hold:

$$12 \leq H/a \leq 15$$

If the ratio of H:a is too small, the jet does not fully develop before it strikes the electrode surface and if the ratio is too large, the free-jet spreads out before it impinges on the electrode surface.
5) The diameter of the free-jet should be negligible, therefore the electrode diameter should be at least 10 times larger than that of the inlet diameter [1,16].

3.3.1) Wall-Jet Cell used for the Determination of Arsenic in Gold

The cell designed for this work is illustrated in figure 3.10 and the measurements are shown in figure 3.11. As for the previous cell, this flow cell was made from a polymethylmethacrylate (Perspex) cylinder as it is inert to the solutions used and in order to see what is happening inside during an analysis. There are cavities for a BAS glassy carbon electrode, a platinum wire for the auxiliary electrode and a BAS reference electrode. The platinum wire was soldered to a brass screw and they were sealed into place with epoxy resin. The top and the bottom parts of the flow cell were held together by three bolts (not depicted in the diagram) with an o-ring between to make a good seal. An o-ring held the working electrode in place, so it was easy to adjust the inlet-electrode separation and it could be readily removed to clean. The reference electrode was separated from the cell compartment by a narrow passage which extended the life of this electrode. An outlet was situated in the reference electrode compartment so the solution around the electrode could be renewed. Another outlet was situated at the top of the conical section of the cell for the facile removal of bubbles. The inlet was made from PEEK (polyetheretherketone) and had an inner diameter of 0.3 mm.

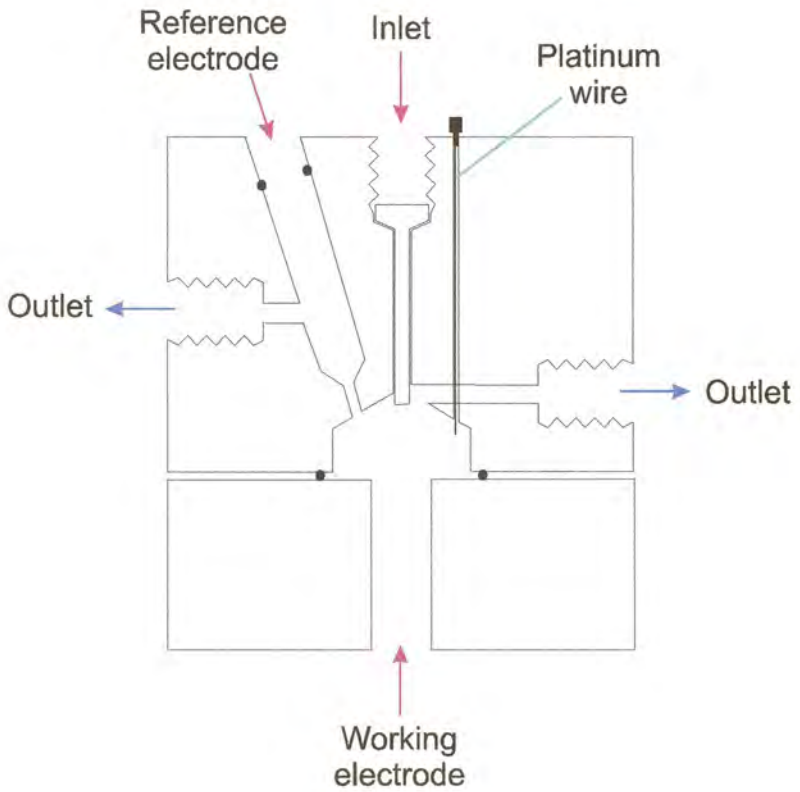

Figure 3.10: Wall-jet cell

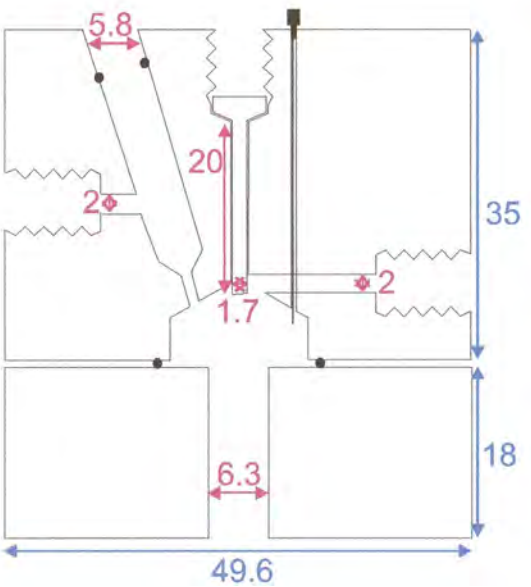

Figure 3.11: Dimensions of the wall-jet cell (values quoted in mm)

The volume of the cell was approximated by calculating the geometric volume from the dimensions. This is shown in figure 6.12.

Figure 3.12: The geometric sections of the cell cavity used to calculate its volume

Total volume = volume of cylinder + volume of pyramid

$= \pi r^2 h + 1/3\pi r^2 h$

$= 795.2\ mm^3 + 217.9\ mm^3$

$= 1013.1\ mm^3$

Therefore the estimated volume is 1 ml. This is a relatively large volume as the volume for thin layer cells is generally of the order of a few µl. There should be no interference with the development of the boundary layer with these cell dimensions. In the case of a WJC, the dead volume is not the same as the geometric volume. It is preferable to have a large geometric volume for a WJC.

3.4) REFERENCES

1) A.J. Bard, Electroanalytical Chemistry, Volume 16, Marcel Dekker Inc., 1989
2) H.B. Hanekamp and H.J. van Nieuwkerk, Anal. Chim. Acta, 121 (1980) 13
3) J. Alpizar, A. Cladera, V. Cerda, E. Lastres, L. Garcia and M. Catasus, Anal. Chim. Acta, 340 (1997) 149
4) A.M. Bond, H.A. Hudson and P.A. van den Bosch, Anal. Chim. Acta, 127 (1981) 121
5) L.A. Mahoney, J. O'Dea and J.G. Osteryoung, Anal. Chim. Acta, 281 (1993) 25
6) U. Baltensperger and R. Eggli, Anal. Chim. Acta, 123 (1981) 107
7) D. Sauer and E. Spahn, Fresenius J. Anal. Chem., 351 (1995) 154
8) W. Lund and L.-N. Opheim, Anal. Chim. Acta, 79 (1979) 35
9) D.C. Johnson, S.G. Weber, A.M. Bond, R.M. Wightman, R.E. Shoup and I.S. Krull, Anal. Chim. Acta, 180 (1986) 187

10) J.A. Wise, W.R. Heineman and P.T. Kissinger, Anal. Chim. Acta, 172 (1985) 1
11) W.J. Albery and C.M.A. Brett, J. Electroanal. Chem., 148 (1983) 211
12) W.J. Albery and C.M.A. Brett, J. Electroanal. Chem., 148 (1983) 201
13) J. Wang and B.A. Freiha, Anal. Chem., 57 (1985) 1776
14) R.G. Compton, A.C. Fisher, M.H. Latham, R.G. Wellington, C.M.A. Brett and A.M.C.F. Oliveira Brett, J. Appl. Electrochem., 23 (1993) 98
15) P. Laevers, A. Hubin, H Terryn and J. Vereecken, J. Appl. Electrochem., 25 (1995) 1017
16) H. Gunasingham, K.P. Ang, C.C. Ngo, P.C. Thiak and B. Fleet, J. Electroanal. Chem., 186 (1985) 51
17) H. Gunasingham, K.P. Ang, C.C. Ngo and P.C. Thiak, J. Electroanal. Chem., 198 (1986) 27
18) P. Laevers, A. Hubin, H Terryn and J. Vereecken, , J. Appl. Electrochem., 25 (1995) 1023
19) H. Gunasingham and B. Fleet, Anal. Chem., 55 (1983) 1409
20) R.J. Rucki, Talanta, 27 (1980) 147
21) H. Gunasingham, Anal. Chim. Acta, 159 (1984) 139

CHAPTER 4

DEOXYGENATION

4.1) INTRODUCTION

The presence of dissolved oxygen in samples often interferes in the application of electroanalytical methods. Oxygen from the atmosphere dissolves in water to produce concentrations of approximately 8.3 $mg.l^{-1}$ at 25°C (1 atm). This value was obtained by averaging a number of values given in the literature [1-3]. At this concentration a high background current is obtained on cathodic reduction of oxygen, which may obscure the analytical signal [4-7]. The dilemma would not be as dramatic if the presence of the oxygen waves were the only interference.

The reduction of oxygen proceeds via a hydrogen peroxide intermediate. In acidic solutions the mechanism is as follows [8]:

$O_2 + 2H^+ + 2e^- = H_2O_2$ $\quad E^0 = 0.69$ V

$H_2O_2 + 2H^+ + 2e^- = 2H_2O$ $\quad E^0 = 1.78$ V

and the overall reaction is:

$O_2 + 4H^+ + 4e^- = 2H_2O$ $\quad E^0 = 1.23$ V

In basic solutions the mechanism is:

$O_2 + 2H_2O + 2e^- = H_2O_2 + 2OH^-$ $\quad E^0 = -0.15$ V

$H_2O_2 + 2e^- = 2OH^-$ $\quad E^0 = 0.55$ V

and the overall reaction is:

$O_2 + 2H_2O + 4e^- = 4OH^-$ $\quad E^0 = 0.40$ V

The H_2O_2 intermediate can function as both an oxidising and reducing agent, and hence act on other electroactive species present. In unbuffered solutions, pH changes can occur in the vicinity of the electrode due to the electro-reduction of oxygen. A resultant increase in pH can lead to precipitation of heavy metal ions close to the electrode and therefore diminish their diffusion currents [4,5]. In stripping voltammetry, the oxygen present leads to the partial dissolution of the metal accumulated by preelectrolysis which lowers the results obtained [4,6].

Deoxygenation also prevents the following non-electrochemical process that can occur in a neutral, unbuffered metal salt solution containing metallic mercury and dissolved oxygen:

$$O_2 + 2Hg + 2Cl^- + 2H_2O = Hg_2Cl_2 + 4OH^- \qquad [4]$$

It is therefore the task of the electrochemist to remove the dissolved oxygen or to nullify the effects thereof, the former being the most widely used.

Sparging the solution with an inert gas is the most frequently used method of deoxygenation. This could, however, lead to sample evaporation and the loss of certain volatile components [6]. It also has limitations in flow analysis. This is mainly due to recontamination of the solution because oxygen can diffuse through the walls of the Teflon tubing generally used in flow analysis. Stainless steel tubing has been used as a substitution where possible, but this leads to metal contamination especially in harsh environments.

A chemical approach comprises of passing the solution through a reactor, in which a reagent that reacts with oxygen is immobilised. Pyrogallol (1,2,3-trihydroxybenzene) in alkaline solutions and ascorbic acid or columns packed with zinc particles in acidic solutions are examples of such reagents [4,6,9]. The drawback of this procedure is the introduction of impurities, particularly when doing trace analysis.

Photochemical methods have also been used. These are based on the reaction of oxygen with organic acids, such as formic, citric or oxalic acids, under UV irradiation. A high concentration of acid and a fairly long irradiation time is required to attain acceptable efficiency, hence this is not an elegant manner to deoxygenate a solution [4].

When determining elements with large negative standard potentials, such as zinc(II), oxygen can be reduced electrochemically prior to the analytical experiment [4,6]. This has a very limited use.

Changes in pressure or temperature can be employed to reduce the concentration of dissolved oxygen. The temperature of the solution can be increased, as the solubility of gases is inversely proportional to the temperature of the solution at a given pressure [4,6,7,9]. The solubility of sparingly soluble gases such as oxygen, nitrogen and carbon monoxide approaches zero at 100°C and ambient pressure [9]. Vacuum degassing and ultrasonication with an applied vacuum are also mechanisms used to reduce the amount of dissolved gases [4,7]. The applied vacuum decreases the pressure above the solution, thus allowing dissolved gases to expel from the solution and be removed by the vacuum [7]. This method could, however, also lead to sample evaporation and the loss of volatile components.

Gas permeable membranes through which the samples pass, with a reduced partial pressure of oxygen surrounding the membranes, have been used in a number of different ways [5-7]. The membrane can be surrounded by a strong reducing agent, such as chromium(II) in the presence of amalgamated zinc. As the oxygen diffuses through the membrane, it is scavenged by the reductant [6,7,10,11]. The mechanism is as follows [8]:

$$4Cr^{2+} + O_2 + 4H_3O^+ \rightarrow 4Cr^{3+} + 6H_2O$$

$$2Cr^{3+} + Zn(Hg) \rightarrow 2Cr^{2+} + Zn^{2+} + Hg$$

The membrane has also been surrounded by nitrogen or a vacuum, or both of these were applied together [4,5,6,11].

An inert gas, instead of air, could be used for segmenting flow streams to remove the dissolved oxygen from solution. The stream should first pass through a time delay coil to achieve more efficient deoxygenation [12]. Sample solutions were also mixed with large excesses of deaerated supporting electrolyte to minimise the effect of dissolved oxygen [4,12]. Neither of these procedures removed oxygen completely, although its concentration is markedly diminished as equilibrium is attained between the oxygen and nitrogen in the flow system [12].

The methods discussed thus far have all involved the removal of oxygen. Another approach is to discriminate against oxygen interference by choosing parameters such as the potential wave form, the chemical form of the analyte and the nature of the working electrode, such that it would alleviate the interference from dissolved oxygen [6].

4.2) SEMI-PERMEABLE MEMBRANES IN A NITROGEN ATMOSPHERE

The first experiments of gas diffusion through a membrane were employed for oxygenation of solutions. It was also a liquid-membrane-gas process. The driving force for the gas exchange was the difference in partial pressures. Eventually a steady state of the partial pressure of gases is reached [13]. This technology has now been employed in deoxygenators, particularly for flow systems.

There are two main properties to consider when choosing a membrane. Firstly, the membrane should be highly permeable to oxygen. The permeability coefficient for oxygen is equal to the product of the solubility coefficient of oxygen in the membrane and the diffusion rate of oxygen through the membrane. Secondly the membrane should be inert to the analyte solution [7,10,11]. In comparison to silicone, most other polymers are much less permeable to gases [4]. Silicone is also inert to a large variety of chemicals, thus making it a suitable membrane material. It is important to have a membrane with a small internal diameter and thin wall thickness to optimise the amount of deoxygenation.

There are numerous other factors affecting the extent of deoxygenation such as the temperature and the viscosity of the analyte solution, the volume ratio of gas to liquid, the pressure of the gas and the initial concentration of oxygen in the gas. The residence time, which is the quotient of the length of the membrane and the flow rate, also needs to be optimised [4,9,10].

Mass transfer by diffusion is the way of transporting a substance under the influence of a chemical potential gradient, generally being a concentration gradient, for stagnant fluids or fluids moving in laminar flow. This takes place at a much smaller rate than eddy or turbulent diffusion, which occurs when the fluid undergoes mechanical stirring or convective movement [12]. Fick's Law governs the rate of diffusion. It expresses the mass transfer rate per unit interfacial area (N_i) as a linear function of the molar concentration gradient.

$$N_i = -D \frac{dC_i}{dy}$$

where N_i is the molar flux of component i, dy is the distance over which the concentration gradient dC_i is present and D is the diffusion coefficient. The negative sign emphasises that diffusion occurs in the direction of the drop in concentration.

Thus Fick's Law can assist in predicting the time required to deoxygenate a solution to a degree suitable for the experiment [9,10,14].

The mass transfer in this membrane deoxygenation system is an important consideration. Firstly, consider a fluid flowing past a flat plate. The velocity at the solid surface is zero, so there must be a layer adjacent to the surface where the flow is predominantly laminar. Here the fluid can be thought of as being made up of thin layers sliding over each other at increasing velocities at increasing distances from the plate. The molecules in one layer, while travelling in their random directions, will move from a fast moving layer to an adjacent slower moving layer. Even when turbulent flow prevails, the layer adjacent to the surface in predominantly laminar. The character of the flow gradually changes as the distance from the surface increases [14]. Therefore Fick's Law should apply for diffusion across a membrane as the flow close to the surface of the membrane is laminar.

From Fick's Law, for diffusion through a flat slab of thickness z, the rate of diffusion per unit area (N) is given by:

$$N = \frac{D(C_1 - C_2)}{z}$$

where C_1 and C_2 are concentrations at opposite sides of the slab [14] and $C_2 > C_1$. The rate of diffusion for other shapes is given by [15]:

$$w = NS_{av} = \frac{DS_{av}(C_1 - C_2)}{z}$$

where S_{av} is the average cross section for diffusion. For radial diffusion through a solid cylinder of inner and outer radius r_i and r_o respectively, and of length ℓ: [14]:

$$S_{av} = \frac{2\pi\ell(r_o - r_i)}{\ln\left(\frac{r_o}{r_i}\right)}$$

and $z = r_o - r_i$

The diffusivity of oxygen in the liquid phase is much lower than that in the gas phase. This is due to resistance in the liquid phase [9,13]. Liquid resistance used to be considered the rate controlling resistance and the membrane resistance was ignored. Tang *et al.* showed the significance of membrane resistance to gas transfer under various operating conditions [13]. Thus, when diffusion through a solid occurs, the structure of the solid and its interaction with the diffusing substance have a profound influence on how diffusion takes place and on the rate of transport [14]. Solid materials through which diffusion can occur are polymers, crystalline solids and porous solids. Since a silicone membrane is a polymer, the mechanism by which diffusion occurs through a polymer will be looked at more closely. Diffusion of solutes through polymeric substances is generally similar to diffusion through liquid solutions, especially for gas solutes. The gas dissolves in the solid at the faces exposed to the fluids and then diffuses from the high to low concentration side of the polymer. The polymeric chains are in a state of constant thermal motion and the diffusing molecules move from one position to another over the potential barrier. A successful move requires that there is an available hole or passage of sufficient size, which in turn depends on the thermal motion of the polymer chains. Therefore diffusion depends on the temperature. In the case of oxygen and nitrogen, the molecules are relatively small, so diffusion is relatively easy [14].

4.3) EXPERIMENTAL

A semi-permeable membrane deoxygenation system was used in this study because it was an efficient way to remove oxygen, particularly for a flow system, and it was also inexpensive and fairly easy to implement. The deoxygenation system consisted of a 3 m length of gas permeable silicone tubing placed inside the same length of impermeable polyethylene tubing. The silicone tubing had an internal diameter of

0.75 mm and a wall thickness of 0.25 mm (Carlin Medical Extrusions, Eden Glen, Johannesburg) and the polyethylene tubing had an internal diameter of 3.8 mm and a wall thickness of 1.2 mm (Controlled Irrigation, Bramley, Johannesburg). A counter flow system, as illustrated in figure 4.1, where the solution flowing through the silicone tubing flows in the opposite direction to the nitrogen flowing in the polyethylene tubing, was used. In this way a concentration gradient for oxygen is maintained throughout the entire length of the tubing, improving the deoxygenation efficiency.

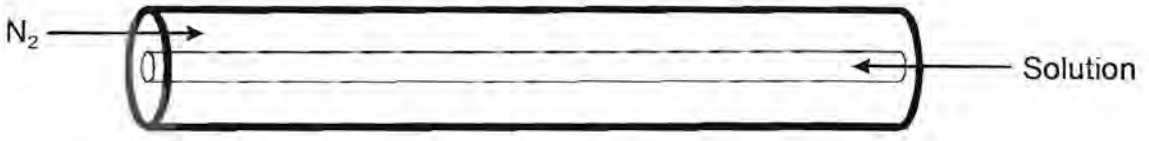

Figure 4.1: Schematic diagram of a counter flow deoxygenation system

Since the nitrogen in the gas cylinder may have contained small quantities of oxygen, the gas was scrubbed. Two scrubbers were employed. The first scrubber contained a vanadous chloride solution with some amalgamated zinc. The vanadous chloride was prepared by boiling 2 g of ammonium metavanadate with 25 ml hydrochloric acid and then diluted to 250 ml. The amalgamated zinc was prepared by covering zinc filings with deionised water, adding 2 drops of hydrochloric acid and then adding mercury. A blue-green solution was produced which turned purple when nitrogen was bubbled through it. When it was exhausted it turned a blue green colour once again. The solution could be rejuvenated by the addition of more amalgamated zinc or a few drops of hydrochloric acid [15]. The mechanism by which the scrubber removed oxygen is:

$$4V^{3+} + O_2 + 4H_3O^+ \rightarrow 4V^{4+} + 6H_2O$$

$$4V^{4+} + 2Zn(Hg) \rightarrow 4V^{3+} + 2Zn^{2+} + 2Hg$$

The second scrubber contained deionised water to trap any vanadous chloride. It was found that gas scrubbing played an important role when the difference in currents were

observed for a new scrubber versus an exhausted one. The flow rate of nitrogen was also estimated by observing the amount of bubbling occurring in the scrubbers.

This membrane deoxygenation system was part of the flow system as shown in chapter 5. It was used with both the flow cell for the SMDE and the WJC. It was tested in both cases due to the different demands of the set-ups.

4.3.1) Testing Deoxygenation using the Flow Cell for the SMDE

In order to investigate the extent of deoxygenation, a solution was tested before and after deoxygenation and the difference in the voltammograms noted. A 0.5 $mol.l^{-1}$ sulphuric acid solution was considered first. Although the effect of deoxygenation was evident, it was difficult to quantify the amount of deoxygenation that had taken place. A copper solution in 1 $mol.l^{-1}$ nitric acid was then tested. The copper reduction peak is close to the first reduction peak of oxygen, thus in a solution exposed to the atmosphere the oxygen peak predominates resulting in the inability to detect the copper [16]. A concentration of 1 $mg.l^{-1}$ copper was first used, but proved to be too high as it diminished the effect of dissolved oxygen in the solution, so a 20 $\mu g.l^{-1}$ copper concentration was used. The differential pulse stripping voltammetry (DPSV) mode was used with the parameters as follows:

initial potential = –300 mV
final potential = 120 mV
deposition time = 180 s
quiet time = 10 s
scan rate = 20 $mV.s^{-1}$
pulse amplitude = 50 mV
sample width = 20 ms
pulse width = 50 ms
pulse period = 200 ms

The effects of the presence of dissolved oxygen, particularly for trace concentration determination, can readily be seen in figure 4.2.

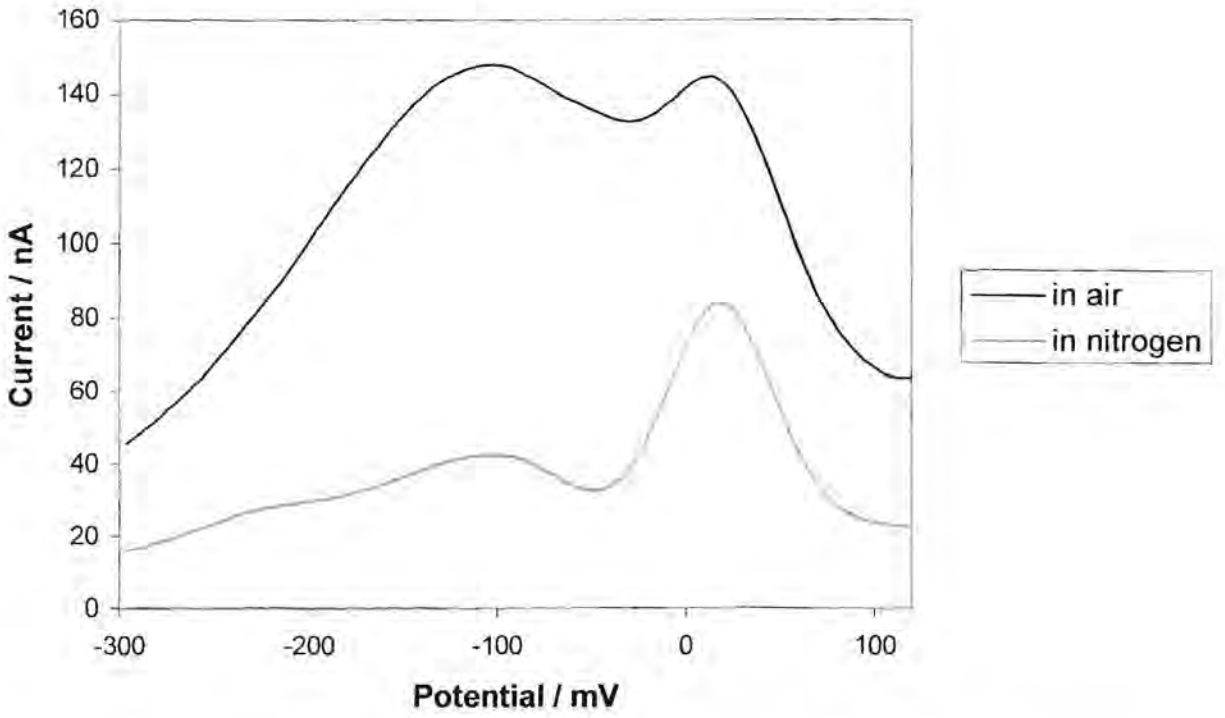

Figure 4.2: 20 $\mu g.l^{-1}$ Cu in 1 $mol.l^{-1}$ HNO_3 measured in an air atmosphere and then in a nitrogen atmosphere

Finally the method used by Pedrotti *et al.* [4], who employed a sodium perchlorate solution under hydrodynamic conditions, was used. A 10 $mmol.l^{-1}$ $NaClO_4$ (that had been recrystallised) solution was made. Linear sweep voltammetry (LSV) was used to collect the data from 200 mV to –1400 mV. A scan rate of 10 $mV.s^{-1}$ and sensitivity of 1 $\mu A.V^{-1}$ was used. Data were collected while the pump was running at a speed setting of 10 which corresponded to 1.5 $ml.min^{-1}$ (see chapter 5). Figure 4.3 shows the difference in currents for an oxygenated versus a deoxygenated solution. The efficiency of oxygen removal was evaluated from the ratio of the initial current before deoxygenating and the steady state current afterwards. Since the deoxygenation system consisted of a long tube, it was necessary to first flush the polyethylene tubing with nitrogen for some time to purge all the oxygen out. It was found that a 30 minute flush was sufficient as longer periods had no further significant effect.

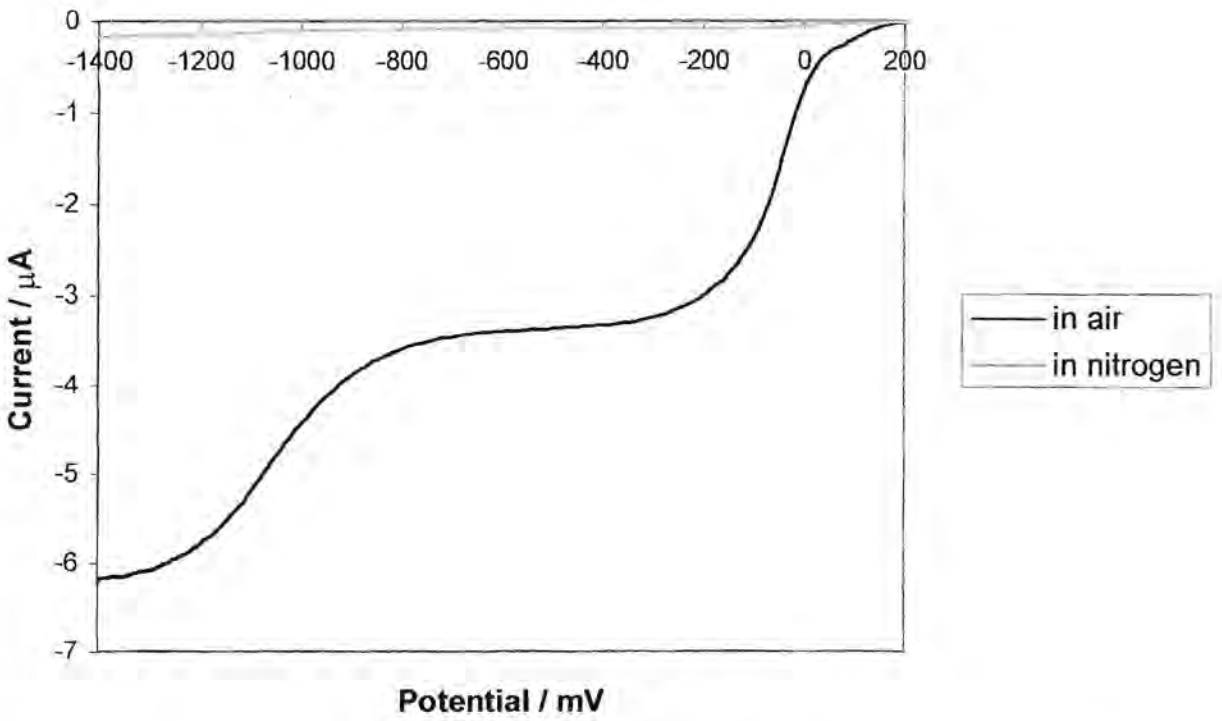

Figure 4.3: The oxygen reduction current in 1 mmol.l^{-1} $NaClO_4$ measured in an air atmosphere and then in a nitrogen atmosphere

Three different deoxygenation set-ups were tested, namely:

1) the deoxygenation tubing alone,
2) the deoxygenation tubing together with sparging the solution in a flask before entering the tubing, and
3) sparging the solution in the flask alone before passing directly into the flow cell.

The steady state currents were measured at -550 mV and the results are presented in table 4.1.

Table 4.1: Deoxygenation efficiencies

Atmosphere	Air	Nitrogen		Air	Nitrogen
Set-up	Tubing	Tubing	Tubing + Flask	Flask	Flask
Steady state current (nA) at -550 mV	3.37×10^3	72.0	39.1	4.27×10^3	372
Current decrease factor	1	47	86	1	11
Residual dissolved O_2 ($\mu g.l^{-1}$)	8.3×10^3	177	96.5	8.3×10^3	755
O_2 removal efficiency (%)		97.9	98.8		90.9

Where:

$$\text{current decrease factor} = \frac{\text{steady state current in air}}{\text{steady state current in nitrogen}}$$

$$\text{residual dissolved } O_2 = \frac{8.3 \times 10^3 \ \mu g.l^{-1}}{\text{current decrease factor}}$$

$$O_2 \text{ removal efficiency} = \frac{8.3 \times 10^3 - \text{residual dissolved } O_2}{8.3 \times 10^3} \times 100\,\%$$

The concentration of dissolved oxygen given as 8.3 $mg.l^{-1}$ is the value for distilled water. This concentration decreases as the concentration of the electrolyte increases [17]. In addition, oxygen is non-polar and hence becomes less soluble as the solvent polarity increases [7]. The dissolved oxygen concentration should thus be significantly lower for the concentrated electrolytes used in this study.

In the case of the flask set-up, a pulse damper, as described in chapter 5, was placed between the pump and the flow cell when the deoxygenation tubing was removed. Data in air was also collected for this set-up as the hydrodynamics may have varied slightly

in the absence of the tubing. A point was reached where increasing the sparging time did not affect the current measured. This proved to be the least efficient method for oxygen removal which was probably due to contamination while passing through the Teflon tubing of the pump which is susceptible to gas diffusion. The pulse damper could also have been a source of contamination as the sealed tube that was perpendicular to the solution flow contained air.

The most efficient method of oxygen removal was using the combination of sparging the solution in the flask before passing into the tubing. The bulk of the oxygen was removed during the sparging and the tubing set-up could remove further traces. Any contamination from passing through the Teflon pump tubing was also removed in the deoxygenation tubing. It was decided, however, that this method would be impractical and time consuming. An alternative would have been to only sparge the stripping electrolyte which would reduce the oxygen signal. However, the oxygen removal efficiency was only one percent lower if sparging was not done first, so the tubing set-up alone was used.

4.3.2) Testing Deoxygenation using the Wall-Jet Cell

The method that was used by Pedrotti *et al.* [4] and in the previous section was tested at the gold film electrode in the wall-jet cell (WJC). Measurements were made firstly in an air atmosphere and then, after flushing the tubing for 30 minutes, measurements of the deoxygenated solutions were made at various flow rates. 10 $mmol.l^{-1}$ sodium perchlorate was pumped through the system and LSV was done between 400 mV and –500 mV at a scan rate of 10 $mV.s^{-1}$. The results are presented in figure 4.4. There was a definite decrease in current at the lower potentials after deoxygenation. Varying the flow rate while deoxygenating yielded at least two variables, namely, as the flow rate increased, the rate at which the analyte was transferred to the electrode increased and the rate of deoxygenation decreased due to a reduced time spent in the deoxygenation system. A third possible variable would be the performance of the wall jet, in other words, was the flow rate fast enough to produce a stable jet and so on. It

was difficult to quantify the extent of deoxygenation in this case, so other options were considered.

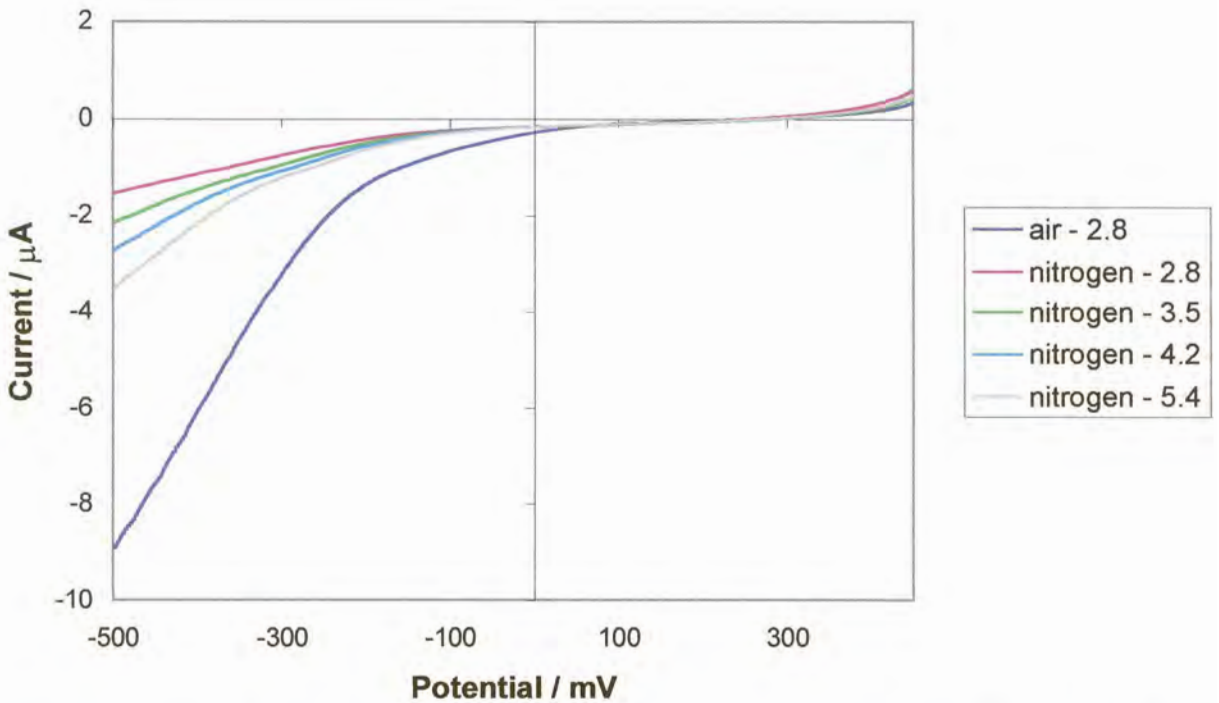

Figure 4.4: The oxygen reduction current in 1 mmol.l^{-1} $NaClO_4$ measured in an air atmosphere and then in a nitrogen atmosphere at varying flow rates (in ml.min^{-1}) at a gold film electrode

A 1 mg.l^{-1} copper solution containing 0.1 mol.l^{-1} potassium nitrate was then studied and the peak currents were measured. DPSV was applied between -300 mV and 200 mV at a scan rate of 20 mV.s^{-1} after a deposition time of 5 s at -300 mV. The other parameters were the default values as used in the previous section. The presence of oxygen would result in a higher background current and hence a smaller copper peak. Deoxygenation took place firstly in the tubing only and then in the tubing after sparging the solution in a flask. In the latter case, sparging with nitrogen first took place for 30 minutes before the analyses began. The results depicted in figure 4.5 clearly show the effect of deoxygenation. Deoxygenation merely through the tubing was not sufficient as the responses increased with additional deoxygenation in the flask. When the solution was

deoxygenated in the tubing only, the slope of the line was slightly greater than that in air. This indicates that the faster copper mass transport, which would increase the peak current, balanced with the reduced deoxygenation at higher flow rates, which would decrease the peak current. However, when deoxygenation took place in both the flask and the tubing, the slope increased to a greater extent. In this case smaller amounts of oxygen needed to be removed, so at the greater flow rates, the extent of mass transport predominated. It was thus evident that at higher flow rates, the tubing system was not sufficient on its own.

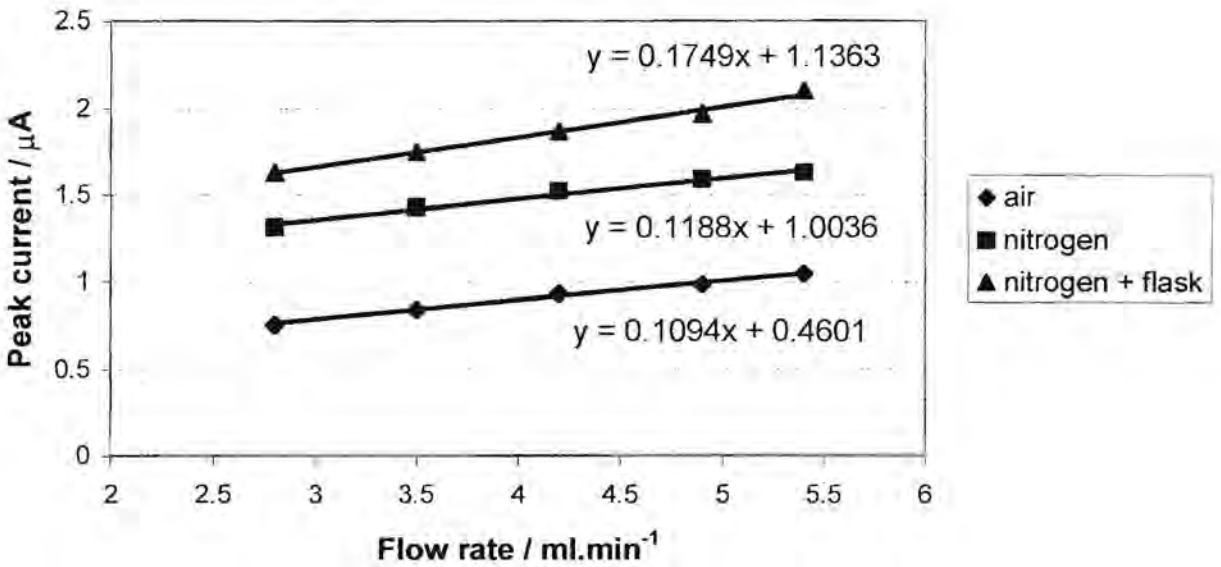

Figure 4.5: Graph of peak current versus flow rate for a 1 $mg.l^{-1}$ copper solution in an air atmosphere and then after deoxygenation in both the tubing system and a flask + the tubing system

Lastly, the GCE was plated with a mercury film and the method by Pedrotti *et al.* [4] was attempted again. The mercury film was plated from a 1.4 $mmol.l^{-1}$ Hg^{2+} (added as $HgCl_2$) solution containing 8 $mmol.l^{-1}$ hydrochloric acid. This was done in a cup cell while stirring the solution. The film was deposited at –1200 mV for 60 s. Data were collected using LSV between 100 mV and –1400 mV at 10 $mV.s^{-1}$. The voltammograms in figure 4.6 clearly show the reduced background current due to deoxygenation, which only took place in the tubing, and the results are presented in table 4.2. These showed

that at lower flow rates, the extent of deoxygenation was greater. A flow rate of 4.2 $ml.min^{-1}$ was used in the WJC (see chapter 5) which led to a deoxygenation efficiency of 94.7%.

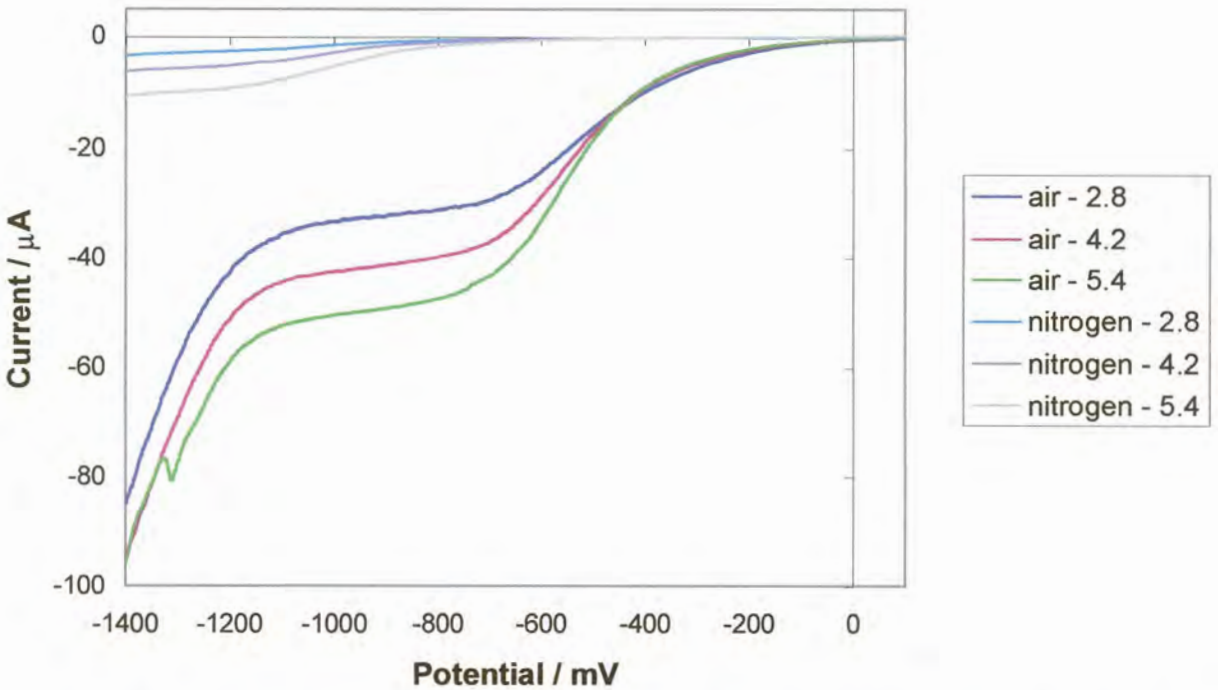

Figure 4.6: The reduction of oxygen in 1 $mmol.l^{-1}$ $NaClO_4$ measured in an air atmosphere and then in a nitrogen atmosphere at varying flow rates (in $ml.min^{-1}$) at a mercury film electrode

Table 4.2: Deoxygenation efficiencies

Atmosphere	Air			Nitrogen		
Flow rate ($ml.min^{-1}$)	2.8	4.2	5.4	2.8	4.2	5.4
Steady state current (μA) at –950 mV	32.8	42	50.1	1.28	2.21	4.24
Current decrease factor	1	1	1	25.6	19.0	11.8
Residual dissolved O_2 ($\mu g.l^{-1}$)	$8.3x10^3$	$8.3x10^3$	$8.3x10^3$	324	437	702
O_2 removal efficiency (%)				96.1	94.7	91.5

The gold samples that were to be analysed for arsenic were dissolved in alkaline cyanide solutions in the presence of oxygen. It was feared that the excess cyanide in the alkaline sample solution would attack the gold film electrode if there was still oxygen (be it only about 440 $\mu g.l^{-1}$ oxygen) present. This would lead to rapid electrode degradation and irreproducible results. In order to improve deoxygenation, the tubing could be lengthened to increase the residence time of the solution in the deoxygenation system, however, this could lead to severe dispersion problems. Purging the solutions in a flask beforehand seemed to be the best option. This was done using a separate nitrogen cylinder and inserting a number of T-pieces between the tubing so that several samples could be purged simultaneously. This ensured that the analysis time was not extended unnecessarily which could also lead to the electrode degrading on standing for prolonged periods in the sample solutions.

4.4) DISCUSSION

The semi-permeable membrane deoxygenation system was a convenient way to deoxygenate samples in a flow system. It was very efficient in oxygen removal and not

at all time consuming. The degree of deoxygenation efficiency depended on the flow rate on the solution, and at higher flow rates this method was supplemented by purging the samples beforehand. This, however, would not always be necessary and would depend on the experimental requirements. It also functioned as a pulse damper. The drawbacks of using this system were that work had to be done within the constraints of the tubing length and the extent of dispersion also increased.

4.5) REFERENCES

1) G.W. Kaye and T.H. Laby, Tables of Physical and Chemical Constants (15th ed.), Longman Group Ltd, 1986

2) W.F. Linke, Solubilities – Inorganic and Metal-Organic Compounds (4th ed.), Vol. 1, American Chemical Society, 1958

3) W.F. Linke, Solubilities – Inorganic and Metal-Organic Compounds (4th ed.), Vol. 2, American Chemical Society, 1958

4) J.J. Pedrotti, L. Angnes and I.G.R. Gutz, Anal. Chim. Acta, 298 (1994) 393

5) Trojanek and K. Holub, Anal. Chim. Acta, 121 (1980) 23

6) G.G. Wallace, Trends in Anal. Chem., 4 (1985) 145

7) M.E. Rollie, G. Patonay and I.M. Warner, Ind. Eng. Chem. Res.,26 (1987) 1

8) Colombo and C.M.G. van den Berg, Anal. Chim. Acta, 377 (1998) 229

9) X.-S. Chai and L.-G. Danielsson, Anal. Chim. Acta, 332 (1996) 31

10) M.E. Rollie, G. Patonay and I.M. Warner, Anal. Chem., 59 (1987) 180

11) R.E. Relm, Anal. Chem., 55 (1983) 1188

12) W. Lund and L.-N. Opheim, Anal. Chim. Acta, 79 (1975) 35

13) T.E. Tang and S.-T. Hwang, AIChE Journal, 22 (1976) 1000

14) R.E. Treybal, Mass-Transfer Operations (3rd ed.), McGraw-Hill Inc., Singapore, 1980

15) Model 303 static mercury drop electrode operating and service manual, EG&G Princeton Applied Research, Princeton, 1978

16) J.F. van Staden and M. Matoetoe, Fresenius J. Anal. Chem., 357 (1997) 624

17) H. Eskilsson, C. Haraldsson and D. Jagner, Anal. Chim. Acta, 175 (1985) 79

CHAPTER 5

FLOW SYSTEMS

The flow system incorporates both the flow cell and the deoxygenation system and how they operate together. It also includes the control of the pump and valve, as well as data collection.

5.1) THEORY

A large number of cell geometries with forced convection have been designed. The general equation, in Cartesian coordinates, to describe the mass transfer of an electroactive species by convective diffusion is [1]:

$$\frac{\partial c}{\partial t} = D\left(\frac{\partial c}{\partial x} + \frac{\partial c}{\partial y} + \frac{\partial c}{\partial z}\right) - \left(V_x\frac{\partial c}{\partial x} + V_y\frac{\partial c}{\partial y} + V_z\frac{\partial c}{\partial z}\right)$$

where D is the diffusion coefficient and V_x, V_y, and V_z are the velocity distribution functions. The first group of terms refers to the diffusive mass transfer and the second group to the convective mass transfer processes. The influence of migration is ignored as it is negligible when the electroactive species contributes negligibly to the ionic strength.

The limiting current can be written as [2]:

$$i_\ell = nFI_{max}$$

where I_{max} is the maximum diffusion mass flow towards the electrode surface, n is the number of electrons involved and F is Faraday's constant. It is therefore necessary to describe the diffusion towards the electrode in order to find the limiting current. Equations for the limiting currents under steady-state conditions have been derived for various cell geometries as shown in figure 5.1 [1]. These are displayed in table 5.1 [1].

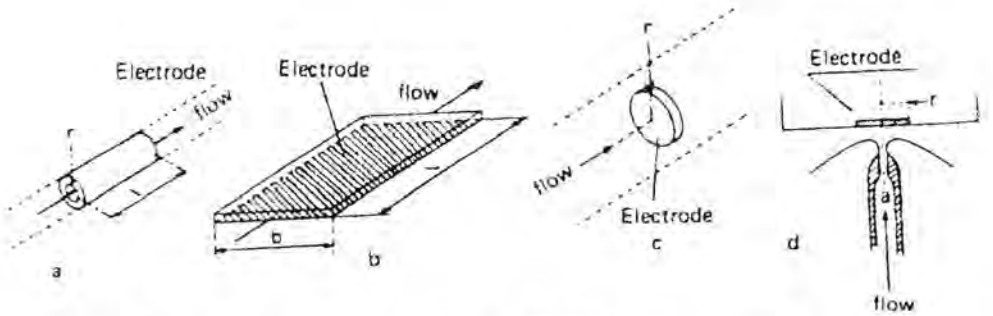

Figure 5.1: Electrode geometries for flow systems with electrochemical detection: a) tubular, b) planar with parallel flow, c) planar with perpendicular flow and d) wall-jet

Table 5.1: Limiting current equations for various cell geometries

Electrode geometry	**Limiting current equation**
Planar (parallel flow)	$i = 0.68\, nFCD^{\frac{2}{3}}\nu^{-\frac{1}{6}}\left(\frac{A}{b}\right)^{\frac{1}{2}}V^{\frac{1}{2}}$
Thin layer	$i = 1.47\, nFC\left(\frac{DA}{b}\right)^{\frac{2}{3}}V^{\frac{1}{3}}$
Planar (perpendicular flow)	$i = 0.903\, nFCD^{\frac{2}{3}}\nu^{-\frac{1}{6}}A^{\frac{3}{4}}u^{\frac{1}{2}}$
Wall-jet	$i = 1.38\, nFCD^{\frac{2}{3}}\nu^{-\frac{5}{12}}a^{-\frac{1}{2}}R^{\frac{3}{4}}V^{\frac{3}{4}}$
Tubular	$i = 1.61\, nFC\left(\frac{DA}{r}\right)^{\frac{2}{3}}V^{\frac{1}{3}}$

where i = limiting current (A)

n = number of electrons

F = Faraday constant ($C.mol^{-1}$)

C = concentration ($mol.l^{-1}$)

D = diffusion coefficient ($m^2.s^{-1}$)

A = electrode area (m^2)

r = radius of tubular electrode (m)

V = average volume flow rate ($m^{-3}.s^{-3}$)

ν = kinematic viscosity ($m^2.s^{-1}$)

b = channel height (m)

R = electrode radius (m)

a = diameter of inlet (m)

u = velocity ($m.s^{-1}$)

The relationships in these hydrodynamic situations apply only to laminar flow, not turbulent flow. The dimensionless Reynolds number, Re, characterises the transition from laminar to turbulent flow. It is the ratio of inertial and viscous forces for a particular electrode geometry and is given by [2]:

$$Re = \frac{Ul}{\nu}$$

where U is the velocity, l is the length and ν is the kinematic viscosity. A critical Reynolds number, Re_{Cr}, indicates the onset of turbulent flow. Thus for laminar flow $Re < Re_{Cr}$ [1]. For example, $Re_{Cr} = 1000$ for a WJC. Laminar flow is also necessary for a low amount of noise [1].

When a fluid flows over the electrode surface, a very thin layer is formed at the surface where the velocity gradient normal to the surface is very large. This layer is called the boundary layer [1,3]. The boundary layer thickness is dependant on the design of the flow cell and is important to optimise the detector's performance. The thickness of the diffusion layer, which defines the concentration gradient at the electrode surface, is a few percent of the boundary layer. Levich approximated the relationship as [1]:

$$\delta_{dl} = \left(\frac{D}{\nu}\right)^{\frac{1}{3}} \delta_{bl}$$

where δ_{dl} is the thickness of diffusion layer, δ_{bl} is the thickness of boundary layer, D is the diffusion coefficient and ν is the kinematic viscosity.

When pumping solutions through the tubing in a flow system, dispersion of the solutions occur. This dispersion depends both on convection and diffusion. It is agreed that convection plays a greater role straight after injection and that diffusion is dominant after a certain time period [4]. A solution moving under laminar flow may be thought of as having a classical parabolic velocity profile which adopts a bullet shape with a hollow tail, as illustrated in figure 5.2(a) and 5.2(b) [5]. This would lead

to rapid dispersion, but radial diffusion reduces this effect. The tip of the slug diffuses outwards to the slower moving solution and is thus retarded. Also, the tail of the slug diffuses inwards into faster moving streams and is accelerated to produce a slug as shown in figure 5.2(c) [5]. There seems to be some conflicting ideas whether the dispersion of a sample zone increases or decreases with decreasing flow rate, but the dominant thought is that dispersion would decrease. For stopped flow systems, the dispersion is practically independent of the time that the flow is ceased [4].

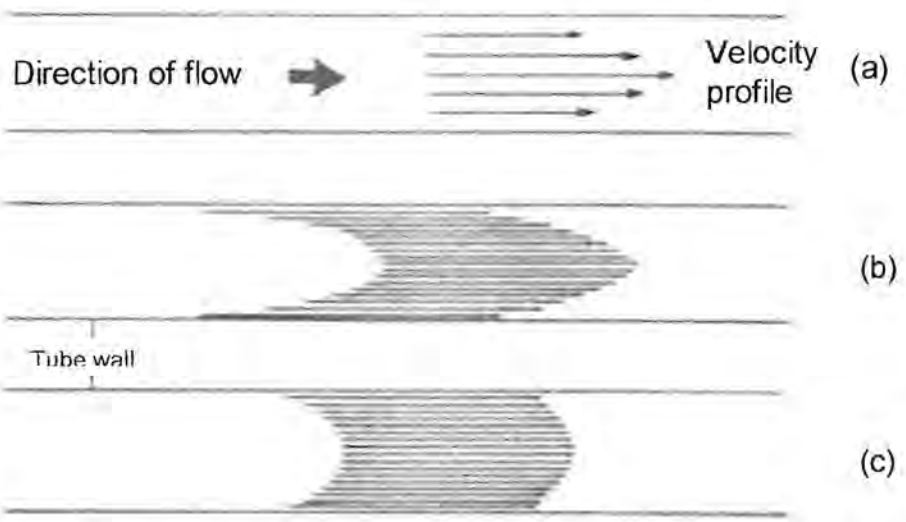

Figure 5.2: Dispersion of a sample slug in a flowing stream: (a) laminar flow velocity profile, (b) dispersion of sample slug caused by convection and (c) sample zone modified by diffusion.

In segmented flow systems, gas bubbles are introduced between slugs to avoid excessive dispersion. The only mixing that occurs is due to the adherent thin film left behind by the solution on the inner tube wall, but this is generally insignificant [6]. The problem with segmented flow is that the bubbles may need to be removed depending on the detector used and their compressibility also creates difficulties.

5.2) DATA COLLECTION

5.2.1) Potential Waveforms

Voltammetry was the electroanalytical technique used in this project. There are a number of variants of the waveforms in this technique, such as linear sweep

voltammetry (LSV), cyclic voltammetry (CV), pulse voltammetry, square wave voltammetry (SWV) and so on. In voltammetry the potential is varied in a defined manner and the current response is monitored [7].

LSV involves varying the potential linearly from an initial to a final value at a constant scan rate, as illustrated in figure 5.3 [7]. However, in practice, this potential waveform is a staircase as a true linear waveform is impossible to generate digitally. The drawbacks of using LSV are the relatively low resolution and the unfavourable effect of the charging current, which interferes especially in the determination of very low concentrations of substances by distorting the stripping curves [8]. CV is a variation of LSV where the scan direction is reversed when the final potential is reached and the scan occurs in the opposite direction. It is frequently used to characterise a redox system and is used to study the kinetics and the mechanism of a system [7].

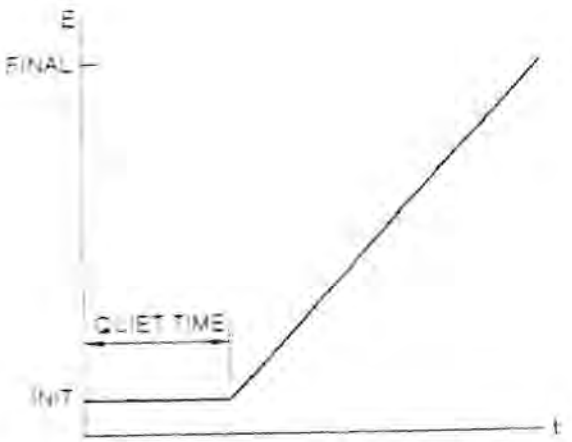

Figure 5.3: Potential waveform for LSV

The BAS workstation offers both normal pulse voltammetry (NPV) and differential pulse voltammetry (DPV). NPV has a waveform that consists of a series of pulses of increasing amplitude, with the potential returning to the initial value between pulses, as demonstrated on figure 5.4 [7]. When the initial potential is significantly positive of the reduction potential, the application of a small pulse does not cause a faradaic reaction, in other words a reaction which involves charge transfer across the electrode-solution interface. When the pulse potential is sufficiently large to cause a faradaic reaction, the magnitude of the current increases. This may be dependent on

both diffusion and the rate of electron transfer. A limiting current is reached when the electron transfer occurs rapidly at sufficiently negative potentials. The current-potential curve produced is thus sigmoidal in shape. In DPV the base potential increases in small steps and the pulse amplitude is constant with respect to the base potential, as shown in figure 5.5 [7]. The current is sampled twice in this technique, just before the pulse and at the end of the pulse. The difference of these currents is then recorded as a function of the base potential. Once again, at potentials significantly positive of the redox potential, there is no faradaic reaction when the pulse is applied. This results in a zero differential current. At potentials around the redox potential, the differential current reaches a maximum and then decreases to zero as the current becomes diffusion controlled. This results in a symmetric peak-shaped curve for the current-potential plot. In this manner DPV is able to discriminate against the charging current [7].

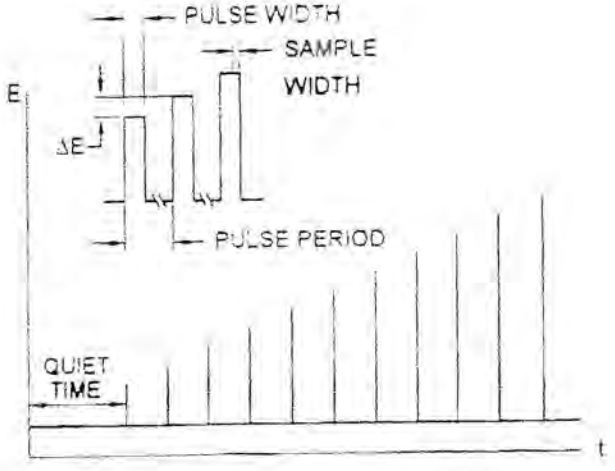

Figure 5.4: Potential waveform for NPV

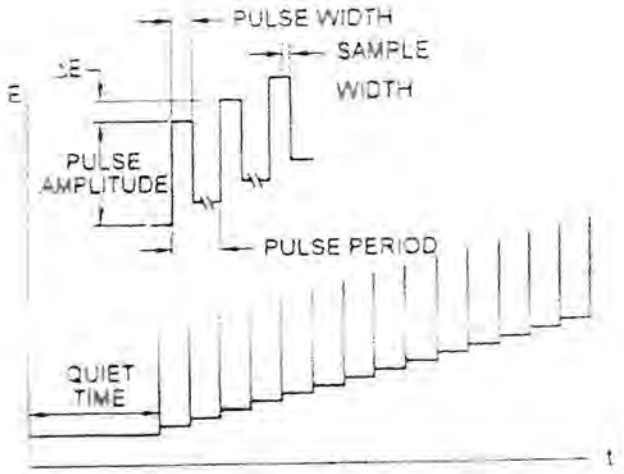

Figure 5.5: Potential waveform for DPV

There are two square waveforms available on the BAS workstation, namely the Osteryoung SWV (OSWV) and the Barker SWV (BSWV). The potential waveform for OSWV is a series of pulses alternating in direction as shown in figure 5.6 [7]. The current is sampled at the end of each pulse or half-cycle. The forward current, reverse current and the difference between these can be viewed. The differential current response is also a symmetric peak with discrimination against background charging currents. The technique has a greater sensitivity and faster speed than DPV [7]. BSWV is similar to OSWV, except the samples are collected and averaged over a number of cycles (as illustrated in figure 5.7), thus making it slower than OSWV [11].

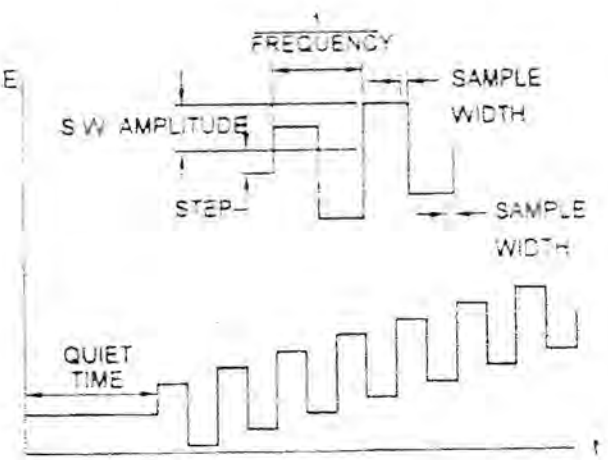

Figure 5.6: Potential waveform for OSWV

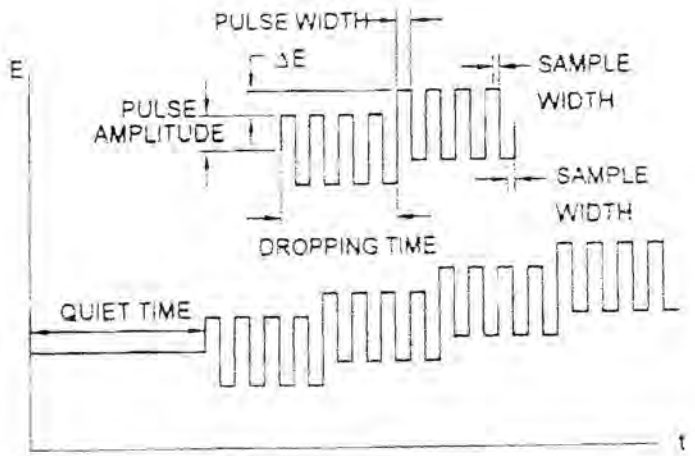

Figure 5.7: Potential waveform for BSWV

The waveforms discussed above (except for CV) can all be applied to stripping voltammetry. This is when the analyte is first accumulated onto or into the electrode as discussed in chapter 1. The analyte is accumulated at a given potential and then the waveform is applied during the stripping step. This enhances sensitivity and hence allows for very low detection limits [7].

In this work, DPV was mainly used due to its sensitivity and ease of use. OSWV was also briefly looked at. It proved to be more sensitive, but more complex to produce a well-defined peak.

5.2.2) iR Compensation

iR compensation was used in all experiments. This was necessary as it could have affected the true value of the operating potential of the cell. This is demonstrated by considering an electrochemical cell as represented in figure 5.8.

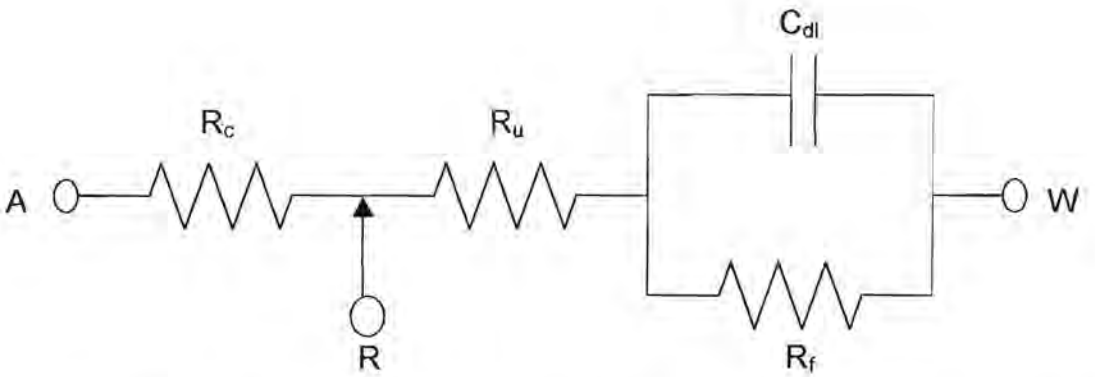

Figure 5.8: Equivalent circuit of an electrochemical cell. A = auxillary electrode, R = reference electrode, W = working electrode, R_c = compensated resistance, R_u = uncompensated resistance, R_f = faradaic impedance and C_{dl} = double layer capacitance [9].

The potential applied (E_{app}) across the reference and working electrodes is related to the true operating potential (E_w) across the working electrode and the solution interface by:

$$E_w = E_{app} - iR_u - \varphi_{ref}$$

where ϕ_{ref} is the reference electrode interfacial potential

or E_w (vs ref) = $E_{app} - iR_u$

If iR_u is large, it would substantially lower E_w from E_{app}, thus making the data obtained meaningless. There are generally three ways to minimise iR drop, namely: using a highly concentrated electrolyte, placing the reference electrode as close to the working electrode as possible and having an adjustable positive feedback (f) in the potential control loop such that E_w is related to the other circuit components as follows:

$$E_w \text{ (vs ref)} = E_{app} - iR_u + ifR_u$$

The positive feedback is gradually increased until the current response starts to oscillate. At this point $iR_u = ifR_u$ and the solution resistance is assumed as totally compensated for. However, this does not necessarily lead to 100% compensation as the circuit may become unstable before this is achieved. Another drawback of using this method is that the electrode surface structure may be destroyed or altered when the system starts to oscillate [9].

The BAS potentiostat uses a different approach to solve this problem [9]. Firstly a test potential is required where only capacitive response would occur at the working electrode and solution interface, i.e. no faradaic processes should occur. The instrument applies a potential step of 50 mV to the working electrode at this potential and then monitors the current response as follows:

$$i = i_o \exp\left(-\frac{t}{R_u C_{dl}}\right)$$

Two data points are sampled at 54 and 72 μs respectively and are assumed to be shorter than the R_uC_{dl} time constant. The exponential current decay can be approximated with a linear plot under this circumstance. It is extrapolated to t_o and the uncompensated resistance can hence be calculated using:

$$R_u = \frac{\Delta E}{i_o}$$

where ΔE is the potential step applied. The instrument then stepwise inserts a fraction of R_u in the positive feedback loop and tests the circuits stability. The stability test is performed by once more applying a potential step of 50 mV to the working electrode at the given test potential. The current response is then sampled at a frequency of 20 kHz for 50 ms. The maximum and minimum current is found and used to calculate the % overshoot as follows:

$$\%\,\text{overshoot} = \frac{i_{min}}{i_{max}} \times 100$$

This procedure is repeated until iR compensation is achieved in accordance with preset levels of both overshoot and compensation extent [9]. (The default values of 10% and 100% respectively, were used in this work.) The instrument now slightly decreases the iR compensation and inserts a capacitor between the auxilliary and reference leads to stabilise the cell system.

5.3) FLOW SYSTEM FOR THE SMDE

5.3.1) Set-up

The set-up for the experimental work in this study is depicted in figure 5.9.

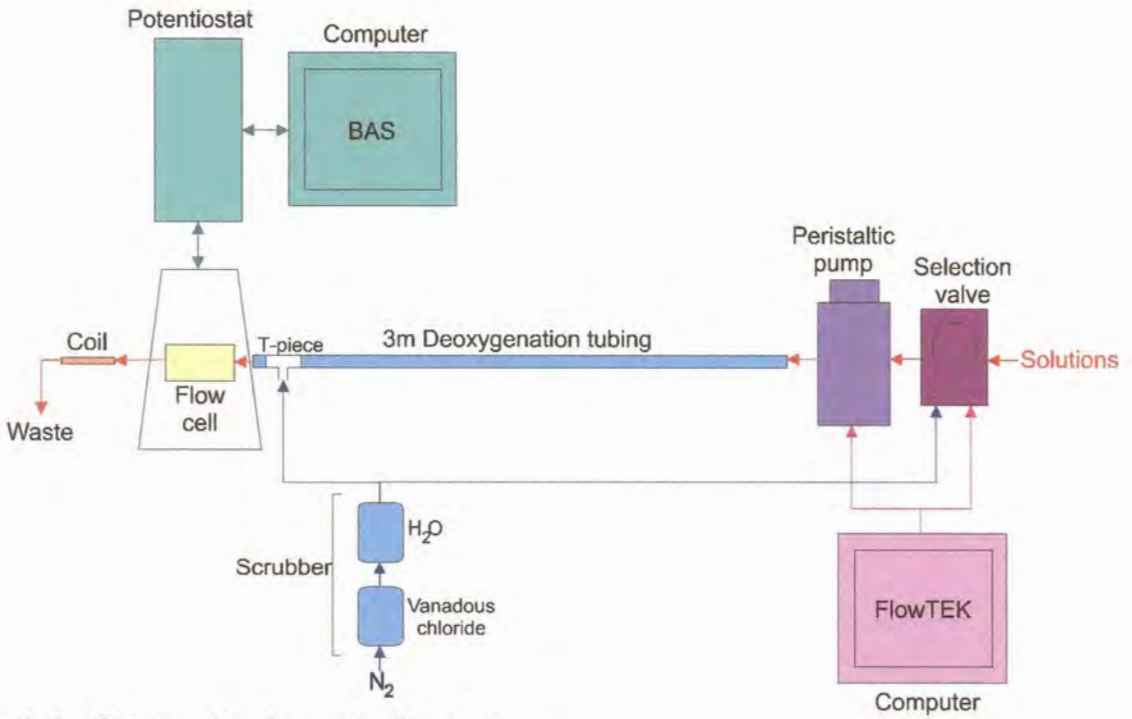

Figure 5.9: Schematic diagram of set-up

A Gilson Minipuls 3 peristaltic pump (Gilson, Villiers, France) and a VICI model EMHMA selection valve with the multiple-position actuator control module (Valco Instruments Co. Inc., USA) was used. The software used to control the pump and the valve was FlowTEK (Mintek, SA). The hardware needed for control was an interface card and a distribution board. The interface card used was an Eagle Electric PC-30B card (Eagle Electric, SA), which is a high accuracy analogue and digital input/output (I/O) board. It can be plugged into any of the fully bussed slots in an IBM or compatible computer. The distribution board (Mintek, SA) enabled the convenient connection of devices to the interface card. It also has optional features such as an amplifier and a filter [10]. FlowTEK could also be used to collect data, but it does not have the infrastructure for particular electrochemical experiments. The electrochemical experiments were done on a BAS 100B/W Electrochemical Workstation (Bioanalytical Sysytems, West Lafayette, USA) which was comprised of a potentiostat and a computer running the BAS software with a MS Windows interface. An EG&G Princeton Applied Research Model 303 SMDE (EG&G, New Jersey, USA) was used in the flow cell that was designed and was controlled by the BAS system.

Flow systems can be broadly classified as segmented and non-segmented systems. In a segmented flow system, solution plugs are separated by air or some inert gas [1,11]. This was initially done to prevent cross-contamination of samples, but it was later found that the extent of contamination was insignificant [11]. The system used here was a pseudo-segmented system as a nitrogen bubble was introduced after the matrix exchange solution, which directly proceeded the sample solution, in order to dislodge the mercury drop. Once the cell was rinsed with water, another nitrogen bubble was introduced so that the beginning of the sample plug could be seen. There was no bubble between the sample solution and the matrix exchange electrolyte or else the mercury drop would have been washed out of the cell after the plating step and before stripping could occur.

The presence of the nitrogen bubbles increased the compressibility of the contents in the tubing. When the pump was stopped, the solutions continued to flow for a short period thereafter. This was not adequate because a greater amount of control was needed over the positioning of the various solutions with respect to the flow cell. A coil of tubing with a small internal diameter was placed at the outlet of the flow cell to provide a back-pressure and improve control. On hindsight, the nitrogen slugs could also have been made smaller to reduce the extent of compressibility.

The use of a peristaltic pump in flow systems leads to periodic oscillations in the flow rate. This is particularly a problem for electrochemical detectors. For example, in voltammetric detectors the transfer of electroactive substance to the electrode surface must be done under reproducible, invariable transport conditions when measuring the current [12]. When a HMDE is used under pulsating flow conditions, it leads to irreproducible results. The pulsating flow causes the drop to vibrate and alters the geometry of the drop, as well as gives rise to different mass transport conditions [12].

Various methods have been used for pulse damping. An air chamber was introduced after the pump which acted as a pressure filter as shown in figure 5.10 [1,12]. A pump was placed at the outlet of the detector so that the solution is in effect drawn through [1]. Gas-driven systems have also been used to curb the problem of pulsation [1].

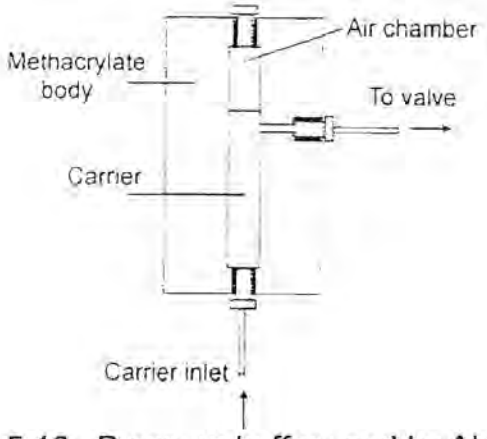

Figure 5.10: Pressure buffer used by Alpizar *et al.* [12]

In this study, a pulse damper consisting of a T-piece with a sealed piece of tubing on the vertical leg, as illustrated in figure 5.11, was introduced just after the pump. As the solution passed though the T-piece, the air in the sealed tube compressed and expanded thus reducing the pulsation. However, some problems were experienced with this pulse damper. The sealed tubing contained air which contaminated the nitrogen bubbles and solutions that passed though the damper, but this was a minor problem as the damper could be placed before the deoxygenation system. As the solution initially passed though the pulse damper, the air in the sealed tubing was compressed and some solution was pushed into this tube. This solution also vibrated as the solution flowed through the T-piece and a certain amount of mixing occurred. The most serious problem transpired when the solution was halted to do the stripping phase in a stationary solution in order to reduce the noise. The solution and some air would slowly creep back into the main tubing, causing contamination and air bubbles that would dislodge the mercury drop at inappropriate times.

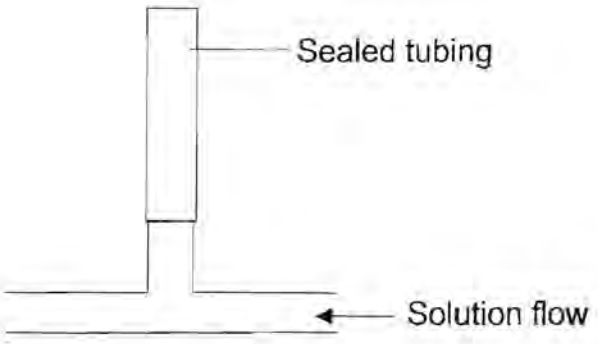

Figure 5.11: Pulse damper

It was found that, together with the solution having to pass through the 3m long deoxygenation tubing and with the coil placed at the outlet of the flow cell to provide a back pressure, the pulsation was reduced such that there was very little or no pulsation by the time the solution was pumped into the flow cell. The pulse damper could thus be omitted from the set-up.

Alternative flow system set-ups were considered with respect to the positioning of the components and the pro's and cons of these. Three examples are shown below.

1) The sample would be the only solution to flow through the deoxygenation tubing in the first alternative set-up, as shown in figure 5.12. The rinse solution and stripping electrolyte could be continuously purged by nitrogen in flasks as these solutions remained the same throughout the analyses. This would result in less dispersion as the solutions would have a shorter distance to travel while they were in contact with each other and there would be greater control over the positioning of the various solutions with respect to the flow cell. However, the solutions would be contaminated by oxygen when passing through the selection valve and the pump. A pulse damper would also be needed as the pump would be adjacent to the flow cell.

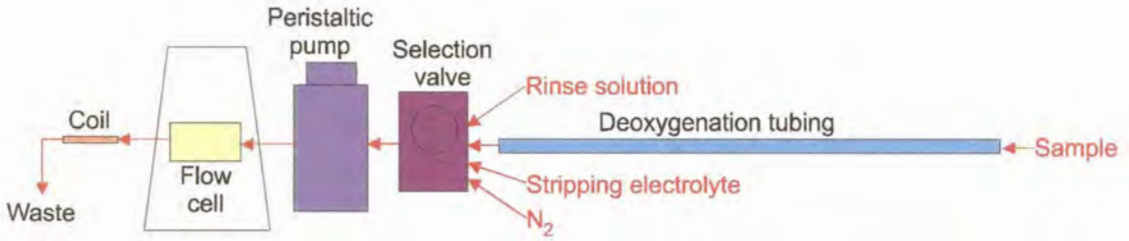

Figure 5.12: Alternative set-up 1

2) Placing the pump after the flow cell would result in the solutions being sucked through the system as depicted in figure 5.13. This would reduce pulsation and dispersion. The flow system would have to be thoroughly sealed to prevent air from being sucked into the system. This would not be the best option when using a HMDE as it could lead to fouling of the capillaries and affect the mercury flow.

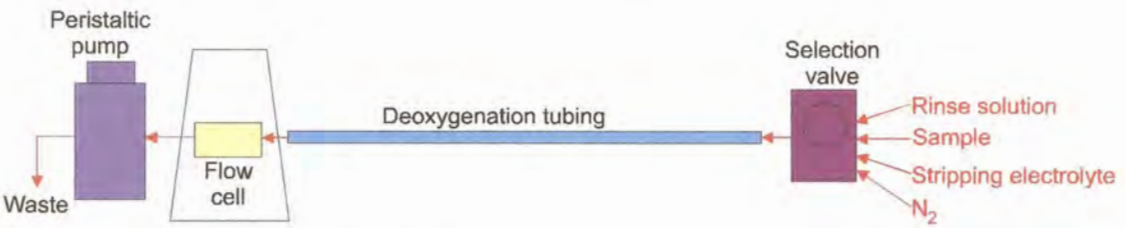

Figure 5.13: Alternative set-up 2

3) Introducing an injection valve was also considered, where the stripping electrolyte would be the carrier stream. A selection valve would also be needed to introduce the nitrogen to dislodge the mercury drop and a large sample loop would be required when long plating times were used. This would complicate the system and with the control that is afforded by using a program such as FlowTEK, the use of an injection valve does not provide considerable advantages.

5.3.2) Testing the Flow System

The flow system was tested to ensure that it would produce adequate and reproducible results.

5.3.2.1) Flow Rate

The flow rate was calibrated against the readings on the peristaltic pump by measuring the volume of solution that emerges from the system in a minute. The results are shown in table 5.2 and figure 5.14. It can be seen that the pump settings were directly proportional to the flow rates.

Table 5.2: Calibrating the Gilson peristaltic pump

Pump setting	**Flow rate / ml.min^{-1}**
10	1.5
20	2.9
30	4.4
40	5.8

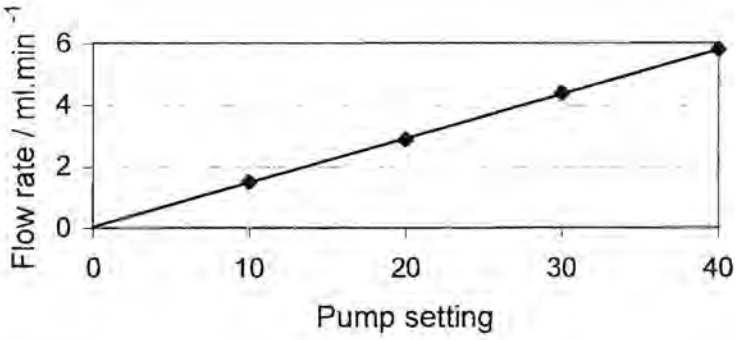

Figure 5.14: Graph flow rate of versus pump settings

5.3.2.2) Reproducibility

The reproducibility of the set-up was tested by measuring the peak height produced by a sample of 1 mg.l^{-1} copper (as $CuSO_4$) in 10% (v/v) nitric acid. A 5 s deposition time was used with a deposition potential of –300 mV. The mode applied was DPSV, with the scan rate set to 20 mV.s^{-1} and the final potential to 200 mV. The pulse amplitude was 50 mV, the pulse width was 50 ms, the sample width was 20 ms and the pulse period was 200 ms. During accumulation the flow rate was 1.5 ml.min^{-1} and stripping took place in a quiescent solution. The FlowTEK procedure (refer to section 5.3.3), shown in figure 5.15 below, allowed three sets of solutions to be stacked in the deoxygenation tubing at a time. The positions of the selection valve were as follows: position 1 was a water rinse, position 2 was the sample solution and position 3 was the nitrogen. The RSD obtained for 10 results was 3.5% which is

sufficient. The results also appeared to be random, in that the values obtained did not follow a trend.

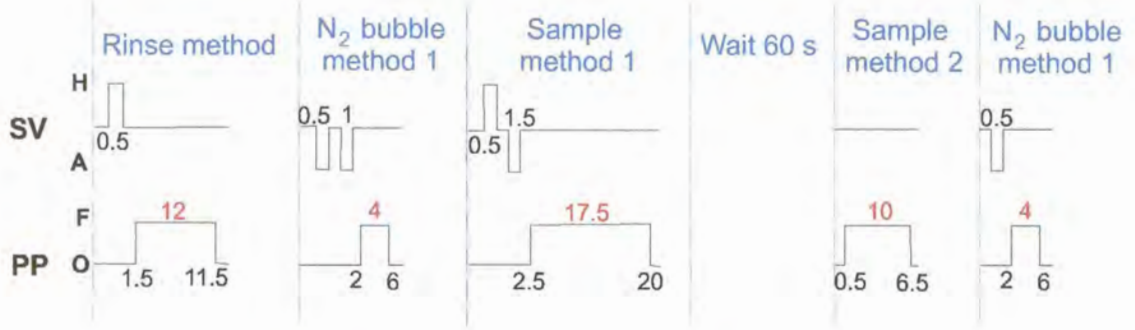

Figure 5.15: FlowTEK procedure for testing reproducibility

5.3.2.3) Flow Cell Characteristics

The characteristics of the flow cell were tested to see which cell type the designed cell best fits.

5.3.2.3a) *Effect of flow rate*

Firstly a copper solution was looked at where flow was maintained only during a 5 s plating step and then stripping was performed in a quiescent solution using the DPSV mode. The initial and final potentials were –200 mV and 120 mV respectively, and the deposition potential was –300 mV. The other conditions were as above. Deoxygenation took place through the membrane set-up.

The results given in table 5.3, were manipulated to ascertain which cell type the design fitted best. These results are also depicted in figure 5.16. The relationship between the peak current and the flow rate varies according to the cell type as was shown in table 5.1. It can be seen that for a planar electrode with perpendicular flow, the current in proportional to $(\text{velocity})^{1/2}$ and for a thin layer detector (TLD), the current is proportional to $(\text{volume flow rate})^{1/3}$.

Volume flow rate is given in units of $ml.min^{-1}$.

$$\frac{ml}{min} = \frac{cm^3}{s} \times \frac{60\ s}{1\ min}$$

$$\frac{cm^3}{s} \times \frac{1}{cm\ (diameter)} \times \frac{1}{cm\ (length)} = \frac{cm}{s}$$

Velocity is given in units of $cm.s^{-1}$. Since the diameter and the length of path are constant, it follows that the peak current is proportional to (volume flow rate)$^{1/2}$ for a planar electrode with perpendicular flow.

Table 5.3: The effect of flow rate on peak current

Pump speed setting	**Flow rate / ml.min^{-1}**	**(Flow rate)$^{1/2}$**	**(Flow rate)$^{1/3}$**	**Peak Current / μA**
5	0.8	0.894	0.928	0.4141
10	1.5	1.22	1.14	0.4193
20	2.9	1.70	1.43	0.4289

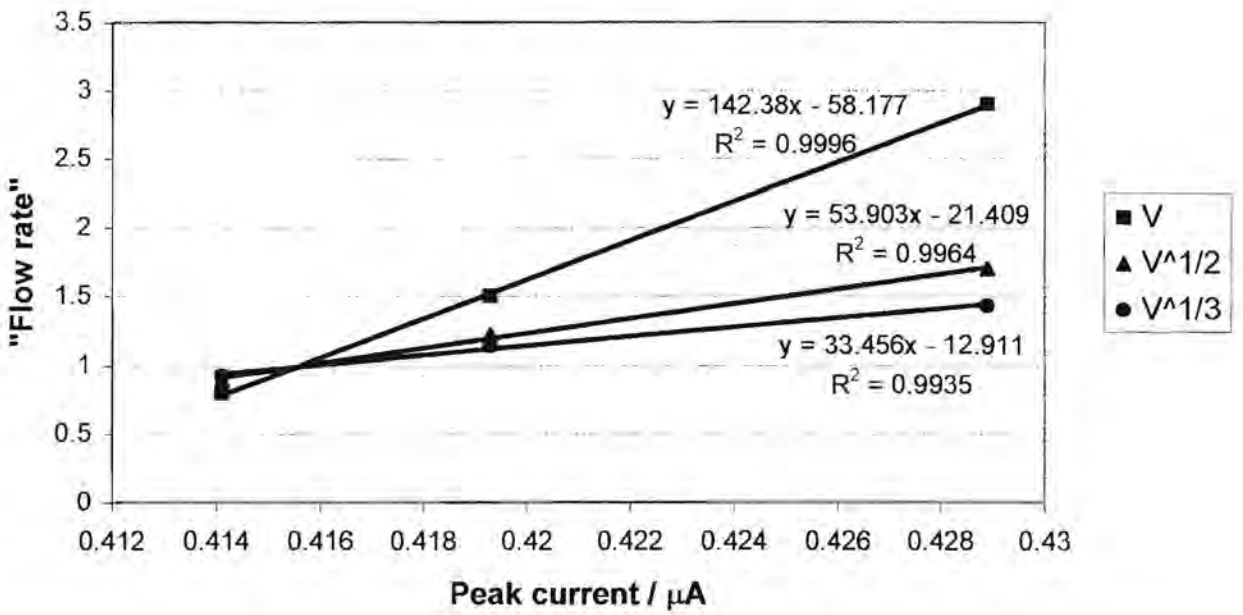

Figure 5.16: Graph of peak current versus flow rate, (flow rate)$^{1/2}$ and (flow rate)$^{1/3}$ for a 1 mg.l^{-1} copper solution deoxygenated in the tubing set-up

From figure 5.16 it could be deduced that a direct proportionality fitted the data best with a correlation coefficient of 0.9996. This did not correspond to either the TLD or a planar electrode with perpendicular flow.

It was, however, decided that passing the solution through the deoxygenation tubing would add another variable to the investigation, namely the extent of deoxygenation. In this case the slower the flow rate, the greater the residence time, hence the more the deoxygenation. Thus the solution was sparged in a flask before passing through a pulse damper (as described previously) and the flow cell. Data were collected in a manner similar to the previous experiments. The results obtained are shown in figure 5.17.

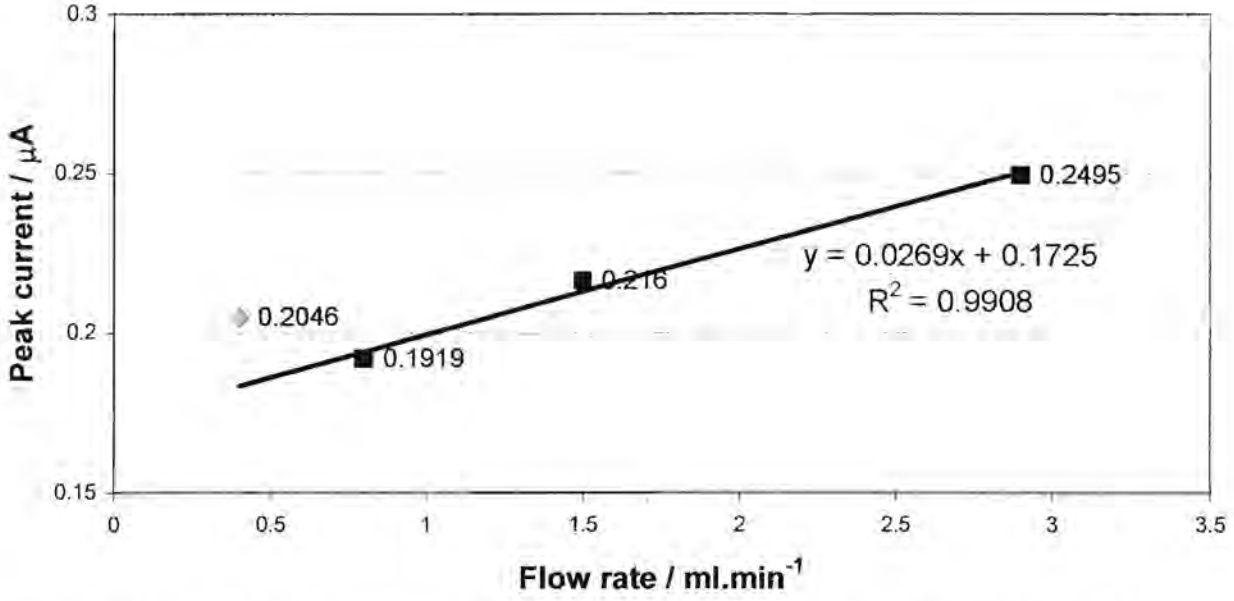

Figure 5.17: Graph peak current of versus flow rate for a 1 mg.l^{-1} copper solution deoxygenated in a flask

As the flow rate decreased, the peak current decreased in a linear manner, but then rapidly increased for the slowest flow rate of 0.4 ml.min^{-1}. The steady decrease in current was expected due to a decrease in mass transfer at slower flow rates, but the first datum point did not follow the trend. This could possibly show that there was laminar flow only at very low flow rates, and as the flow rates increased some turbulence set in. As the flow rate increased from there, the flow was still turbulent, but the increase in mass transport led to a slow increase in the peak current.

It was then decided not to use a stripping technique, but to simply use DPV in flowing solutions. A cadmium solution was used with no deoxygenation taking place, but still passing the solution through a pulse damper. The effect of oxygen present when

examining the cadmium reduction peak would be less than that for a copper peak as the first reduction peak for oxygen in close to that for copper. Data was collected from –300 to –800 mV at a rate of 10 $mV.s^{-1}$. The results obtained are presented in figure 5.18.

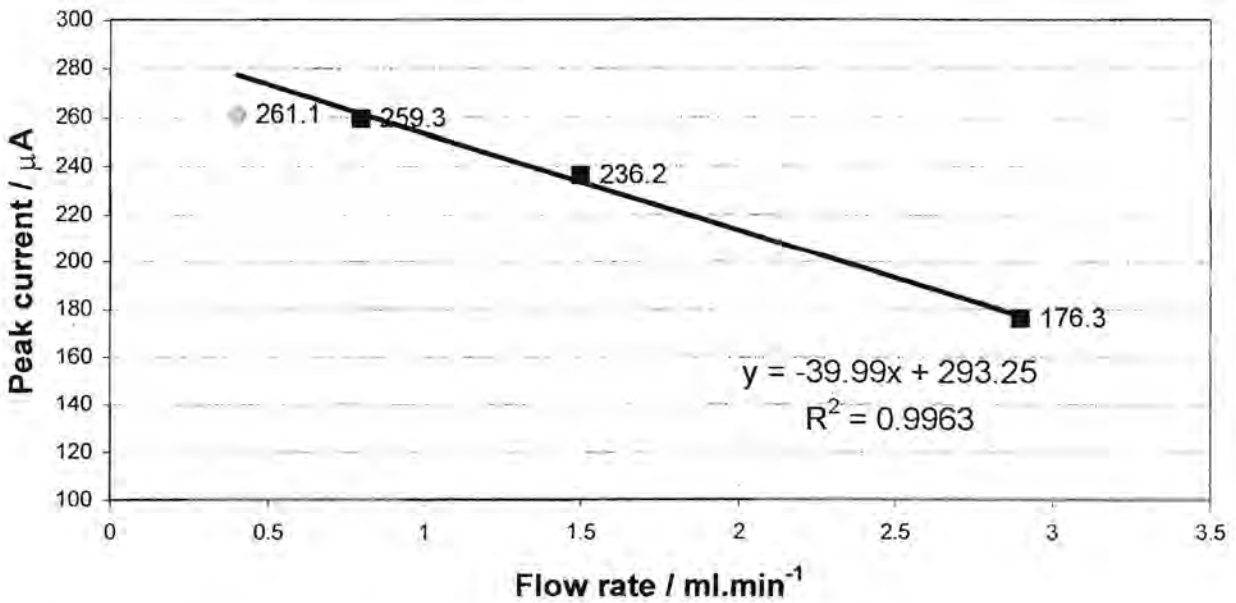

Figure 5.18 : Graph of peak current versus flow rate for a 1 $mg.l^{-1}$ cadmium solution with no deoxygenation

This produced totally unexpected results because the current was decreasing with increasing flow rate. It was later established that the faster the flow rate, the smaller the mercury drop was that formed in the flowing solution. At a flow rate of 5.8 $ml.min^{-1}$ a mercury drop did not form at all. The drop even became more unstable at low flow rates with time. This behaviour indicated that the capillary needed to be resiliconised. It appeared that the relatively large pressure led to the fast degradation of the capillary and would have to be examined periodically.

It was concluded that the hydrodynamics of the flow cell design did not fit into the category of either a thin layer detector or a planar electrode with perpendicular flow. Thus with the geometry of the flow cell being less well defined, the prediction of the absolute values of the current was not possible. A flow rate of 1.5 $ml.min^{-1}$ was used in the work from here on, unless stated otherwise. This would give a fair sensitivity due to the rate of mass transport and the mercury drop was stable at this flow rate.

5.3.2.3b) *Effect of scan rate*

The peak current was measured for varying scan rates in a cadmium solution. DPV was used and data was collected from –400 mV to –800 mV in a solution flowing at a rate of 1.5 ml.min^{-1}. The results are represented in figure 5.19.

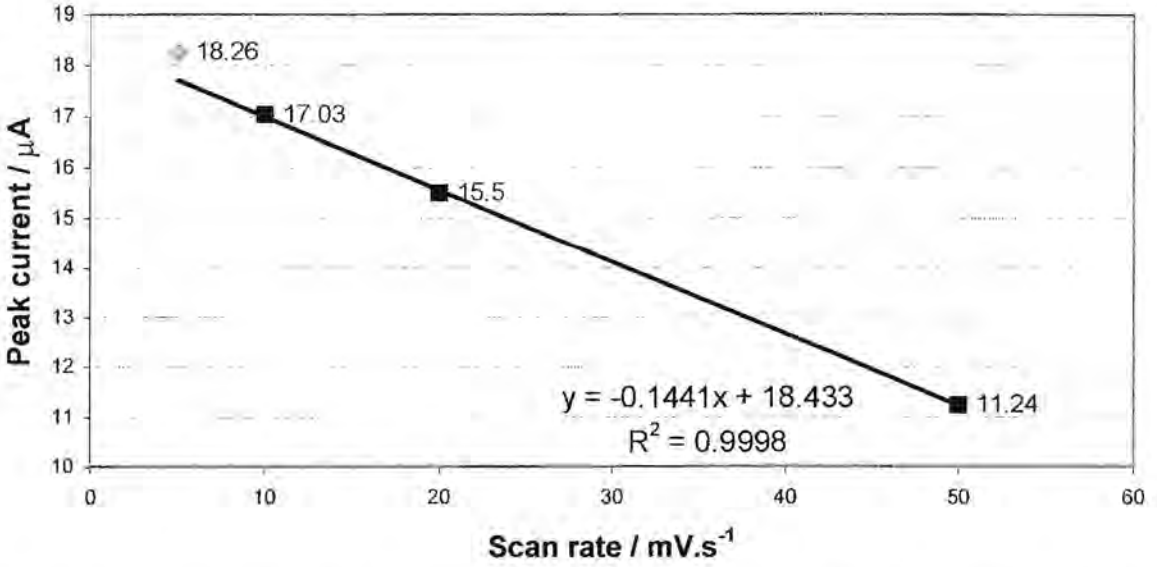

Figure 5.19: Graph of peak current versus scan rate for a 1 mg.l^{-1} cadmium solution

Data could not be collected at faster scan rates, as there were not enough data points for the software to calculate the peak height. Except for the scan rate of 5 mV.s^{-1}, the peak current decreased linearly with an increase in scan rate. A scan rate of 20 mV.s^{-1} was used in future work, unless stated otherwise, as this gave good sensitivity and also took a reasonable time for the run.

5.3.2.3c) *Effect of concentration*

The peak current was measured for various cadmium concentrations. Once again DPV was applied between –400 mV and –800 mV and data was collected in deoxygenated solutions flowing at a rate of 1.5 ml.min^{-1}. The voltammograms are shown in figure 5.20 and the results are depicted in figure 5.21.

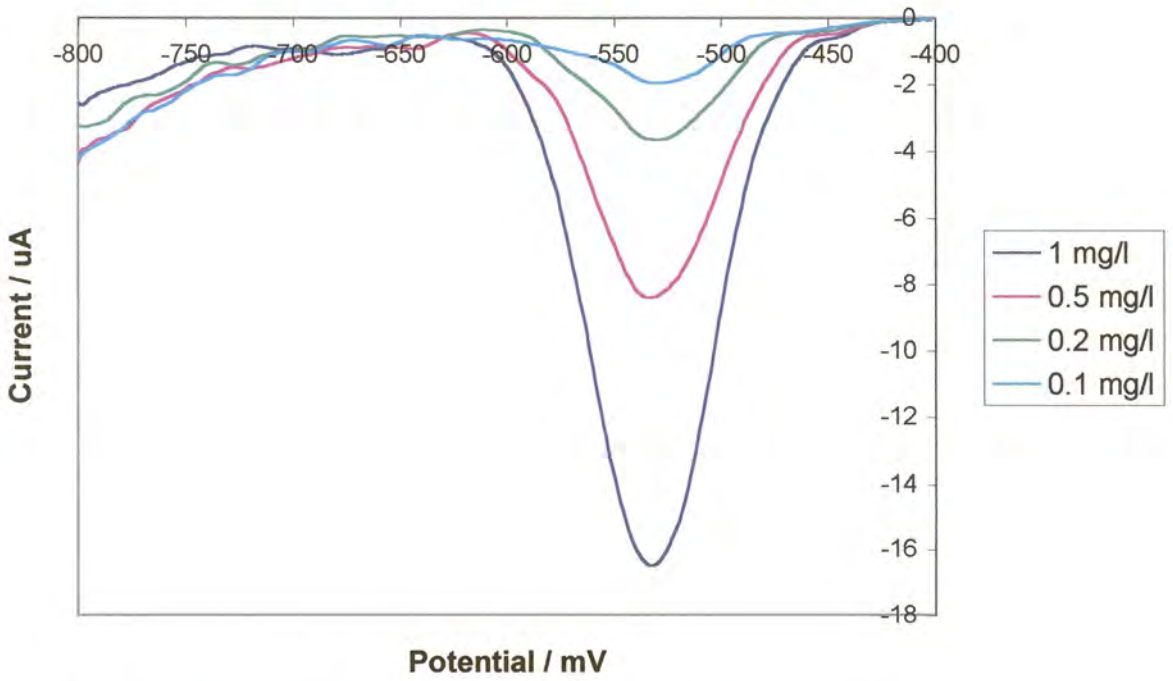

Figure 5.20: Voltammograms for varying cadmium concentrations

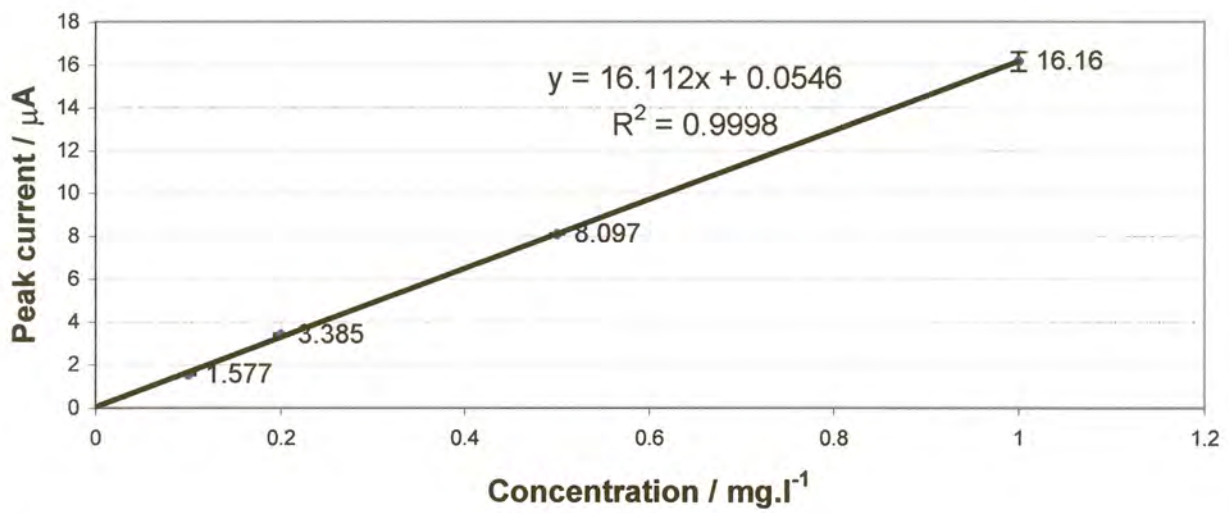

Figure 5.21: Graph of peak current versus concentration for a cadmium solution

This clearly shows a linear relationship between the concentration of the electroactive species and the peak current produced. This an important result when considering whether the design of the flow cell is feasible or not. Work was continued using the flow cell for determining cobalt in a zinc electrolyte.

5.3.3) FlowTEK Procedures

The FlowTEK software was used to control the peristaltic pump and the selection valve. This was done by first establishing the logic that controls the devices and then defining and configuring the devices (see the appendix). The actions that they could perform were then defined. In the case of the selection valve, the actions were "home", which took the valve to the first position, and "advance", which moved the valve one position forward. The valve could not move backwards, it had to first move to the home position and then move forward from there. The peristaltic pump's actions were "forward", "reverse" and "off", but the reverse option was not necessary for this work.

A method was built by specifying the time at which these actions must occur. A procedure could be built by arranging various methods in sequence and by replicating methods or procedures.

A typical FlowTEK procedure in this project for the determination of cobalt in a zinc electrolyte using matrix exchange is shown in figure 5.22. The solutions were arranged at the selection valve as follows: position1 (home) was water for rinsing, position 2 was nitrogen from the scrubber, position 3 was the sample solution and position 4 was the stripping electrolyte. The analytical procedure had several parts for one determination. Firstly the flow cell was rinsed with water and then a nitrogen bubble was passed through to indicate the start of the sample solution. The sample solution, that had been previously diluted with the supporting electrolyte, was pumped into the flow cell followed by the onset of accumulation of the analyte from a flowing solution. The stripping electrolyte was then introduced into the cell followed by a quiet time where the pump was halted and the solution was allowed to come to rest. Stripping of the analyte by a potential scan while measuring the current occurred in a quiescent solution before another nitrogen bubble was passed through to remove the used mercury drop from the cell.

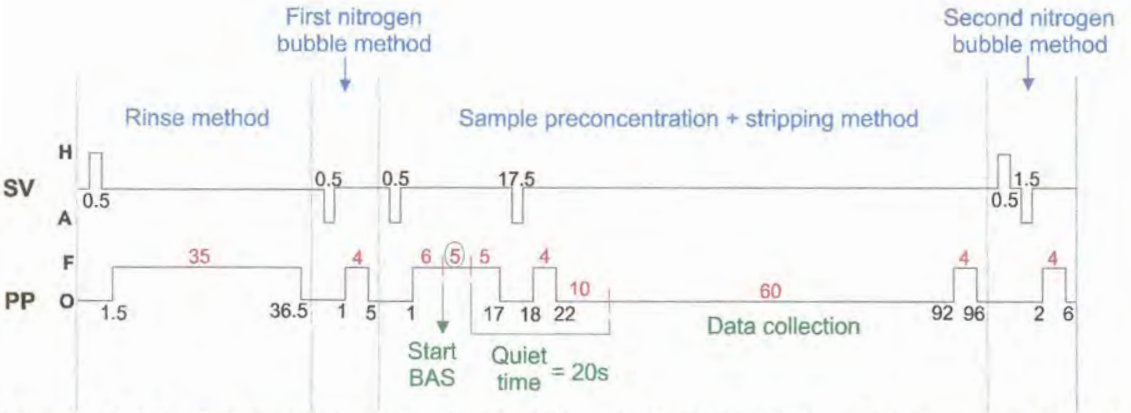

Figure 5.22: Schematic diagram of a FlowTEK procedure. SV = selection valve, H = home, A = advance, PP = peristaltic pump, O = off and F = forward.

The solutions were not pumped directly into the flow cell, but were first pumped through the 3 m long deoxygenation tubing. Due to the time delay, the samples for one determination were always stacked in the length of tubing. Thus as a particular solution was pumped into the tubing, the corresponding solution that was stacked in the tubing, was being pumped into the flow cell. As the accumulation time varied, the rinse time was adjusted to ensure that the tubing was always totally full.

The FlowTEK procedure in figure 5.22 needs some interpretation. The rinse method involved moving the selection valve to position 1 and then pumping water for 35 s. The first nitrogen bubble method shifted the valve to position 2 and pumped nitrogen for 4 s. The sample preconcentration and stripping step comprised moving the valve to position 3 to pump the sample solution through for 16 s. After pumping this solution for 6 s the cell was filled with the sample solution and the BAS system was started manually to apply the deposition potential for the accumulation step. The accumulation time was 5 s in this method and another 5 s of solution was allowed to flow through the cell to ensure that the cell only contained sample solution while accumulating analyte at the electrode. The valve was then shifted to position 4 and stripping solution was pumped for 4 s to ensure the cell contained stripping solution. An effective quiet time of 10 s then followed. The quiet time on the BAS system was given as 20 s, but this included the time to wash out the sample solution and fill the cell with stripping electrolyte. After data were collected in a quiescent solution, the stripping electrolyte was pumped for another 4 s. In effect a stripping electrolyte plug of 8 s was stacked in the tubing and was pumped halfway through the cell, thus

ensuring the whole cell was filled by stripping solution. Lastly, the selection valve was switched "back" to position 2 and another 4 s nitrogen bubble was pumped through.

5.4) FLOW SYSTEM FOR THE WJC

5.4.1) Set-up

The set-up used is represented in figure 5.23.

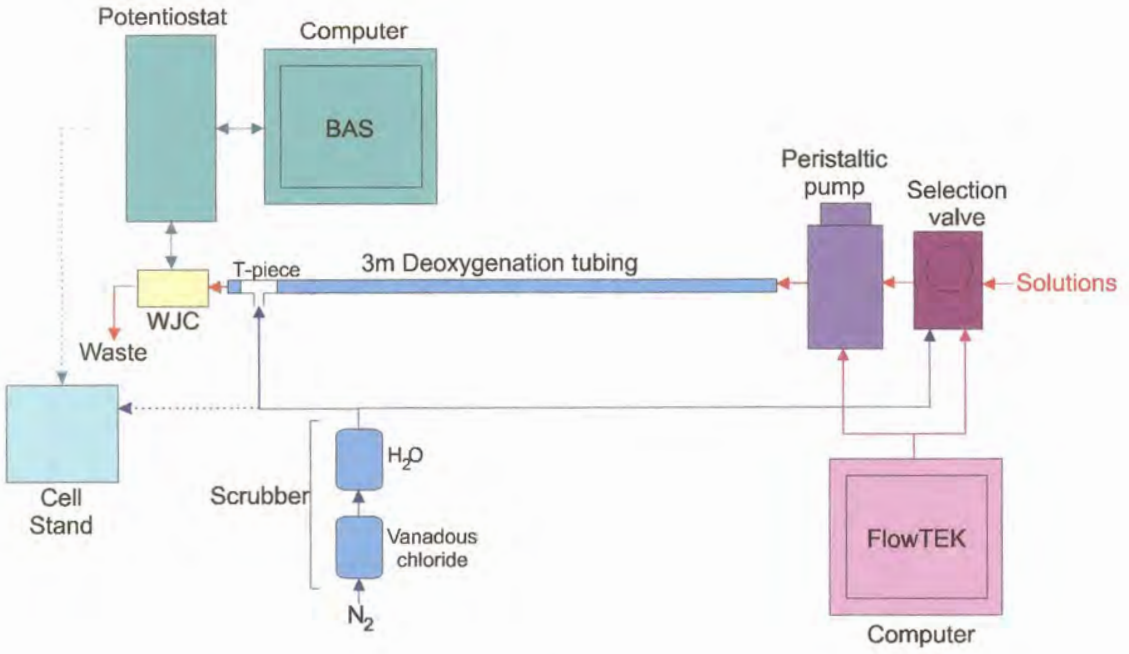

Figure 5.23: Schematic diagram of set-up

The same components as in the previous set-up were used, except the WJC was used and an Alitea C4 peristaltic pump (Alitea, Sweden) replaced the Gilson Minipuls 3 peristaltic pump during the course of this work as the latter pump stopped functioning. The BAS C2 Cell Stand (Bioanalytical Systems, West Lafayette, USA) was also used for the preparation of the gold film electrodes.

A non-segmented flow system was used throughout this work. It was necessary to first remove any air bubbles in the WJC when it was initially filled with solution. Once these bubbles were expelled, the solution would readily flow out of the two outlets at

a similar rate. The deoxygenation tubing once again acted as the pulse damper to prevent pulsating flow at the cell.

5.4.2) Testing the Flow System

5.4.2.1) Flow Rate

The Gilson peristalitc pump was recalibrated as different tubing was used and later the flow rate of the Alitea pump also required calibrating according to the pump settings. This was done as before. The results are displayed in table 5.4 and figure 5.24 for the Gilson pump and in table 5.5 for the Alitea pump.

Table 5.4: Calibrating the Gilson peristaltic pump

Pump setting	**Flow rate / ml.min^{-1}**
10	1.4
15	2.2
20	2.8
25	3.5
30	4.2
35	4.9
40	5.4

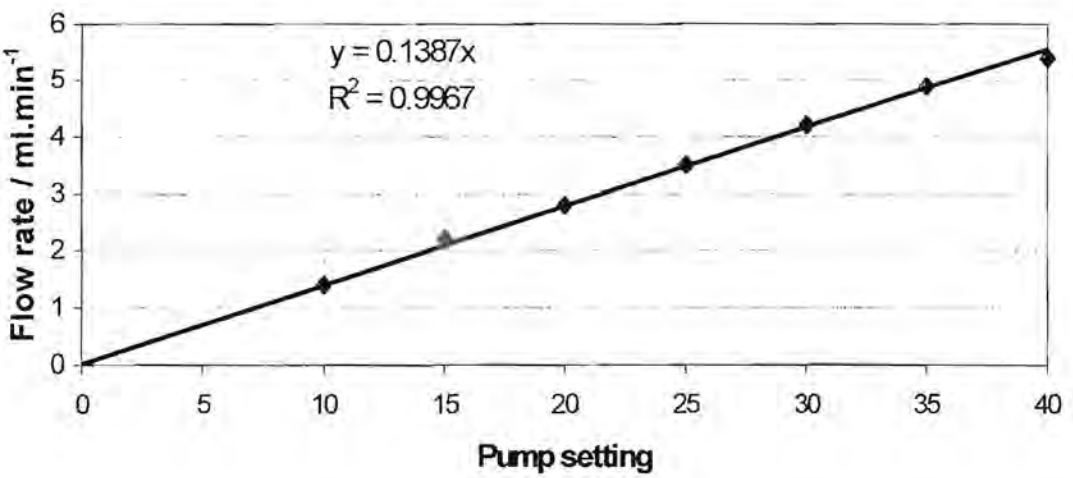

Figure 5.24: Graph of flow rate versus pump settings for the Gilson peristaltic pump

Table 5.5: Calibrating the Alitea peristaltic pump

Pump setting	**Flow rate / ml.min^{-1}**
30	1.3
90	3.9
95	4.0
98	4.2

5.4.2.2) Flow Cell Characteristics

The flow cell was investigated to determine which flow rates and inlet-electrode separations were required for the cell to exhibit wall-jet behaviour.

5.4.2.2a) *Effect of flow rate*

The WJC, with an inlet- electrode distance of 3 mm, was tested at flow rates of 2.8, 3.5 and 4.2 ml.min^{-1}. First a gold film electrode was prepared and a 10 mg.l^{-1} arsenic (III) solution in 20% (v/v) hydrochloric acid was analysed. DPSV was used from –300 mV to 400 mV at a scan rate of 50 mV.s^{-1} and a deposition time of 10 s. The other parameters were the default values of 50 mV pulse amplitude, 50 ms pulse width, 200 ms pulse period and 20 ms sample width. The results are presented in table 5.6. The peak current at the lowest pump speed was less than at the higher pump speeds. This could be due to the jet breaking up slightly before it reaches the electrode. The RSD was best for the highest pump speed. It was decided to work at a flow rate of 4.2 ml.min^{-1} which corresponded to the pump setting of 30 on the Gilson pump and 98 on the Alitea pump.

Table 5.6: Effect of flow rate on the peak current

Flow rate / ml.min^{-1}	**Peak current / μA**	**RSD / %**
2.8	11.4	7.3
3.5	12.5	1.7
4.2	12.2	0.4

5.4.2.2b) *Effect of inlet-electrode separation*

The limiting current is directly proportional to (flow rate)$^{3/4}$ for a WJE [13,14,15]. Therefore a plot of log(peak current) versus log(flow rate) should produce a straight

line of slope 0.75. Thus a 10 $mg.l^{-1}$ arsenic (III) solution in 20% (v/v) hydrochloric acid was analysed using LSV from –200 mV to 400 mV at a scan rate of 50 $mV.s^{-1}$. This was done for various inlet-electrode distances and the results are displayed in figure 5.25 and table 5.7. The greatest slope of 0.62 was for a 3.1 mm separation between the inlet and the electrode surface. Laevers *et al.* [1] suggested that for true wall-jet behaviour the relationship between the nozzle diameter (a) and the nozzle-electrode separation (H) should be:

$$12 \leq H/a \leq 15$$

With the nozzle diameter of 0.3 mm, it can be calculated that H/a = 3/0.3 =10. This does not fit in with the above relationship. A separation closer to 4 mm would give the required result. This would probably imply that the wall-jet was not fully developed when the solution struck the electrode surface. The results for the 2.9 mm separation produced a curve for which the best fit was not a linear relationship, but a polynomial. An inlet-electrode separation of 3 mm was used throughout this work. This distance was chosen as it produced a slope close to the maximum slope as shown in table 5.7.

Table 5.7: Table depicting the slopes and correlation coefficients for various inlet-electrode separations

Inlet-electrode separation / mm	**Slope**	**Correlation coefficient (R^2)**
2.9	0.47	0.9110
3.0	0.59	0.9986
3.1	0.62	0.9918
3.2	0.51	0.9990

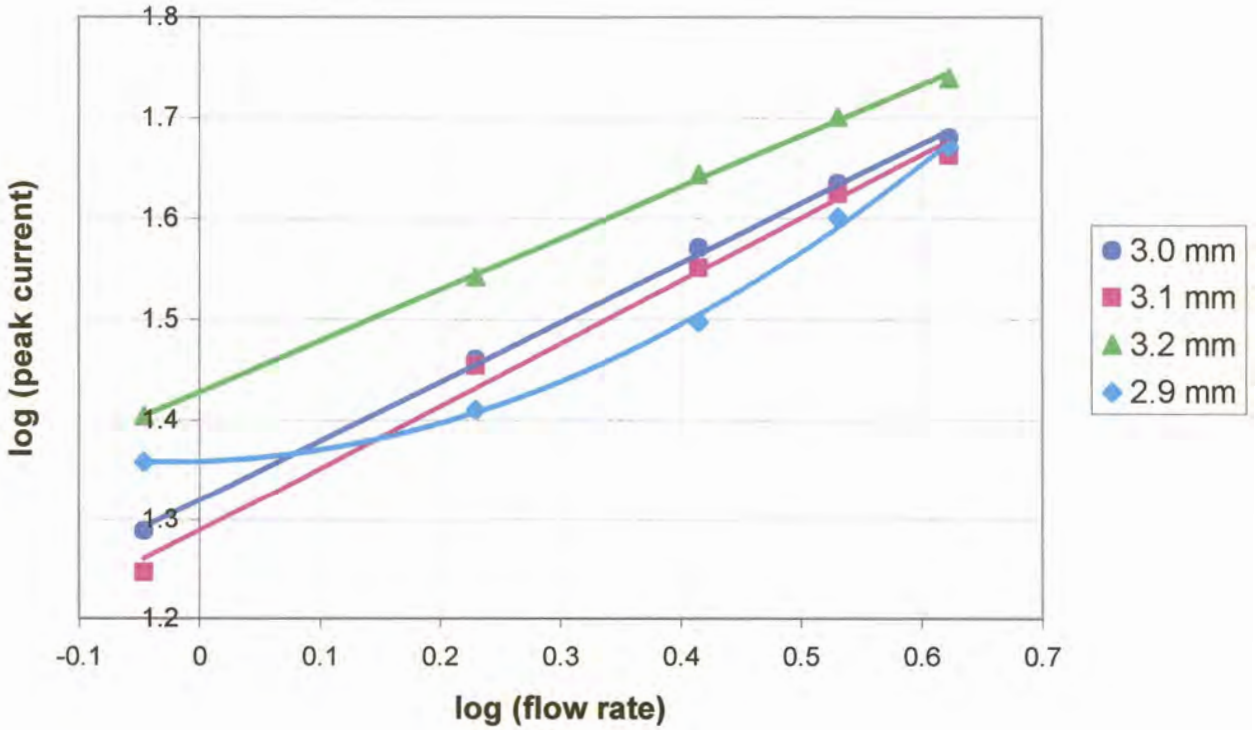

Figure 5.25: Graph of log(peak current) versus log(flow rate) at different inlet-electrode separations

5.4.3) FlowTEK Procedures

The FlowTEK software was once again used to control the peristaltic pump and selection valve as before. It took the solution 42 s to flow from the valve through the tubing to the flow cell when a flow rate of 4.2 $ml.min^{-1}$ was used. This interval affected the way in which the FlowTEK methods were created. Examples of procedures employed when matrix exchanged was used are described below.

Figure 5.26 depicts a FlowTEK method for a 20 s deposition time. Actually it is one method and then the start of the next, which is merely the same method that is repeated. This was done in order to clearly demonstrate what was happening at the various flow system components and how they influenced each other. The sample solution was at the first position and the stripping electrolyte was at the second position of the selection valve. The sample solution was pumped through the system for 42 s so that it was at the entrance of the flow cell when the valve was switched and the stripping solution was pumped through. As the stripping electrolyte was

pumped into the flow system, the sample solution flowed into the flow cell and the analyte could be collected at the electrode surface. A 12 s interval was given before accumulation began to ensure that unmixed sample solution was striking the electrode. Stripping solution flowed through the flow cell once sample solution was being pumped into the system again. Stripping occurred in a flowing solution because in a WJC, only the solution impinging on the electrode is seen by the electrode, not the bulk solution. This made it unnecessary to rinse the cell between analyses. The quiet time was introduced not in the true sense of the concept, as a quiet time is not necessary when using a WJE. Instead it allowed time for the excess sample solution to be pumped out of the deoxygenation tubing, the valve to be switched and to introduce the stripping electrolyte into the cell.

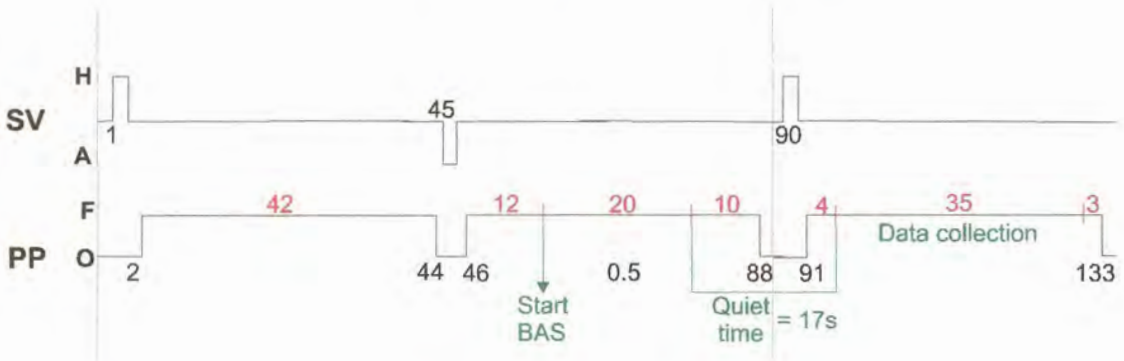

Figure 5.26: Schematic diagram of a FlowTEK method for a 20 s deposition time

Using longer deposition times such as 60 s changed the scenario as there was only space for 42 s worth of solution in the tubing at a time. Such a FlowTEK procedure is illustrated in figure 5.27. The first 42 s was spent loading the tubing with sample solution and thereafter it could be pumped through the flow cell for as long as required. When it came to stripping the analyte from the electrode in the stripping solution, the sample solution first had to be flushed from the tubing and the stripping electrolyte loaded. The quiet time encompassed this activity. Stripping could then take place in the flowing electrolyte. The data collection times for these two methods varied since it depended on the scan rate and the potential range used during this step.

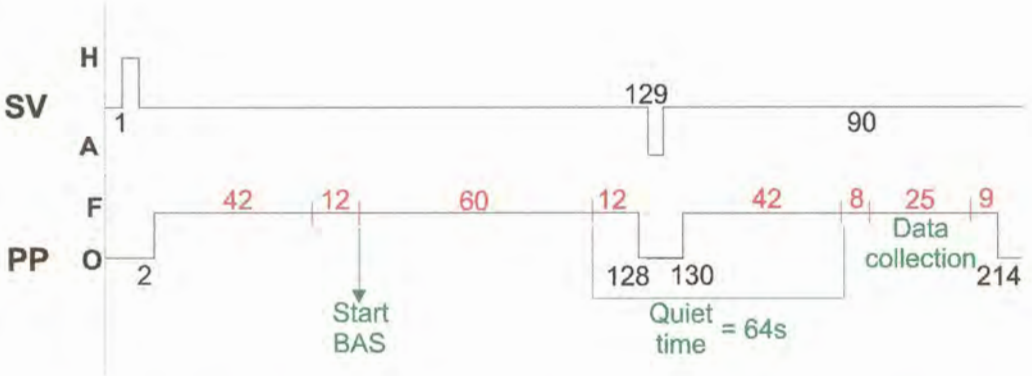

Figure 5.27: Schematic diagram of a FlowTEK method for a 60 s deposition time

If there were more than one sample to be analysed, it would probably be best to have the stripping electrolyte at position 1 and the sample solutions at the other positions. Thus after accumulation of the analyte, the valve would move to the home position and the stripping electrolyte will be pumped through the system.

5.5) REFERENCES

1) A.J. Bard, Electroanalytical Chemistry, Volume 16, Marcel Dekker Inc., 1989
2) H.B. Hanekamp and H.J. van Nieuwkerk, Anal. Chim. Acta, 121 (1980) 13
3) R.J. Rucki, Talanta, 27 (1980) 147
4) E.B. van Akker, M. Bos and W.E. van der Linden, Anal. Chim. Acta, 378 (1999) 111
5) E.A. Jones, Reference unknown
6) Z.-I. Zhi, Trends in Anal. Chem., 17 (1998) 411
7) BAS 100B/W Instrument Manual ,Version 2, 1995
8) F. Vydra, K. Stulik and E. Julakova, Electrochemical Stripping Analysis, Ellis Horwood Ltd, 1976
9) K.-N. Kuo, Communication received from BAS Inc: True iR compensation with the BAS-100 Electrochemical Analyzer
10) FlowTEK manual
11) W. Lund and L.-N. Opheim, Anal. Chim. Acta, 79 (1975) 35
12) J. Alpizar, A. Cladera, V. Cerda, E. Lastres, L. Garcia and M. Catasus, Anal. Chim. Acta, 340 (1997) 149

13) P. Laevers, A. Hubin, H. Terryn and J. Vereecken, J. Appl. Electrochem., 25 (1995) 1017

14) H. Gunasingham, K.P. Ang, C.C. Ngo, P.C. Thiak and B. Fleet, J. Electroanal. Chem., 186 (1985) 51

15) H. Gunasingham and B. Fleet, Anal. Chem., 55 (1983) 1409

CHAPTER 6

DETERMINATION OF COBALT IN A ZINC ELECTROLYTE

6.1) SUPPORTING ELECTROLYTE

The voltammetric determination of cobalt is difficult in the presence of zinc as their reduction potentials are similar in most supporting electrolytes and the resolving power of differential pulse voltammetry is not sufficient to separate these peaks [3]. Electroanalytical methods have been developed for the determination of copper, cadmium, lead, antimony and iron in zinc plant electrolytes [4-7], but these methods are not suitable for the determination of cobalt in the same sample.

There are also problems associated with the determination of cobalt at a mercury electrode, namely, irreversibility of the process and poor sensitivity of stripping methods due to the low solubility of cobalt in mercury [8-10]. Therefore complexing agents have been employed to form a cobalt complex, which is then adsorptively accumulated at the electrode-solution interface prior to the electrode process [8].

The reagent most frequently used for quantitative cobalt determination is dimethylglyoxime (DMG). This forms a complex with the ratio Co:DMG = 1:2 [11]. Due to its surface activity, the $[Co(DMG)_2]$ complex adsorbs onto the electrode surface and thus provides a means of preconcentration. This results in an increased sensitivity [8,12,13]. The mechanism of the electrode process is under dispute for this complex as some believe that the reduction process is accompanied by a catalytic evolution of hydrogen, while the majority maintain that the increase in current is due to the adsorptive accumulation of the complexes on the electrode surface [14].

One of the newest theories on the mechanism for the electrochemical stripping reduction of the cobalt (and nickel) DMG complexes is that by Ma *et al.* [13]. They postulated that it is a 10-electron process in alkaline media. First the complex is adsorbed onto the electrode surface:

$$[Co(II)\text{-}DMG_2]_{(sample)} \rightarrow [Co(II)\text{-}DMG_2]_{(ads)}$$

The central ion is then reduced:

$$[Co(II)\text{-}DMG_2]_{(ads)} + 2e^- \rightarrow Co(0) + 2DMG^-_{(ads)}$$

This is followed by a four-electron reduction of each glyoximate ligand in which hydroxylamine groups are formed:

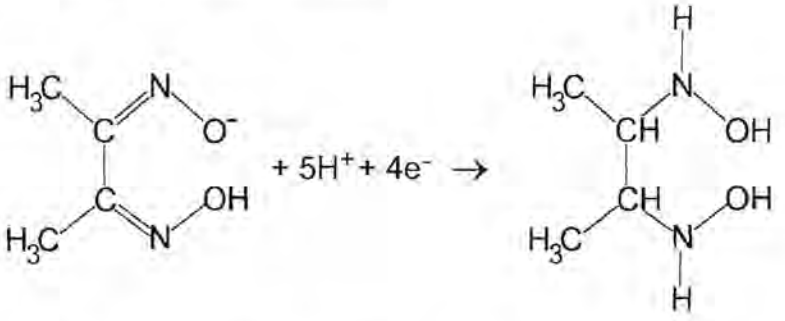

In addition to cobalt(II) the only other metals commonly cited to form stable DMG complexes are nickel(II), copper(II), palladium(II), platinum(II) and bismuth(III) [15]. This should be borne in mind as interferences may not only arise from the overlap of reduction peaks, but could also stem from competitive reactions with the complexing agent and from the competitive adsorption of ions or their complexes on the electrode surface [14]. Thus high concentrations of the other elements which also form complexes with DMG will compete to react with the DMG and possibly for space on the electrode to adsorb too.

Cobalt was determined as a DMG complex in ammonium chloride, but it was susceptible to interference from zinc [3]. The $[Co(DMG)_2]$ complex was also analysed in water with a NH_3-NH_4Cl and $CaCl_2$ supporting electrolyte [16]; or in biological materials [9], pressurised water reactor coolant [12] and iron samples [17] with just a NH_3-NH_4Cl supporting electrolyte [9]; or in water with NH_3 and HEPES (4-(2-hydroxyethyl)-1-piperazineethanesulphonic acid) [18] and so on. A novel way of using the DMG complex to determine cobalt was by making mixed binder carbon paste electrodes (MBCPE) [19]. DMG was mixed with graphite, liquid paraffin and glycerol and made into an electrode. The cobalt in solution then complexes with the DMG on the electrode and once again a sensitive determination for cobalt was produced.

The main disadvantage of using DMG on it own for cobalt determinations is the close proximity of the nickel and especially the zinc reduction peaks to that of cobalt, hence there is strong interference if these elements are present in solution [9,20]. Other complexes, in combination with DMG or on their own, have been studied to overcome problems experienced when using DMG.

The addition of citrate to the DMG and NH_4Cl was used to determine cobalt in an excess of nickel [20]. This approach was extended to overcome the zinc interference, where 2 ppb cobalt could be determined in 150-fold excess of zinc [3,20]. Triethanolamine (TEA) was added to DMG and NH_4Cl to determine cobalt in sea water [21]. It was also used to determine 0.05 $\mu g.l^{-1}$ cobalt in up to 25 000-fold excess of zinc [3]. Tetrabutylammonium fluoride (TBAF) was added to DMG, citrate and NH_4Cl to shift the zinc reduction potential to even more negative values [20]. Diacetyl dioxime (DAD) was also used in this manner [22], but the zinc and cobalt reduction peaks were not sufficiently separated to determine cobalt in a zinc plant electrolyte [22]. The addition of iminodiacetic acid (IDA) was studied as this formed a non-electroactive zinc complex [20]. 1-(benzylsulphonyl)-2-(N-morpholino) ethane (BME) was used to analyse for cobalt in a zinc electrolyte as the Zn^{2+} reduction is retarded without inhibiting the reduction of the cobalt-DMG complex. It was possible to determine 60 $\mu g.l^{-1}$ cobalt in the presence of 40000-fold excess zinc [22]. 2-quinolinethiol has been used to separate the cobalt, nickel and zinc peaks [20]. The use of the cobalt(III)-2-nitroso-1-naphthol complex in an ammoniacal supporting electrolyte made it possible to determine 2 $\mu g.l^{-1}$ cobalt in 1000-fold excess of zinc without interference [3]. Ethylenediamine with KNO_3 was used to determine cobalt in zinc [23]. Both dioxime [14] and nioxime [24], as well as thiocyanate [25], were used in conjunction with nitrite to determine cobalt. The reduction current was catalytically enhanced by the presence of nitrite, thus it was more sensitive. Other complexes studied include oxine [26], nioxime (cyclohexane-1,2-dione dioxime) [14,24,26], α-furil dioxime [14], diphenylglyoxime [24], dithiocarbamate [10], a synthesised azo compound 1-(2-pyridylazo)-2,7-dihydroxynaphthalene (2,7-PADN) [27] and so on.

Although many of the complexes improved the separation between the cobalt and the nickel and zinc peaks, they were insufficient to determine cobalt in a zinc plant

electrolyte as the high zinc concentration interfered. Bobrowski [14] developed a method using α-benzil dioxime as complexing agent which also forms a complex with the ratio of 1:2 for Co: α-benzil dioxime. Cobalt could be determined in solutions containing zinc concentrations 10^7 times higher than that of cobalt. The resolution and sensitiivity were futher enhanced by the addition of the nitrite ion, which, as described before, gives rise to a catalytic effect. Mrzljak *et al.* [10] used this method in determining cobalt in a zinc plant electrolyte and obtained excellent sensitivities, but a very small working range of 0.25 $\mu g.l^{-1}$ to 30 $\mu g.l^{-1}$ cobalt under the specific working conditions were obtained.

Mrzljak *et al.* [10] also looked at a matrix exchange method to determine cobalt in a zinc plant electrolyte using DMG and citrate. This method produced a lower sensitivity, but a wider working range up to 600 $\mu g.l^{-1}$ under the particular conditions. It was decided to look at this electrolyte as it best fitted the requirements for the limits that cobalt could be tolerated in the zinc electrolyte. Below a certain value, the exact concentration is not that critical as it would be below the required lower limit and hence within specifications. The starting point was to look at the same supporting electrolytes as proposed by Mrzljak *et al.* and then to optimise them for the flow system that has been developed.

6.2) ADSORPTIVE STRIPPING VOLTAMMETRY

Adsorptive stripping voltammetry involves the formation of an appropriate metal chelate, followed by its controlled interfacial accumulation onto the working electrode. The adsorbed metal chelate is then reduced by the application of a negative-going potential scan. The reduction can proceed though the metal or the ligand [1]. This technique is very sensitive and only short accumulation times are required.

The amount of adsorbate accumulated at the electrode surface depends on both the size and orientation of the molecule or ions. There are a number of forces leading to adsorption such as: the solubility of the reactant in the solvent (the lower the solubility, the stronger the adsorption), the electrostatic forces between an ionic adsorbate and the charged electrode, the field-dipole interaction between the

electrode double layer and the functional groups of the organic reactant, and the chemisorption of certain groups on metallic electrode surfaces [2].

Adsorption isotherms have been derived to indicate the equilibrium relationships between the concentration of the adsorbate on the surface of the electrode and that in the bulk solution [2]. The most popular of these isotherms in the Langmuir isotherm, given by [1,2]:

$$\Gamma = \Gamma_m \left(\frac{BC}{1+BC} \right)$$

where Γ is the surface concentration of adsorbate, Γ_m is the surface concentration corresponding to monolayer coverage, C is the bulk concentration of adsorbate and B is the adsorption coefficient. From this it can be deduced that when $BC<<1$, $\Gamma = \Gamma_m BC$. In other words, when the adsorbate concentration is very low, its surface concentration is directly proportional to its bulk concentration [2]. The Langmuir isotherm does not always apply. For example, it does not take the interactions between the adsorbate on the electrode surface into account. Therefore there are more complex isotherms.

For AdSV, the peak current is directly proportional to the surface concentration of the adsorbate at low concentrations. At high concentrations, a deviation from linearity is evident which is due to the electrode surface approaching full surface coverage and becoming saturated with adsorbate. To extend the linear range, the sample can be diluted, a shorter preconcentration time can be used or the rate of forced convection can be reduced. It is suggested that when using a method of standard addition, three additions be made to ensure that the response lies within the linear range [2].

6.3) BACKGROUND

The work by Mrzljak *et al.* [10] was used as a basis for this part of the project. The flow system designed was tested by using a proven flow method. The flow system could then be used in other trace determinations in various complex matrices.

Their work takes many factors into account. The cobalt sensitivity was enhanced by forming the DMG complex and hence AdSV was employed. The interference from

the extremely high zinc concentrations present were reduced in two ways, namely, by complexing the zinc with sodium citrate which moved the zinc reduction peak to more negative potentials and by utilising a matrix exchange method where stripping occurred in a comparatively uncontaminated solution. [10]

Mrzljak *et al.* [10] used a bottom-drain cell displayed in figure 6.1. The zinc electrolyte was first diluted six times with a supporting electrolyte. The sample was then injected directly over the HMDE from the flow adapter and during that time the analyte was collected at the working electrode that was held at a fixed potential. Due to the greater density of the sample versus the stripping electrolyte contained in the cell, the sample sank to the bottom of the cell and stripping occurred in a relatively uncontaminated solution, thus reducing zinc interference. The contaminated stripping electrolyte was then drained and replaced by fresh electrolyte [10]. This cell design restricted its use to samples more dense than the stripping electrolyte, whereas the cell design for this project was aimed at producing a cell that would be more versatile.

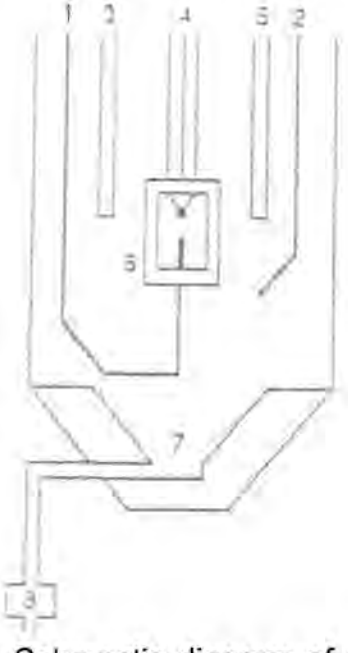

Figure 6.1: Schematic diagram of the bottom-drain cell used by Mrzljak *et al* [10]. (1) Sample inlet line; (2) nitrogen purge line; (3) reference electrode; (4) Metrohm HMDE; (5) auxiliary electrode; (6) PAR 310 flow adapter; (7) sample-electrolyte drain to waste; (8) control valve

The composition of the supporting and the stripping electrolytes are given in table 6.1. It was decided to begin this work with the same compositions and then to optimise the components.

Table 6.1: The composition of the supporting and the stripping electrolytes as used by Mrzljak *et al.* [10]

	Supporting electrolyte	Stripping electrolyte
Trisodium citrate	0.5 mol.l^{-1}	0.1 mol.l^{-1}
Ammonia	0.4 % (v/v)	0.04 % (v/v)
Ammonium chloride	-	0.1 mol.l^{-1}
DMG	5 x 10^{-4} mol.l^{-1}	3 x 10^{-3} mol.l^{-1}
pH	6.4	8.4

In the current project, a synthetic zinc electrolyte was used so that the contaminants could be controlled. This was made up according to the typical feed electrolyte found at Zincor. It consisted of 140 g.l^{-1} zinc, 10 g.l^{-1} manganese, 10 g.l^{-1} magnesium and 0.7 g.l^{-1} calcium. This was in a sulphate medium so the sulphate salts were used and the pH was adjusted to 5.

6.4) EXPERIMENTAL AND RESULTS

6.4.1) Supporting and Stripping Electrolyte Compositions

The composition of the supporting and stripping electrolytes is important as it reduces interference, enhances sensitivity, reduces resistance and so on. The compositions of these electrolytes were optimised for the designed flow system.

6.4.1.1) Sodium Citrate Concentration

Due to the large concentration of zinc present in the sample electrolyte, it was necessary to reduce the extent of interference. Sodium citrate was added to complex the zinc, thus reducing interference by shifting the zinc reduction peak potentials more negative. However, the presence of sodium citrate reduces the cobalt response, hence its concentration was reduced in the stripping electrolyte [10].

The concentration of the sample, and hence the zinc, was also reduced by diluting 4 ml and making it up to 25 ml with the supporting electrolyte.

The concentration of sodium citrate in the stripping electrolyte was investigated by looking at the effect it had on the zinc reduction peak. Matrix exchange DPSV was used with the following parameters:

Initial potential = -600 mV
Final potential = -1100 mV
Deposition time = 5 s
Scan rate = 10 $mV.s^{-1}$
Pulse amplitude = 50 mV
Sample width = 20 ms
Pulse width = 50 ms
Pulse period = 200 ms
Quiet time = 20 s
Drop size = medium
Flow rate = 1.5 $ml.min^{-1}$

The flow system describe in chapter 5 was used with deoxygenation taking place. The solutions were positioned at the selection valve as follows: position 1 was water for rinsing, position 2 was nitrogen, position 3 was the sample already diluted with the supporting electrolyte and position 4 was the stripping electrolyte. The FlowTEK procedure used is depicted in figure 6.2. The peak currents quoted were an average of 3 to 5 measurements and iR compensation was always used.

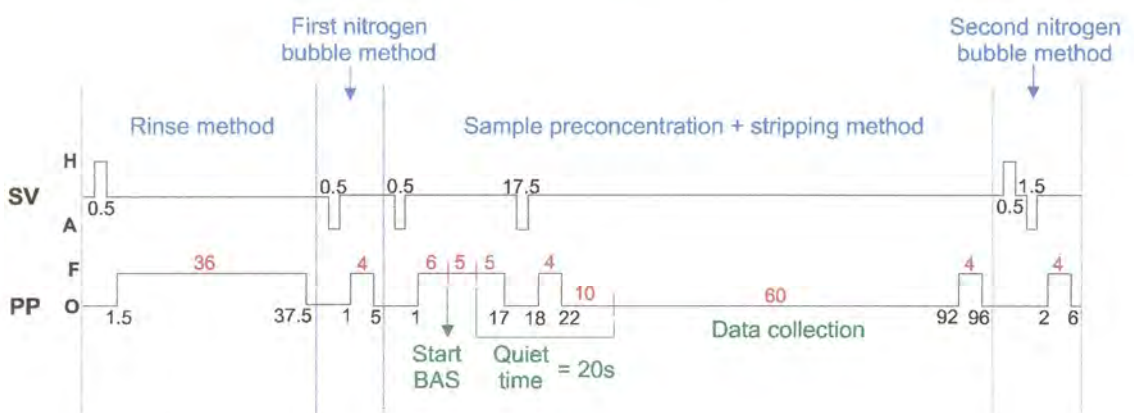

Figure 6.2: Schematic diagram of the FlowTEK procedure with a 5 s adsorption time

The supporting and stripping electrolytes were made up as specified in table 6.1, except the sodium citrate concentration in the stripping electrolyte was varied. The voltammograms in figure 6.3 indicate that varying the concentration of sodium citrate in the stripping electrolyte did not affect the zinc peak much, therefore it could be omitted from this solution. This is beneficial to the sensitivity of the cobalt reduction peak as mentioned above. This result was not surprising because when using the bottom-drain cell, there could still have been zinc in the stripping electrolyte as the only separation mechanism between the sample and stripping electrolyte was the difference in specific gravities. In the flow cell used in this study, the sample was washed out of the cell, so there could only be trace amounts zinc left behind. The slight positive potential shift at the lower citrate concentrations would not be sufficient to interfere with the cobalt reduction peak.

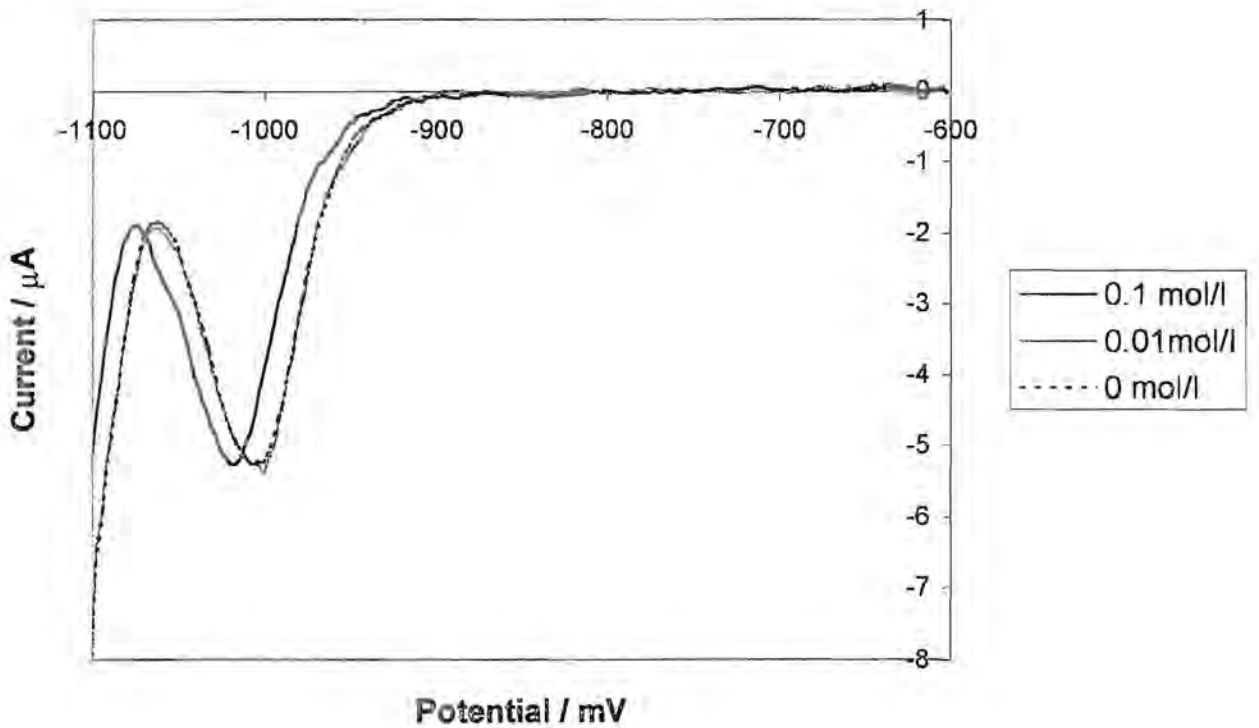

Figure 6.3: Voltammograms showing the effect of varying the sodium citrate concentration in the stripping electrolyte

Varying the concentration of sodium citrate in the supporting electrolyte was then perused under the same conditions as above. The voltammograms in figure 6.4 show that a high concentration of sodium citrate was essential to reduce the interference of the large concentration of zinc present by shifting the zinc reduction

peak to more negative potentials. A concentration of 0.5 mol.l^{-1} was thus used in future work.

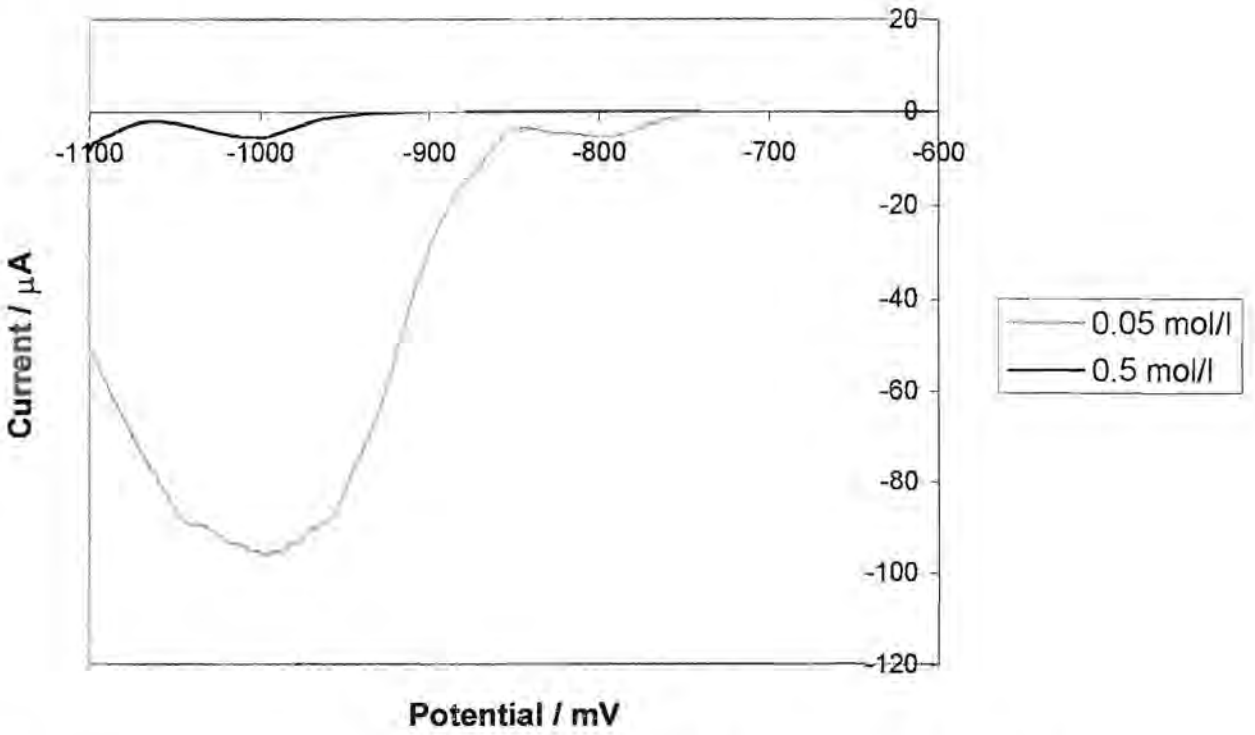

Figure 6.4: Voltammograms showing the effect of varying the sodium citrate concentration in the supporting electrolyte

6.4.1.2) pH

The optimum pH for determining cobalt is between 8 and 9, but precipitates in the zinc electrolyte are formed under those basic conditions. The pH of the complexing electrolyte was kept at a pH of 6.4 by Mrzljak *et al.* [10], where precipitates were not formed but the $[Co(DMG)_2]$ complex was still formed. Stripping could then occur at a more basic pH of 8.4 to increase the sensitivity of the determination.

The pH of the supporting electrolyte was considered in order to improve the sensitivity. A zinc electrolyte containing 1 mg.l^{-1} cobalt was used and the conditions were the same as those used previously, but with a 20 s accumulation time. An increase in pH from 6.4 to 6.7 led to an increase in the peak height of the cobalt peak as seen in figures 6.5 and 6.6. The increase in peak height became more significant at the higher pH values. It was decided not to look at even higher pH values as the limiting factor was the formation of basic precipitates. There was no visible

precipitation at pH 6.7 in the synthetic zinc electrolyte, but a real zinc electrolyte could behave differently. Any slight precipitation could also lead to blocking of tubes in the flow system which had to be avoided. When dealing with a real sample, it would be advantageous to use the highest pH tolerated before precipitation occurs. For the synthetic sample the pH of the supporting electrolyte was thus kept at 6.4 in order to deal with the worst scenario for the real sample.

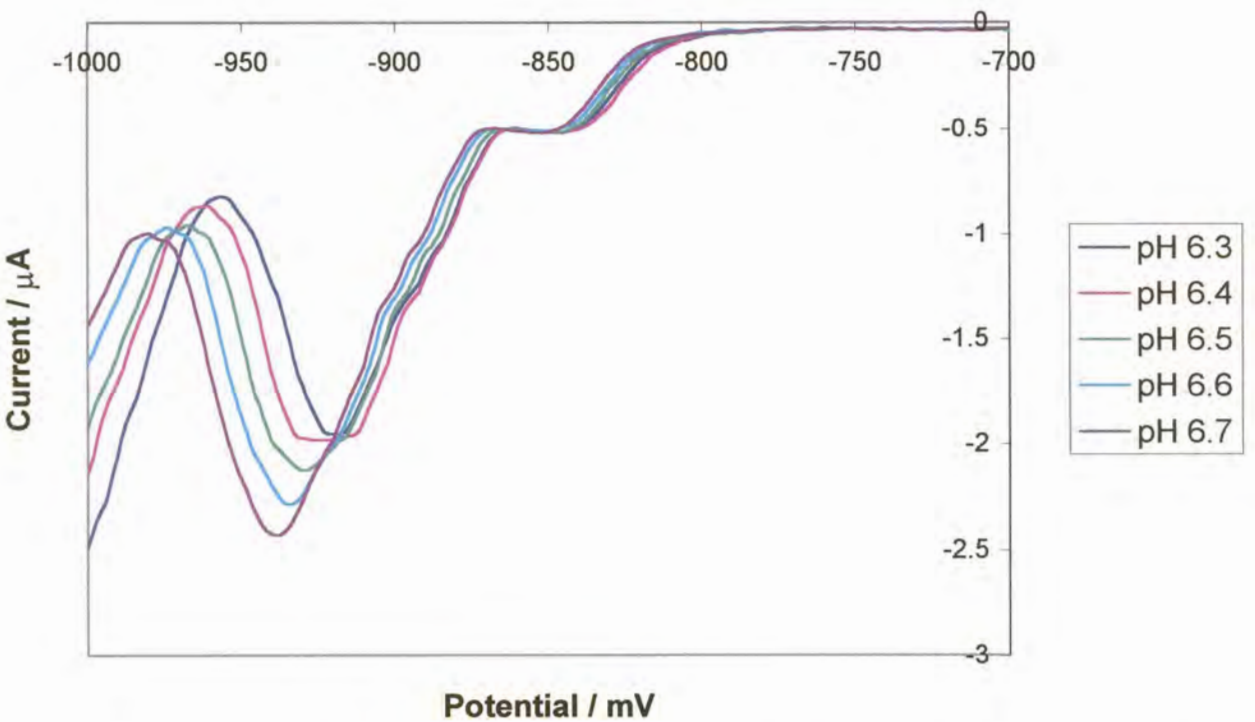

Figure 6.5: Voltammograms showing the effect of varying the pH of the supporting electrolyte

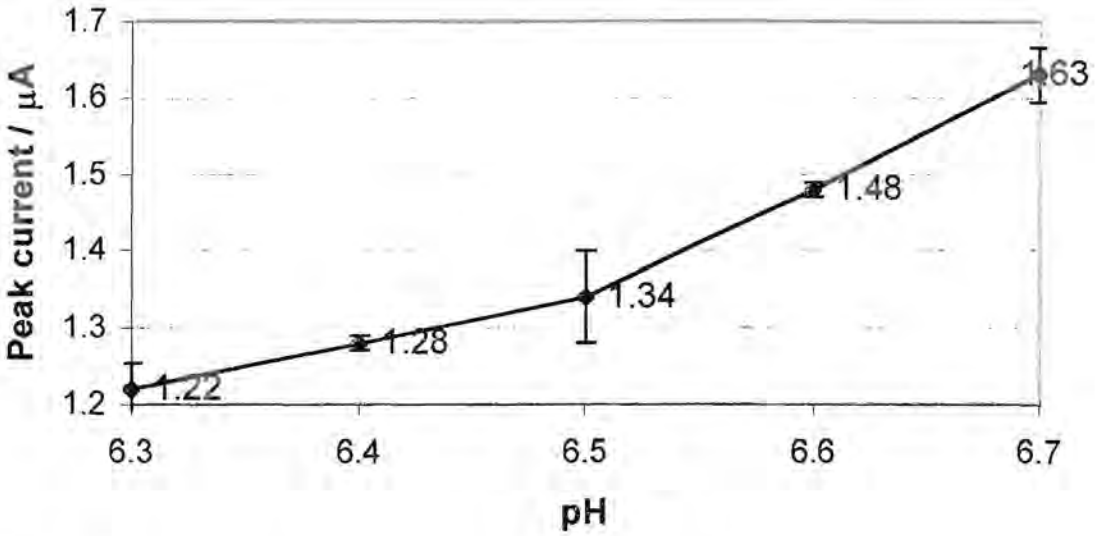

Figure 6.6: Graph of peak current versus pH of the supporting electrolyte

6.4.1.3) Cobalt Concentration

It was decided at this point to look if the change in peak height with cobalt concentration in a zinc electrolyte would yield a linear curve. The DPSV parameters were the same as before, but a deposition time of 20 s was used. The voltammograms are shown in figure 6.7. As depicted in figure 6.8, a linear curve was produced for the cobalt concentration of 0.2 to 1 $mg.l^{-1}$, yielding a correlation coefficient of 0.9979. A 0.1 $mg.l^{-1}$ cobalt concentration did not produce a peak for a 20 s deposition time, thus a longer deposition time would be required for greater sensitivity.

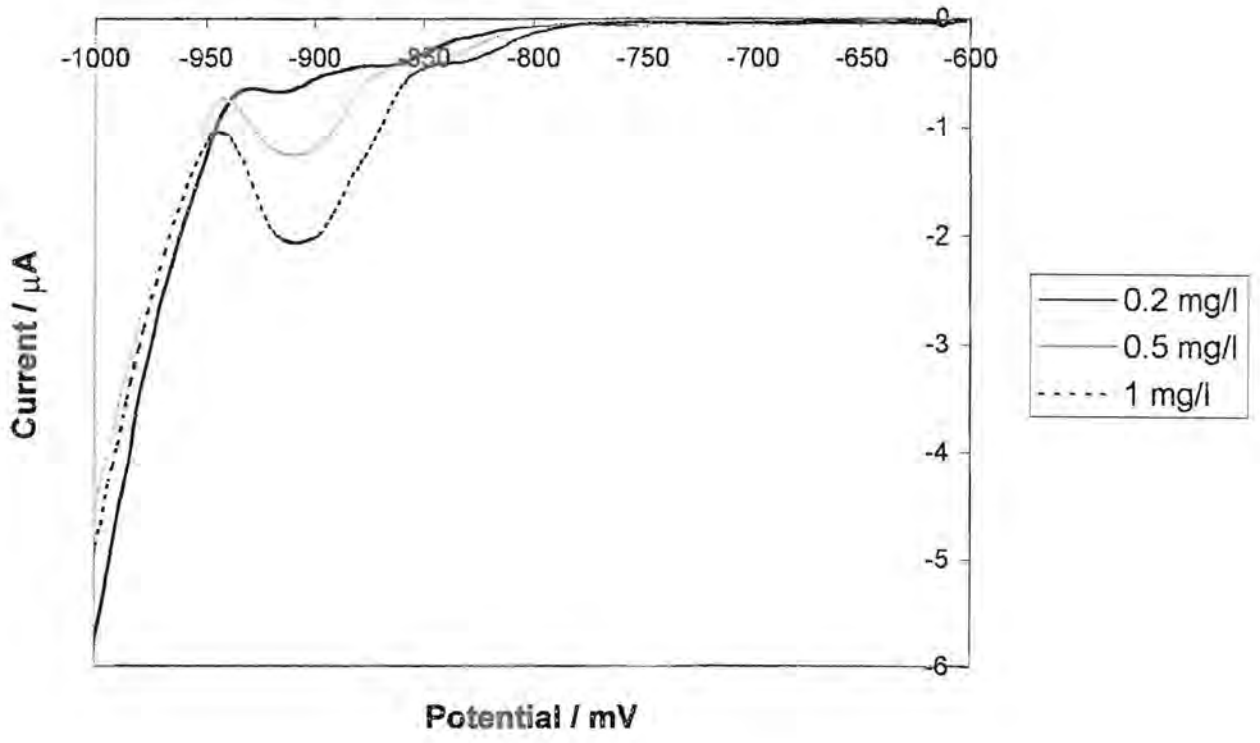

Figure 6.7: Voltammograms showing the effect of varying the cobalt concentration in the zinc electrolyte

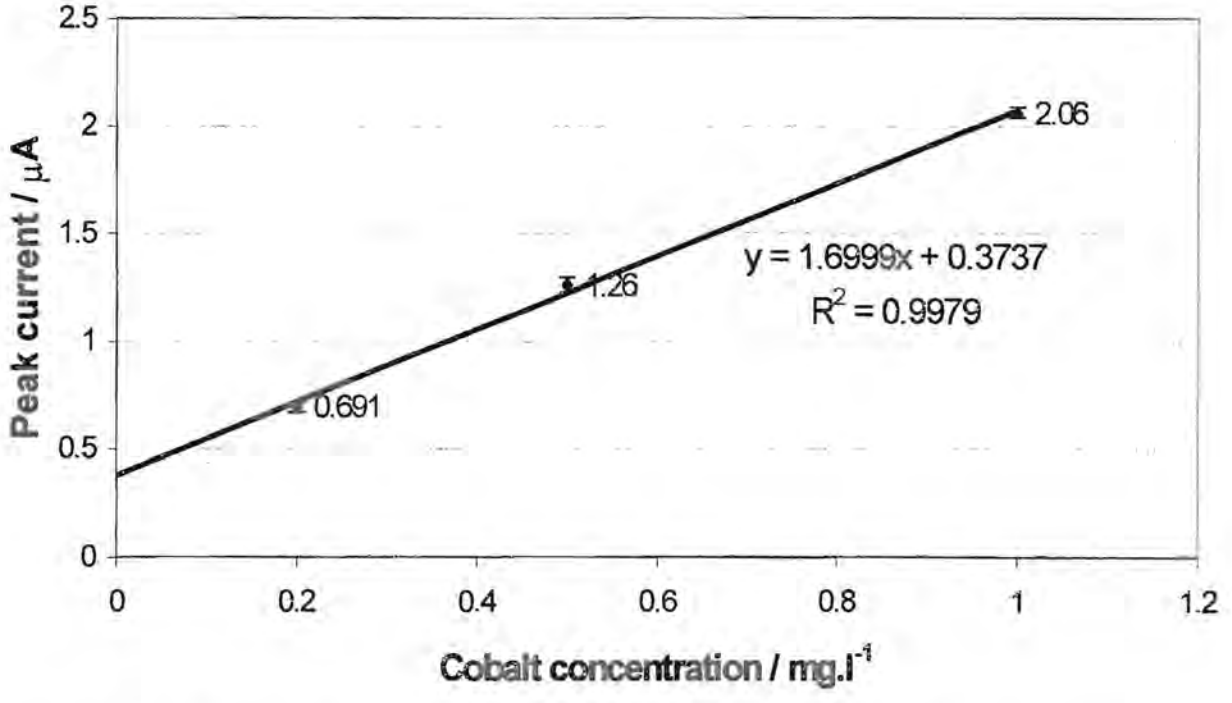

Figure 6.8: Graph of peak current versus cobalt concentration in a zinc electrolyte

6.4.1.4) DMG Concentration

The concentrations of DMG in the supporting and stripping electrolytes were investigated. The conditions were the same as before, but a 20 s deposition time and a 0.5 $mg.l^{-1}$ cobalt concentration in the zinc electrolyte were used. First the DMG concentration in the adsorbing electrolyte was varied as shown in figure 6.9. In the original work a $5x10^{-4}$ $mol.l^{-1}$ DMG concentration was used. From the voltammograms in figure 6.9 it can be seen that at lower DMG concentrations the cobalt peak is not seen, and that the peak height is greater for a $1x10^{-3}$ $mol.l^{-1}$ DMG concentration. This may have been related to the ratio of cobalt to DMG concentration. The initial drop in current, before a steady current was reached, could have been obscuring the cobalt peak at lower DMG concentrations, however it seemed unlikely. This change in current was due to some redox reaction of a component of the background electrolyte. Thus an increase in DMG concentration enhances the sensitivity for cobalt determination. A DMG concentration of $1x10^{-3}$ $mol.l^{-1}$ was used in further work.

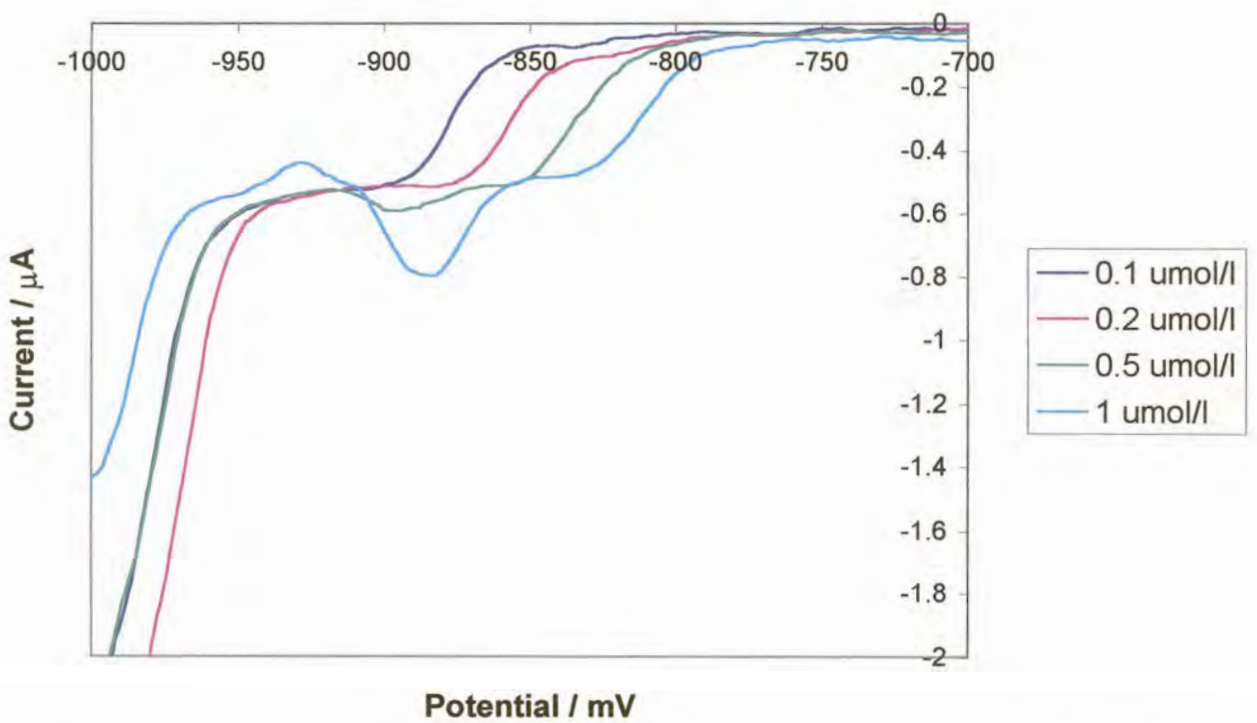

Figure 6.9: Voltammograms showing the effect of varying the DMG concentration in the supporting electrolyte

The influence of the DMG concentration in the stripping electrolyte was also explored. The conditions were the same as that for the above experiment, but the DMG concentration in the stripping electrolyte was varied from $5x10^{-4}$ mol.l^{-1} to $5x10^{-3}$ mol.l^{-1}. The results are depicted in figures 6.10. It was found that the lower the DMG concentration in the stripping electrolyte, the lower the sensitivity for the cobalt reduction peak. The peak heights did not differ much when the electrolyte contained $3x10^{-3}$ mol.l^{-1} DMG versus $5x10^{-3}$ mol.l^{-1} DMG. This was due to the incomplete dissolution of the DMG at the higher concentration. Thus a concentration of $3x10^{-3}$ mol.l^{-1} DMG was used in further work.

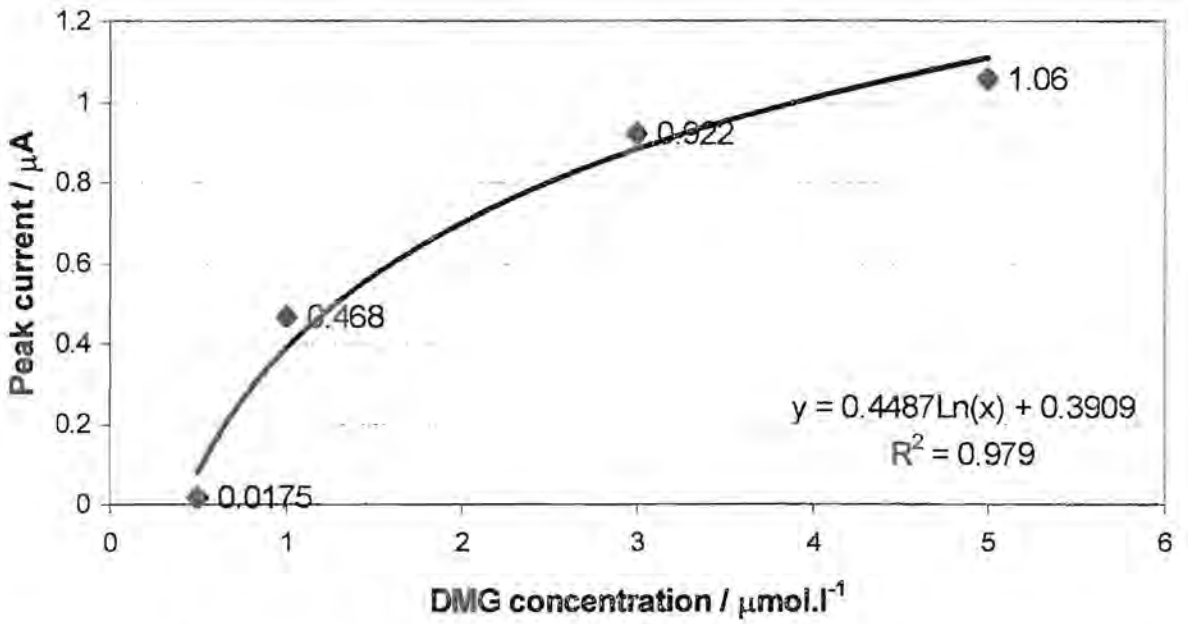

Figure 6.10: Graph of peak current versus DMG concentration in the stripping electrolyte

6.4.1.5) Dilution Factor of the Zinc Electrolyte

The zinc electrolyte was diluted 6.25 times by the supporting electrolyte. In other words, if a zinc electrolyte sample contained 0.25 mg.l^{-1} of cobalt, after the dilution 40 µg.l^{-1} of cobalt needs to be detected. It was therefore decided to see if it was feasible to make a smaller dilution. The function of the dilution was not only to introduce the supporting electrolyte, but also to reduce the zinc concentration and so reduce interference; thus it could not be too small. The usual dilution was 4 ml sample made up to 25 ml with supporting electrolyte. This was compared to taking 6

ml, 8 ml and 10 ml respectively and making it up to 25 ml in each case. In the case of 8 ml and the 10 ml sample aliquot, precipitation occurred at a pH of 6.4. Using a lower pH would not be beneficial to improving the sensitivity as conditions need to be favourable for cobalt-DMG complex formation. The conditions were the same as before and the cobalt concentration in the zinc electrolyte was 0.25 $mg.l^{-1}$. Thus the results for a 6.25 and a 4.17 times dilution were compared and are shown in figure 6.11. It should be noted that not only do the cobalt and zinc concentrations increase, but the concentrations of the various constituents in the supporting electrolyte also decrease. The voltammograms displayed an increase in the cobalt reduction peak height which indicates that a smaller dilution could be made if greater sensitivity was needed. However, once again it would be necessary to ensure that no precipitation occurred for a smaller dilution when analysing a real sample. The concentration of the various components in the supporting electrolyte could also be adjusted so that the different dilution does not affect the resultant concentrations.

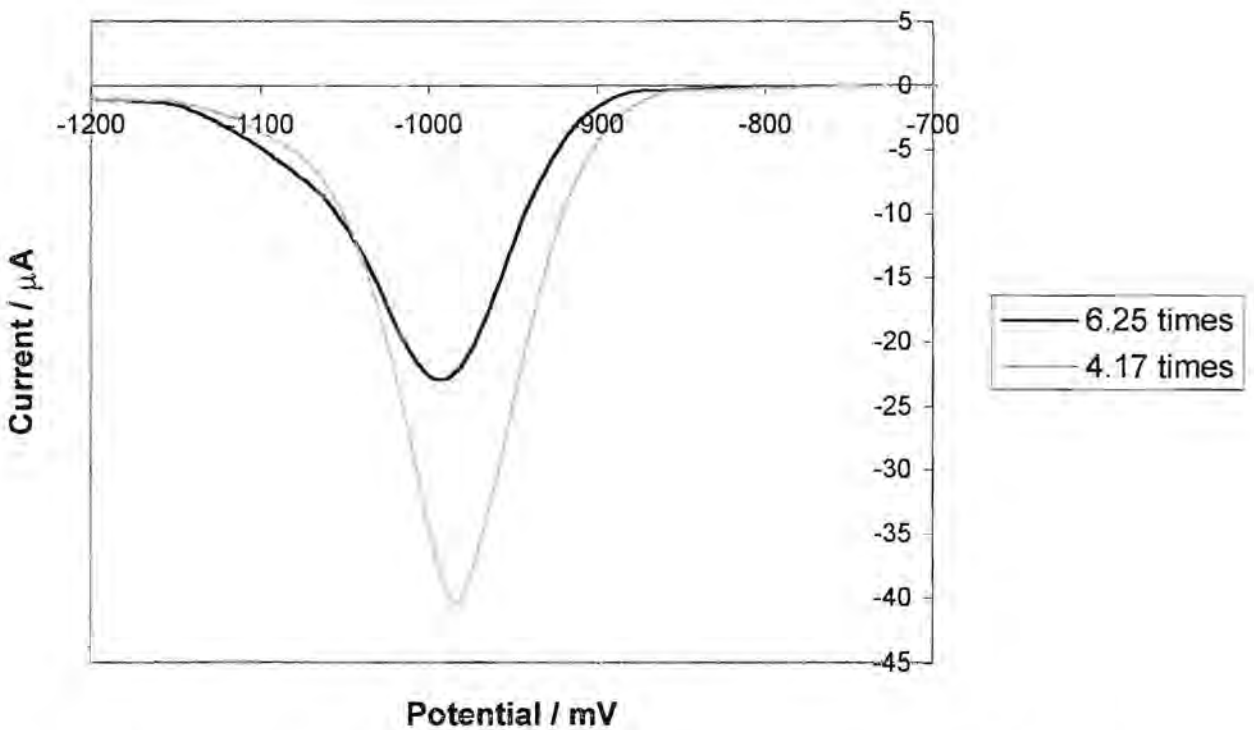

Figure 6.11: Voltammograms showing the effect of varying the sample dilution factor

6.4.2) Experimental Conditions

Not only is the composition of the supporting and stripping electrolytes important, but so are the experimental conditions such as the deposition time, the deposition potential, the potential wave form and so on.

6.4.2.1) Adsorption Time

The FlowTEK methods used for various adsorption times are depicted in figures 6.12 to 6.15. These show how the rinse times were adjusted in order for the solutions to fit in the deoxygenation tubing. A 1 $mg.l^{-1}$ cobalt concentration in the zinc electrolyte was studied. The conditions were the same as that used in the above work.

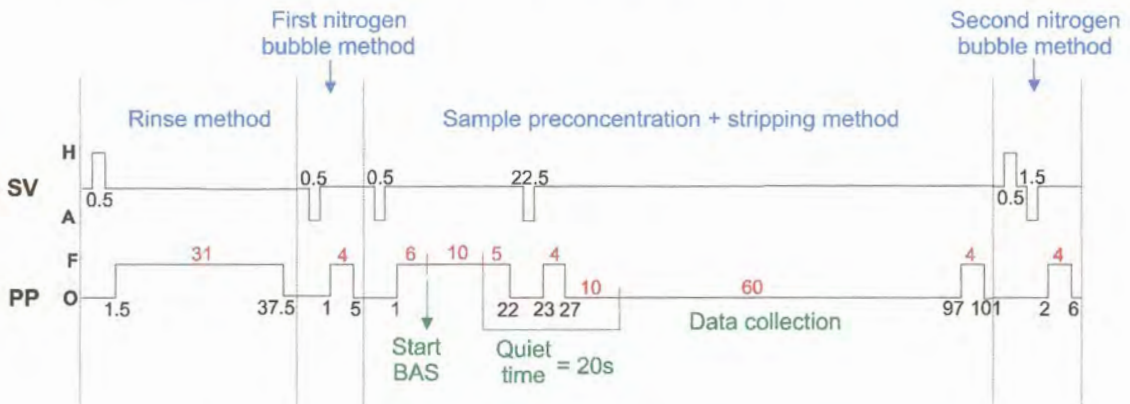

Figure 6.12: Schematic diagram of the FlowTEK method used for a 10 s adsorption time

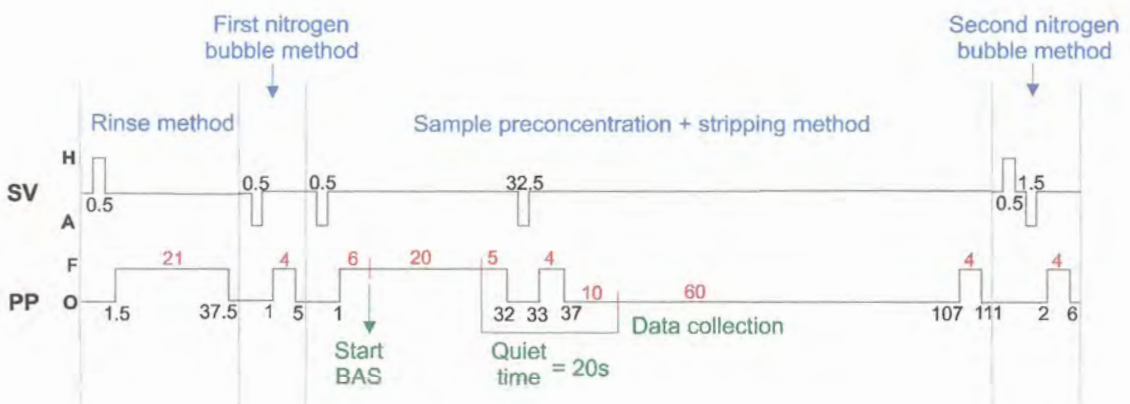

Figure 6.13: Schematic diagram of the FlowTEK method used for a 20 s adsorption time

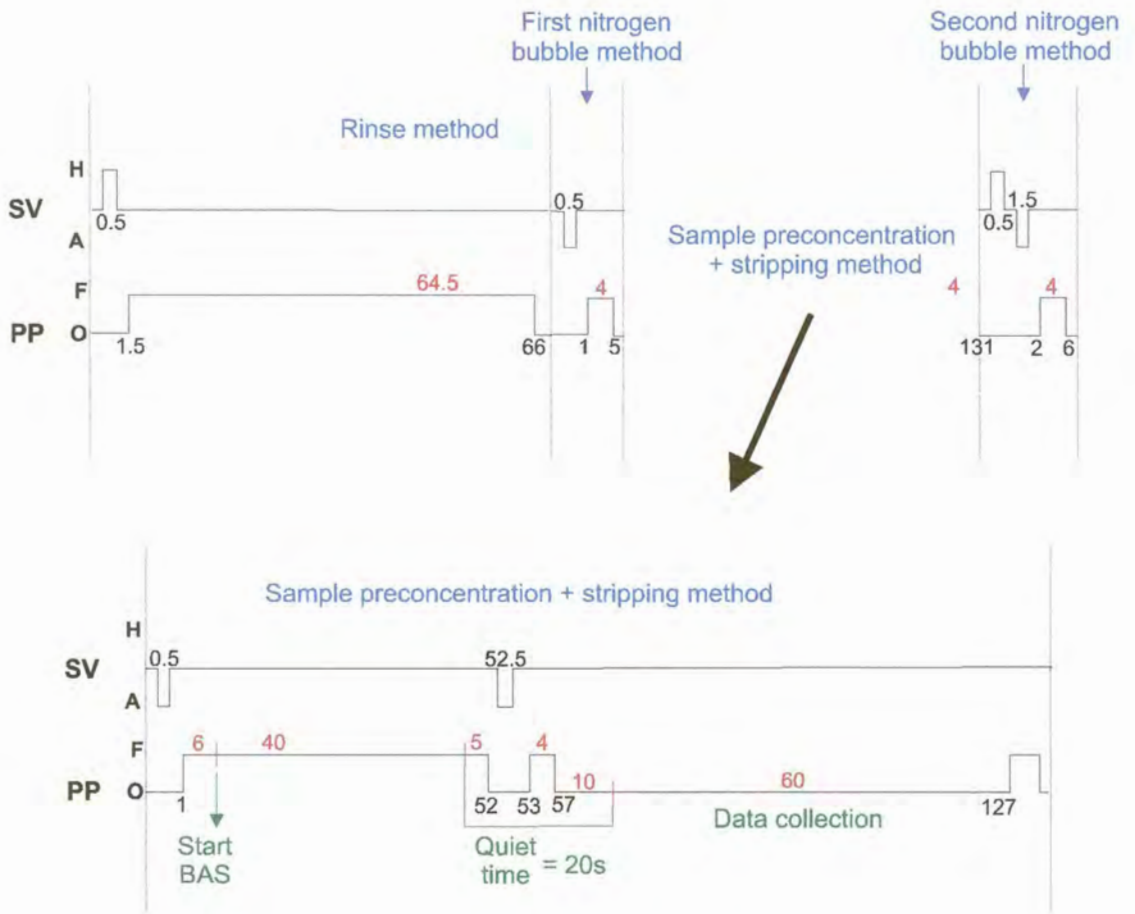

Figure 6.14: Schematic diagram of the FlowTEK method used for a 40 s adsorption time

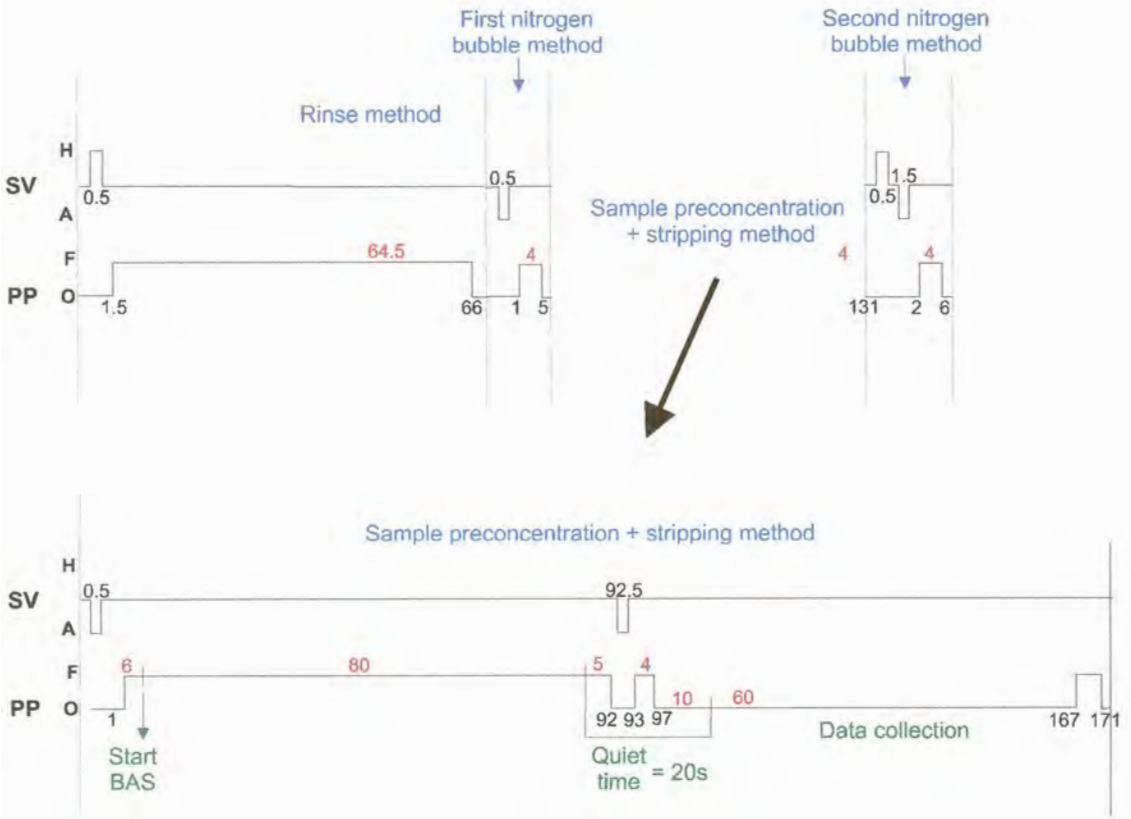

Figure 6.15: Schematic diagram of the FlowTEK method used for a 80 s adsorption time

The results obtained were somewhat erratic as shown in figures 6.16 and 6.17. There were various factors that could contribute to the erratic behaviour, such as the varying rinse times, starting a run when the position of the solution in the flow cell was at different points, the saturation coverage of the electrode surface by the complex and so on. However, the most probable explanation would be the relative positioning of the solution in the flow cell. A way to overcome this problem would be to ensure that when analysing a sample, a method of standard addition is used and that all the conditions remain consistent throughout the determination.

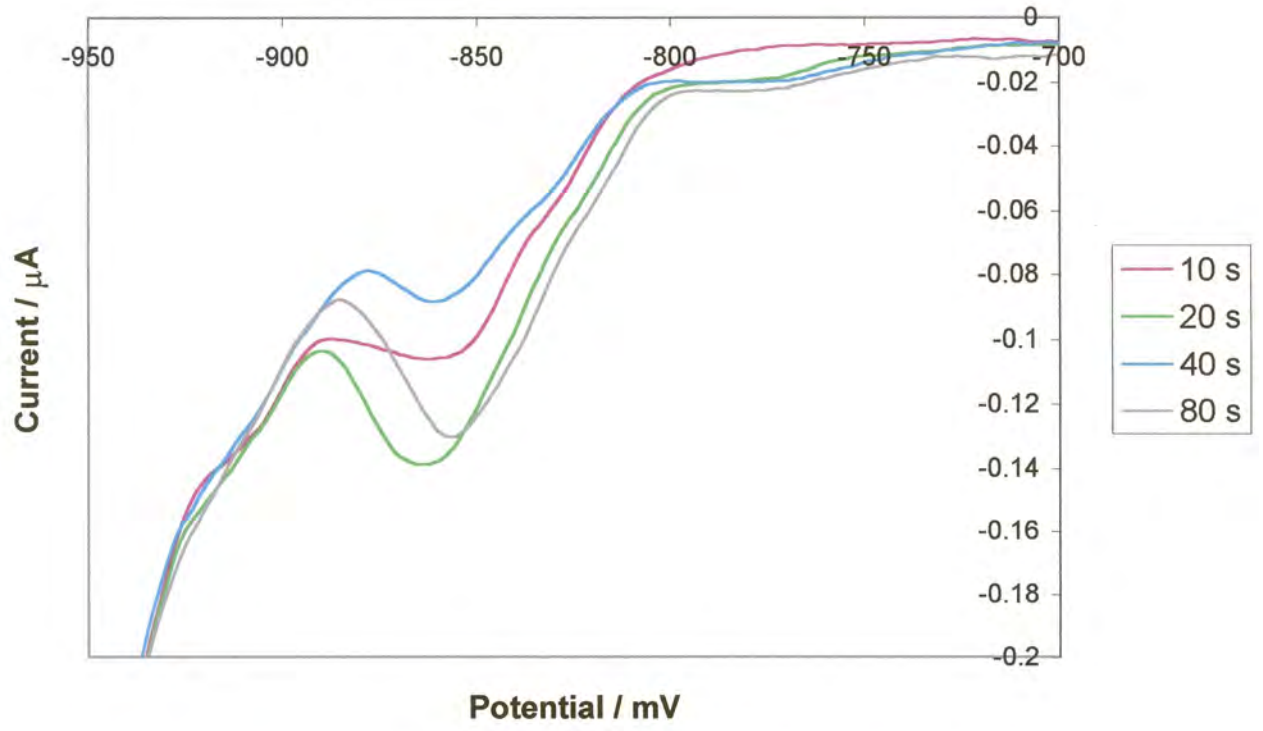

Figure 6.16: Voltammograms showing the effect of varying the adsorption time

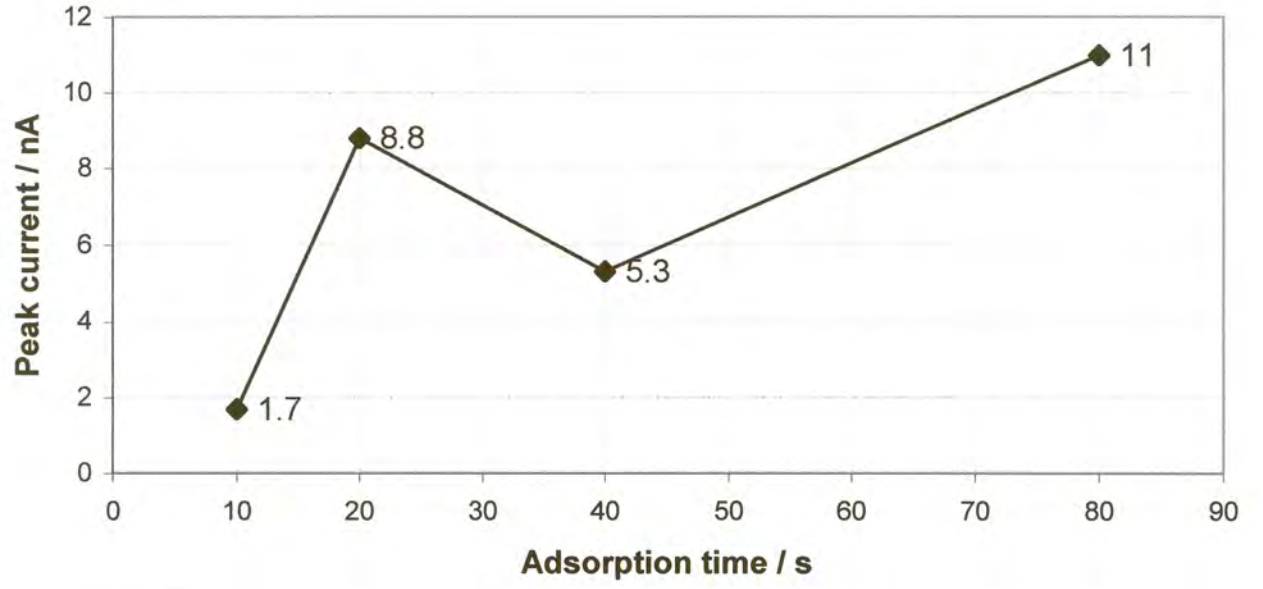

Figure 6.17: Graph of peak current versus adsorption time

6.5) DISCUSSION

In summary, the composition of the supporting and stripping electrolytes is given in table 6.2. Increasing the pH of the supporting electrolyte and diluting the sample to a lesser extent would be preferable if no precipitation occurs.

Table 6.2: The composition of the supporting and the stripping electrolytes

	Supporting electrolyte	Stripping electrolyte
Trisodium citrate	0.5 mol.l^{-1}	0 mol.l^{-1}
Ammonia	0.4 % (v/v)	0.04 % (v/v)
Ammonium chloride	-	0.1 mol.l^{-1}
DMG	1 x 10^{-3} mol.l^{-1}	3 x 10^{-3} mol.l^{-1}
pH	6.4	8.4

The method provided sufficient separation of the zinc and cobalt peaks, even when the amount of zinc present was more than 10^6 times that of the amount of cobalt present. The other main interference, which was not considered in this work, is that from nickel. Nickel and cobalt behave similarly under the conditions of the experimental work, as nickel also forms a $[Ni(DMG)_2]$ complex which is adsorbed onto the electrode and would interfere if present at high concentrations. At least the sensitivity for the $[Co(DMG)_2]$ complex was greater than for the $[Ni(DMG)_2]$ complex under the same conditions [28]. The use of higher ammonium buffer concentrations reduced the amount of interference by increasing the peak separation between the nickel and cobalt reduction peaks, as well as depressing the nickel signal [9,10]. It was shown that varying the ratio of cobalt to nickel concentration led to the interdependent influencing of the respective peak heights due to competition between nickel and cobalt for DMG [28]. The change in nickel concentration only had a slight effect on the cobalt peak height, but the change in cobalt concentration had a more severe effect on the nickel peak height. This effect was reduced by employing a matrix exchange method. It was, however, shown that the nickel levels in the zinc plant electrolyte were too low to be problematic [10].

One of the main problems experienced was that the cobalt reduction peak height did not increase with an increase in the adsorption time. Rather the results obtained

were erratic and showed no trend. This was ascribed most probably to the relative positioning of the solution in the flow cell varying with the different FlowTEK methods used. The longer adsorbing times could also have led to a more pronounced effect from turbulent flow in the flow cell. Employing a method of standard addition when analysing a sample and ensuring that all the conditions remain constant throughout the determination could obviate the problem. However, this is not an ideal situation.

The cobalt reduction peaks produced were very broad and span about 100 mV which is not ideal for analytical purposes. When considering the complicated matrix in which this determination is performed, however, the fact that there was no interference from the large excess of zinc present is significant. The cobalt peak potential occurred between 900 mV and 950 mV. The peak would have been totally overlapped by that for zinc if sodium citrate was not introduced as a complexing agent for the zinc. A fair sensitivity was obtained for cobalt and 0.2 $mg.l^{-1}$ could be determined with an accumulation time of only 20 s. As mentioned previously, due to the dilution of the sample an actual concentration of 32 $\mu g.l^{-1}$ was detected. Mrzljak *et al.* [10] estimated that 0.3 $mg.l^{-1}$ cobalt could be tolerated in the presence of other impurities, thus the detection limit for these conditions was sufficient.

A persistent concern throughout this work was that the resistance was measured between 200 Ω to 300 Ω, when calculating the iR compensation. This resistance seemed to be high for the conducting electrolyte solution in which it was measured. The high resistance was found in both the flow cell and the normal cup cell, when using different capillaries, when using different mercury, when using different electrodes and so on. It seemed that there was probably a dirty contact somewhere in the SMDE causing the problem.

Mechanical failure of the SMDE prevented real samples from being considered, as well as other matrices from being studied using this flow system. This work did, however, show that it was possible to determine impurities in complex matrices by employing electrochemical techniques.

6.6) REFERENCES

1) P.T. Kissinger and W.R. Heineman, Laboratory Techniques in Electroanalytical Chemistry, 2nd edition, Marcel Dekker Inc., New York, 1996
2) A.J. Bard, Electroanalytical Chemistry, Volume 16, Marcel Dekker Inc., New York, 1989
3) M. Geissler and R. Da Maia, Fresenius Z. Anal. Chem., 330 (1988) 624
4) A.M. Bond, R.W. Knight and O.M.G. Newman, Anal. Chem., 60 (1988) 2445
5) A.M. Bond, H.A. Hudson, D.L. Luscombe, K.L. Timms and F.L. Walter, Anal. Chim. Acta, 200 (1987) 213
6) M. Geissler and R. Kunze, Fresenius Z. Anal. Chem., 318 (1984) 15
7) A.M. Bond, B.V. Pfund and O.M.G. Newman, Anal. Chim. Acta, 277 (1993) 145
8) B. Pihlar, P. Valenta and H.W. Nurnberg, Fresenius Z. Anal. Chem., 307 (1981) 337
9) S.B. Adeloju, A.M. Bond and M.H. Briggs, Anal. Chim. Acta, 164 (1984) 181
10) R.I. Mrzljak, A.M. Bond, T.J. Cardwell, R.W. Cattrall, R.W. Knight, O.M.G. Newman, B.R. Champion, J. Hey and A. Bobrowski, Anal. Chim. Acta, 281 (1993) 281
11) I.V. Pyatnitskii, Analytical Chemistry of Cobalt, Oldbourne Press, 1966
12) K. Torrance and C. Gatford, Talanta, 32 (1985) 273
13) F. Ma, D. Jagner and L. Renman, Anal. Chem., 69 (1997) 1782
14) A. Bobrowski, Anal. Chem., 61 (1989) 2178
15) R.P. Baldwin, J.K. Christensen and L. Kryger, Anal. Chem., 58 (1986) 1790
16) M.I. Abdullah and L.G. Royle, Anal. Chim. Acta, 58 (1972) 283
17) A. Economou and P.R. Fielden, Talanta, 46 (1998) 1137
18) J.A. Herrera-Melian, J.M. Dona-Rodriguez, J. Hernandez-Brito and J. Perez-Pena, J. Chem. Ed., 74 (1997) 1444
19) Z.-Q. Zhang, H. Liu, H. Zhang and Y.-F. Li, Anal. Chim. Acta, 333 (1996) 119
20) M.G. Paneli and A. Voulgaropoulos, Fresenius J. Anal. Chem., 341 (1991) 716
21) H. Zhang, R. Wollast, J.-C. Vire and G.J. Patriarche, Analyst, 114 (1989) 1597
22) T. Schmidt, M. Geissler, G. Werner and H. Emmons, Fresenius Z. Anal. Chem., 330 (1988) 712
23) E.S. Pilkington, C. Weeks and A.M. Bond, Anal. Chem., 48 (1976) 1665
24) M. Vega and C.M.G. van den Berg, Anal. Chem., 69 (1997) 874
25) Z. Goa, K.S. Siow and L. Yeo, Anal. Chim. Acta, 320 (1996) 229

26) Colombo and C.M.G. van den Berg, Anal. Chim. Acta, 337 (1997) 29

27) Z.-Q. Zhang, S.-Z. Chen, H.-M. Lin and H. Zhang, Anal. Chim. Acta, 272 (1993) 227

28) R.I. Mrzljak, A.M. Bond, T.J. Cardwell, R.W. Cattrall, R.W. Knight, O.M.G. Newman and B.R. Champion, Analyst, 119 (1994) 1057

CHAPTER 7

DETERMINATION OF ARSENIC IN HIGH PURITY GOLD

7.1) DISSOLUTION OF GOLD IN CYANIDE

The following excerpt [1] shows how long ago it was found that gold could be dissolved in a cyanide solution: "The first definite report of solubility of gold in an aqueous solution of an alkali-metal cyanide is given in a memoir by K.W. Scheel, published in 1783, and in 1846 the importance of oxygen in the dissolution was recognised." Many have studied the mechanisms by which the dissolution occurs and tried to optimise conditions for dissolution [2-9].

Gold will readily dissolve in dilute solutions of alkali-metal cyanide where concentrations of 0.05% to 0.2% are used to leach gold from its ore [1,10]. The $[Au(CN)_2]^-$ complex formed is extremely stable, with a stability constant of $2x10^{38}$ [11].

The accepted reaction mechanism is given as [1,2,11]:

$$4Au + 8CN^- + O_2 + 2H_2O = 4[Au(CN)_2]^- + 4OH^-$$

However, the reduction of oxygen to the hydroxide ion occurs via a hydrogen peroxide intermediate as shown [11]:

$$O_2 + 2H_2O + 2e^- = H_2O_2 + 2OH^-$$

$$H_2O_2 + 2e^- = 2OH^-$$

As H_2O_2 is a strong oxidant, it also promotes the formation of $[Au(CN)_2]^-$. Thus the intermediate route could be as follows:

$$2Au + 4CN^- + O_2 + 2H_2O = 2[Au(CN)_2]^- + 2OH^- + H_2O_2$$

$$2Au + 4CN^- + H_2O_2 = 2[Au(CN)_2]^- + 2OH^-$$

The mechanism is evidently electrochemical [1,2].

The rate of the reaction is governed by the rate of diffusion of dissolved oxygen or cyanide to the surface of the gold, depending on their relative concentrations. Air (21% oxygen) is sufficient for the reaction to occur, but it was shown that using oxygen instead resulted in faster reaction rates [2]. Small amounts of sodium

hydroxide (about 0.01%) are also added to the cyanide solution to prevent the cyanide from hydrolysing to HCN, but sodium hydroxide retards the dissolution of gold by cyanide somewhat, so large quantities should be avoided [1,11].

Reaction rates for gold dissolution in cyanide solutions were compared at various temperatures, namely, 20°, 60° and 80°C. The optimum temperature was at 60°C. The slower dissolution at higher temperatures is probably due to the lower solubility of oxygen in solution [2].

Passivation of the gold surface can occur which slows down the rate of dissolution of gold in cyanide. It has been shown that the presence of small amounts of thallium almost eliminated passivation and accelerated the dissolution of gold about 7-fold [11].

The $[Au(CN)_2]^-$ complex can be electrolysed to form gold metal from an alkaline solution as follows:

$$4[Au(CN)_2]^- + 4OH^- = 4Au + 8CN^- + O_2 + 2H_2O$$

In practice, the liberated oxygen oxidises considerable cyanide to cyanate and carbonate [1].

7.2) ARSENIC

Arsenic has oxidation states of –3, 0, 3 and 5 of which the main ones are 3 and 5 [12]. Arsenic (III) is electrochemically active whereas arsenic (V) is not [12-14]. Arsenic (V) is thus reduced to arsenic (III) when total arsenic needs to be determined electrochemically. This has been done by using various reductants including sulphur dioxide [12,14,15], sodium sulphite [13,16,17], hydrazine [13,18-20], cuprous chloride [13,14,21], potassium iodide [13], ascorbic acid with potassium iodide [22], potassium bromide [18], hydroxylamine hydrochloride [13] and L-cysteine [23,24]. When making up the standard arsenic (III) solutions, reductants such as hydrazine chloride [12,18] or ascorbic acid [14] were added to ensure that none of the arsenic was oxidised; however, it was not found necessary. It is important that the reductants ensure rapid quantitative conversion to arsenic (III) and that any excess or by-products do not interfere with the determination. It was found that small amounts of

hydrazinium chloride raised the background current, and the gold film electrode became tarnished when sulphur dioxide was used, probably due to the formation of gold sulphite [12]. Davis *et al.* [21] used a process called reductillation which first involved reduction with cuprous chloride and then the distillation of arsenic (III) to get rid of interference. Arsenic (V) has been directly determined on a heated gold microelectrode where the high temperature increases the reaction rate of the sluggish reduction process [25]. It was also shown that arsenic (V) becomes electroactive in the presence of mannitol [26].

7.3) BACKGROUND

It was decided not to separate of the arsenic from the gold as minimal sample manipulation is preferred for trace analysis. Instead the kinetically inert gold (I) cyanide complex was formed. In this work potassium aurous cyanide ($K[Au(CN)_2]$) was used instead of dissolving the gold in the manner proposed earlier. This offered more controlled conditions as the impurities could be added as needed. Sodium cyanide was added to the solution to make up for any excess cyanide after the gold dissolution. A concentration of 10^{-3} $mol.l^{-1}$ cyanide was used which should have been sufficient to account for the actual excess. Arsenic was added in the form of arsenic (III) oxide (As_2O_3) which was dissolved in a basic solution. Arsenic (III) oxidation is accelerated by acidification, so this was avoided [31].

A suggested method for the dissolution of gold is, however, proposed. Use finely divided gold to increase the dissolution rate if possible. Add a solution of 0.1% (m/v) KCN and 0.01% (m/v) KOH. Heat to 60°C while stirring. Sparging air or oxygen into the solution will also speed up the reaction, but gas flow rates should not be too high or else evaporation or volatilisation could occur. The resultant solution should contain some excess cyanide and the $K[Au(CN)_2]$ complex should have formed.

The initial work was done in a normal cell in the BAS C2 Cell Stand. This acted as a Faraday cage. Once matrix exchange was implemented, the flow system was utilised.

7.4) EXPERIMENTAL AND RESULTS

7.4.1) pH of Plating Solution

Initially cyclic voltammetry (CV) was done for the various solutions to assess the system and to ascertain where the oxidation and reduction peaks were situated. The starting point was to establish whether the gold (I) cyanide complex and the free cyanide oxidation peaks would interfere with that for arsenic. All these voltammograms were run at a scan rate of 20 $mV.s^{-1}$ with an initial negative-going scan. Various pH values were considered, beginning with a pH of 9, which was achieved by the addition of sodium hydroxide. The cyclic voltammograms for cyanide, arsenic + cyanide and gold (I) cyanide + cyanide, where the cyanide concentration in each case was 10^{-3} $mol.l^{-1}$, are shown in figure 7.1. The cyanide does not have an oxidation peak in the potential region looked at, but the gold (I) cyanide does produce peaks overlapping with the arsenic peak.

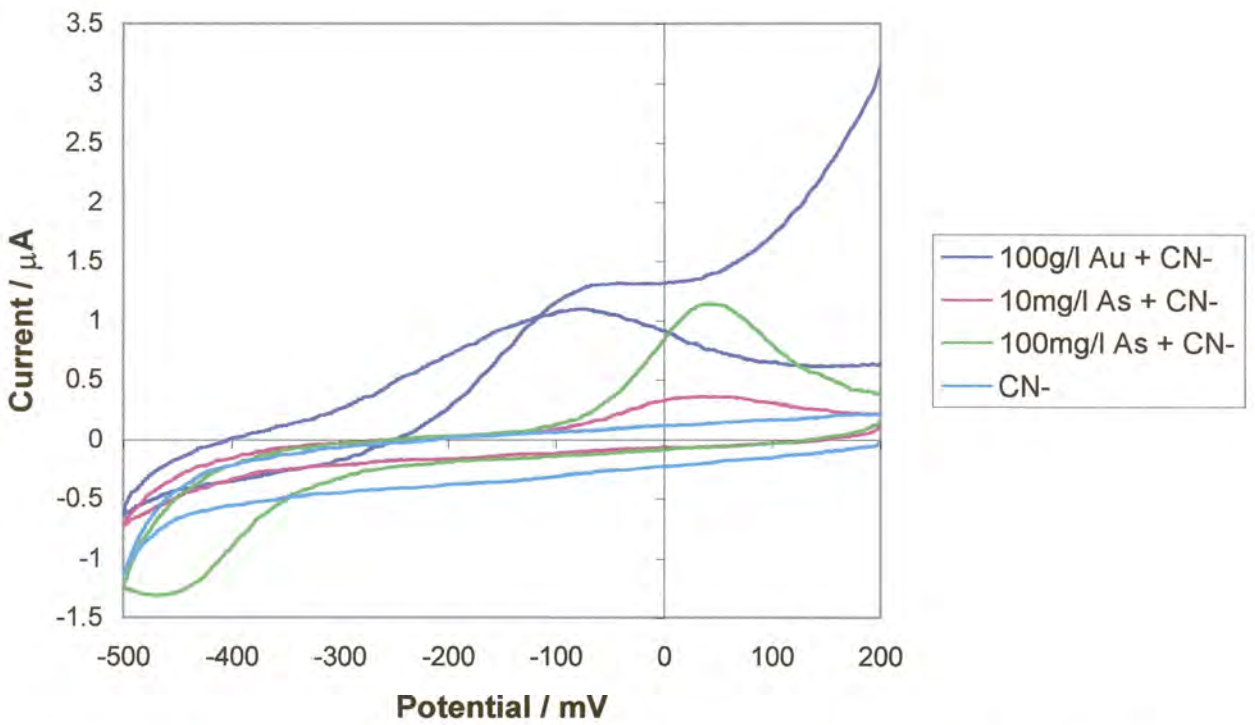

Figure 7.1: The cyclic voltammograms for cyanide, arsenic + cyanide and gold (I) cyanide + cyanide at a pH of 9

It was decided to investigate the effect of a slightly acidic solution at pH 4. In an acidic solution, arsenic (III) exists as the meta-arsenious acid, $HAsO_2$ and the electrochemical process is as follows [27]:

$$HAsO_2 + 3H^+ + 3e^- = As + 2H_2O \qquad E^\circ = +240 \text{ mV}$$

Above a pH of 8, the meta-arsenious acid dissociates to form the arsenite ion, AsO_2^- and the electrochemical process is as follows [27,28]:

$$AsO_2^- + 2H_2O + 3e^- = As + 4OH^- \qquad E^\circ = -680 \text{ mV}$$

Arsenic crystallisation then occurred at the electrode as follows [28]:

$$4As \rightarrow As_4$$

$$nAs_4 \rightarrow (As_4)_n$$

Arsenic dissolves from the electrode into both acidic or alkaline solution [10]. During anodic dissolution, the arsenic passes into solution as the trivalent state, As^{3+} [28].

The pH of solutions similar to those above, was adjusted to 4 by the addition of citric acid. The cyclic voltammograms are shown in figure 7.2. Once again the cyanide does not have an oxidation peak in the potential region studied. In the acidic solution, the gold (I) cyanide had a small peak more anodic than that for arsenic, thus no overlapping occurred. The arsenic peak shifted cathodic by less than 100 mV when moving from a pH 9 to a pH 4 solution. According to Bard [28], the potential for the reversible electrode process for the As/As_2O_3 system depends on the pH according to the following relationship which stems from the Nernst equation:

$$E = 0.234 - 0.059 \text{ pH}$$

The system is reversible from pH 3 to 10 in the absence of air. According to this, the potential at a pH of 9 should be –0.297 V and at a pH of 4 it should be 0.002 V. This implies that a shift of about 300 mV should. This was not observed in this system.

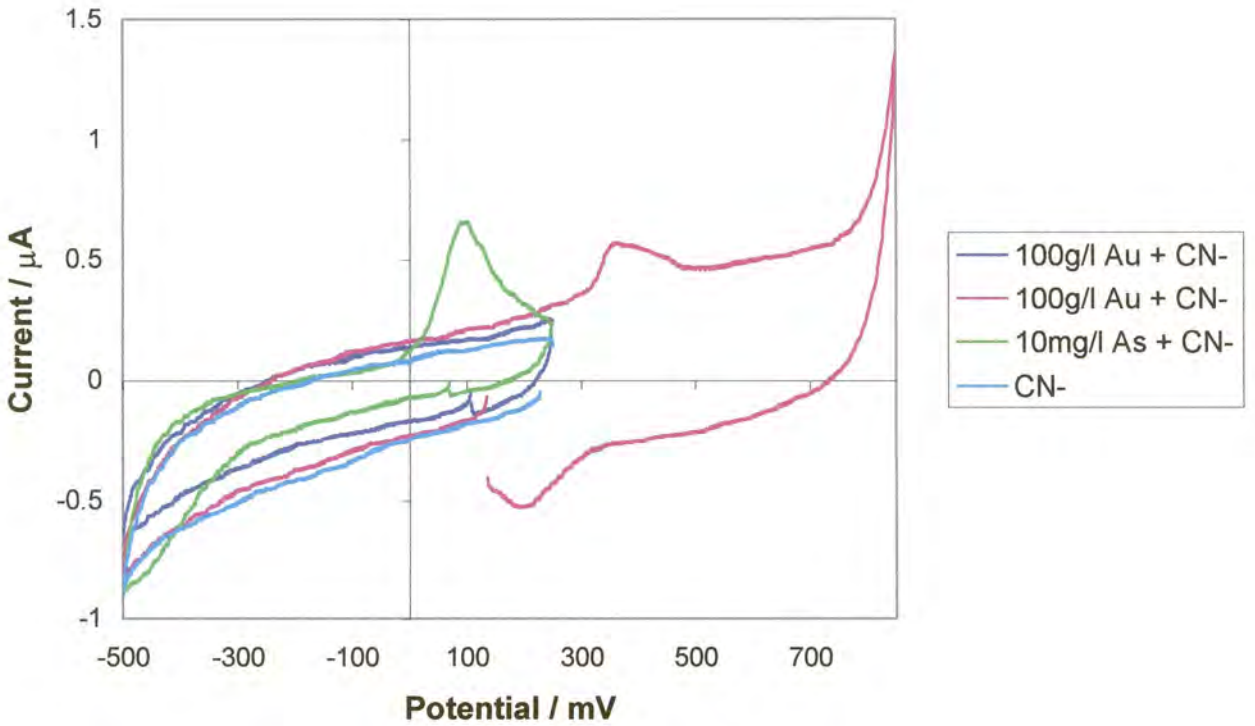

Figure 7.2: The cyclic voltammograms for cyanide, arsenic + cyanide and gold (I) cyanide + cyanide at a pH of 4

An arsenic solution containing cyanide at pH 8 was looked at. The cyclic voltammogram is shown in figure 7.3. The arsenic peak was very broad. Bard [28] pointed out that the compounds of arsenic (III) generate distinctive reduction waves whose nature to a large extent depends on the pH of the solution. In a neutral non-buffered solution, one extended or two closely spaced waves were observed. This was probably the extended peak that is seen in the voltammogram below. Also, when working in a neutral medium As_2O_3 is formed on anodic dissolution as follows:

$$2As + 3H_2O \rightarrow As_2O_3 + 6H^+ + 3e^-.$$

The As_2O_3 will accumulate at the electrode surface and inhibit the anodic dissolution as it is poorly soluble in a neutral solution [28]. It was thus best to avoid neutral or near neutral solutions for this determination.

It was decided to add a supporting electrolyte to improve the conductivity of the solution. KNO_3 was added for this purpose such that the concentration was 0.1 $mol.l^{-1}$. This reduced the iR drop significantly to acceptable levels. This component was added to all solutions from here onward.

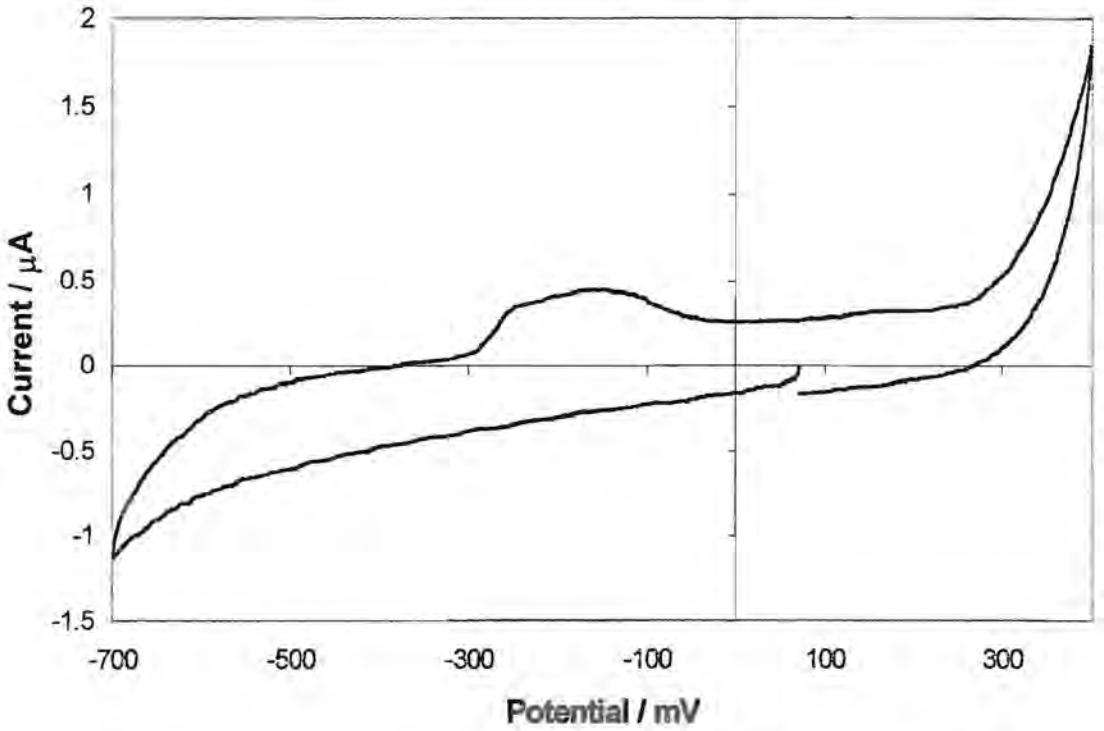

Figure 7.3: The cyclic voltammogram for 100 $mg.l^{-1}$ arsenic + 10^{-3} $mol.l^{-1}$ cyanide at a pH of 8

When working with an arsenic + cyanide solution at pH 10, it was noted that the first run, which was done on a newly formed gold film, showed some kind of peak. However, on the second run, done straight after the first, the peak had disappeared. The cyclic voltammograms are displayed in figure 7.4. The rest potential also became progressively more positive after each run. A similar result was obtained for solutions at pH 11 and 12, where the arsenic peak disappeared or became less sensitive for successive runs. This indicated that the electrode was being passivated under these alkaline conditions.

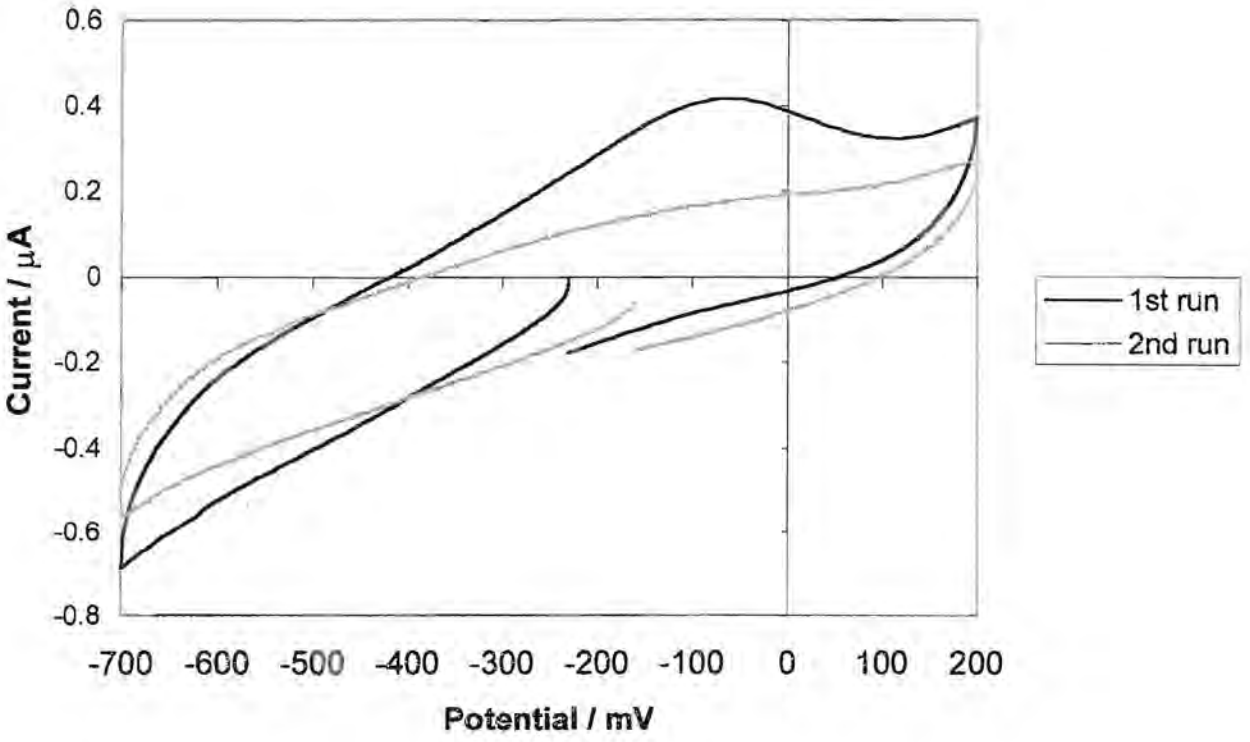

Figure 7.4: The cyclic voltammograms for 100 mg.l^{-1} arsenic + 10^{-3} mol.l^{-1} cyanide at a pH of 10

The two components that could have been responsible for the electrode passivation would be the arsenic or the cyanide. The arsenic concentration was reduced to 10 mg.l^{-1}, but the same trend arose. Two solutions were prepared at a pH of 12: the first contained 10 mg.l^{-1} arsenic + 10^{-3} mol.l^{-1} cyanide and the second only contained 10 mg.l^{-1} arsenic (both of which contained the 0.1 mol.l^{-1} KNO_3). The cyclic voltammograms produced are presented in figure 7.5.

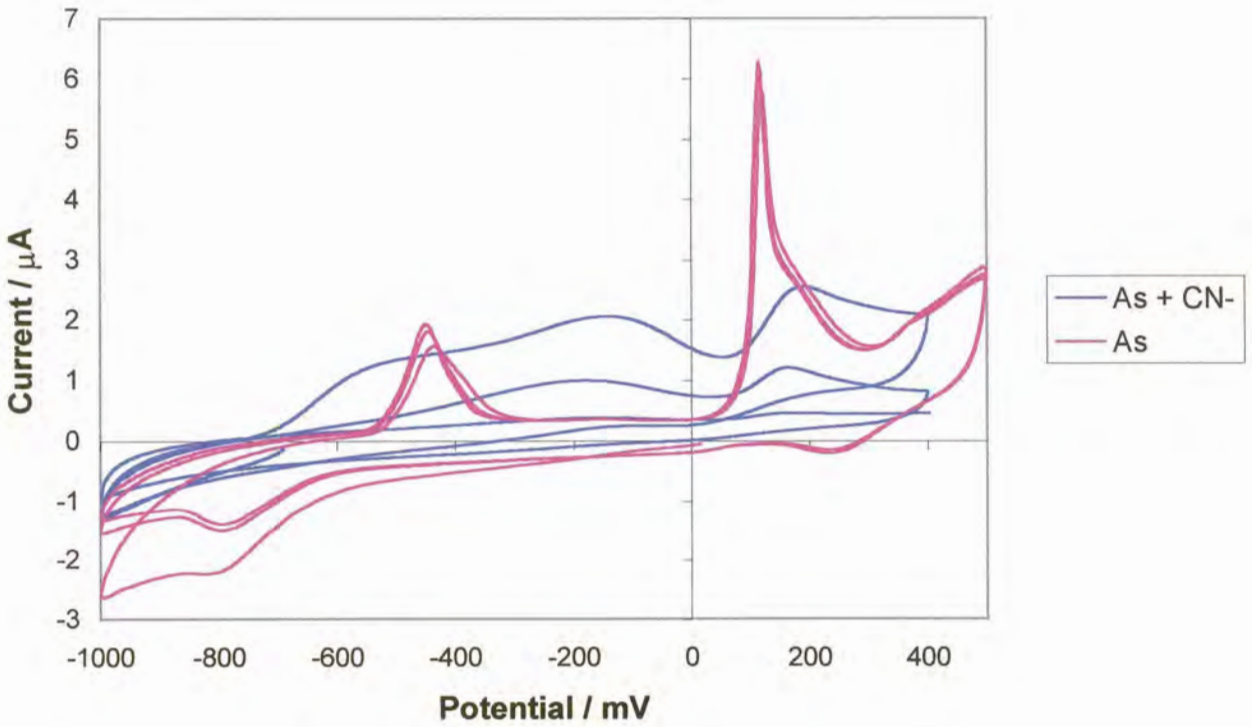

Figure 7.5: The cyclic voltammograms for 10 mg.l^{-1} arsenic + 10^{-3} mol.l^{-1} cyanide and 10 mg.l^{-1} arsenic only at pH 12

A definite passivation of the gold film electrode was observed for the solution containing both arsenic and cyanide. However, the solution containing only arsenic exhibited fairly reproducible results for the successive scans. This pointed to the cyanide being responsible for the passivation effect. This was also found in the leaching of gold from ore, where a passivated gold film could form in the presence of oxygen, cyanide and hydroxide [32]. The voltammograms also showed how the presence of cyanide shifted the arsenic peak potential to more positive values.

The peak at about –440 mV in the absence of cyanide corresponded to the arsenic (III) peak used by Aldstadt *et al.* [27] as shown in figure 7.6. This was also determined in a sodium hydroxide solution at a pH of 12. Bard [28] noted that on moving from a neutral to an alkaline solution, the first wave disappears and the remaining peak shifts to the cathodic region. This too was observed in this work.

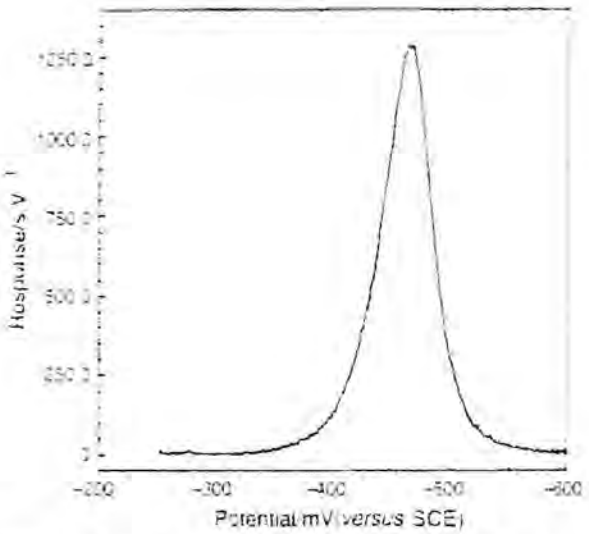

Figure 7.6: The arsenic (III) signal found by Aldstadt *et al.* [27]

Even though using a basic solution to determine arsenic (III) has the advantage of reducing the effects of interfering metals [27], as these would precipitate at high pH values, acidic solutions needed to be considered. The uncomplexed cyanide present in alkaline solutions passivated the gold film electrode which would have resulted in a new gold film having to be formed between each analysis. This would have been tedious and would have resulted in less reproducible results. Also there would be no interference from the gold (I) cyanide.

The sodium cyanide added to the solution should totally dissociate, producing "free" cyanide, CN^-. This would be the uncomplexed cyanide. The CN^- reacts with water to form hydrocyanic acid, HCN. The formation constant is 4.93×10^{-10} [11]. In other words:

$$K_a = \frac{[CN^-][H^+]}{[HCN]}$$

$$K_a = 4.93 \times 10^{-10}$$

Therefore in a solution at pH 12, all the cyanide would be present as CN^- and at pH 3, almost all the cyanide would be present as HCN. HCN is soluble in water giving a weak acid solution. Thus in an acidic solution, there would be very little CN^- to react with the gold film. A pH below 3 could not be considered as the $[Au(CN)_2]^-$ complex would decompose to form AuCN which precipitates under more acidic conditions [33-35].

A 10 $mg.l^{-1}$ arsenic solution was made up as before, containing NaCN and KNO_3, and then the pH was adjusted to 3 by the addition of citric acid. Arsenic (III) oxidation is accelerated by acidification [34], therefore it is important to analyse the samples soon after they have been acidified. The cyclic voltammograms in figure 7.7 showed that no passivation of the gold film occurred at this pH, in both a quiescent and a stirred solution.

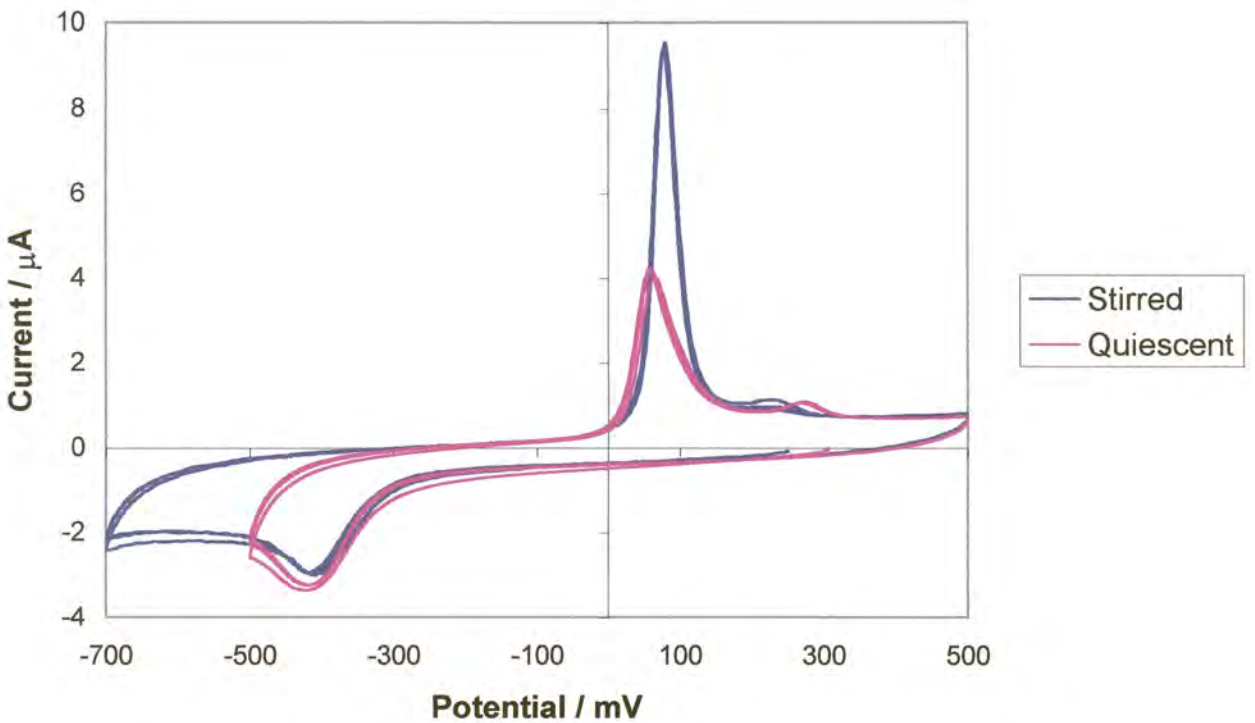

Figure 7.7: Cyclic voltammograms for 10 $mg.l^{-1}$ arsenic (III) + 10^{-3} $mol.l^{-1}$ cyanide at pH 3

The small peak at about 230 mV (in the stirred solution) may have been due to some impurity in the gold that made up the gold film. It was observed that the unknown peak vanished after a number of runs, as shown in figure 7.8, but reappeared once a new film was plated. There was also a slight loss in sensitivity for the arsenic peak, but not sufficient to account for the disappearance of the unknown peak. The change in the arsenic (III) reduction potential indicated that the properties of the gold film were changing. This could have been due to the impurity being stripped from the film. The unknown peak fading faster in the stirred solutions than in the quiescent solutions reinforced this. In the stirred solution the impurity would be rapidly swept away and hence removed from the vicinity of the electrode surface. This would

prevent the impurity from being reduced onto the electrode surface again. In a quiescent solution, the main mass transport process moving the impurity away from the electrode surface would be diffusion, which is a much slower process. Some of the impurity could therefore be redeposited onto the electrode surface, and hence the peak would diminish at a slower rate.

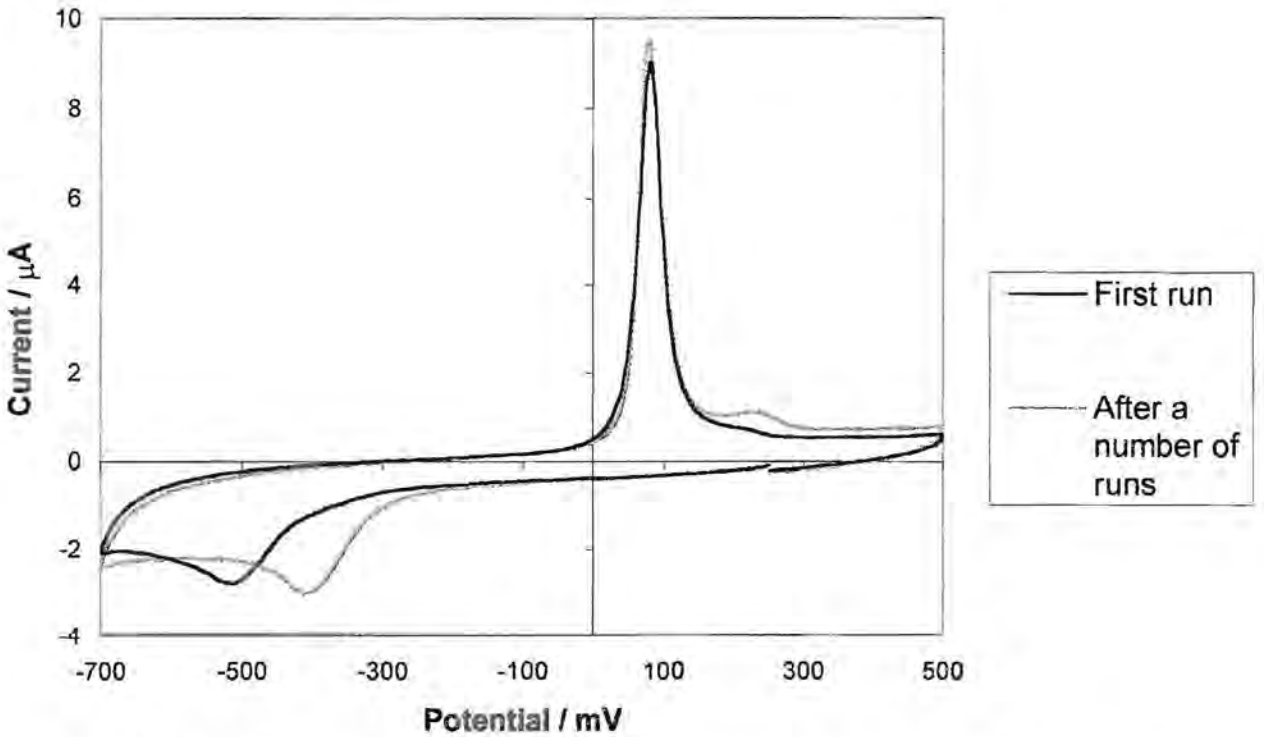

Figure 7.8: Cyclic voltammograms showing the disappearance of the unknown peak for a stirred solution after a number of runs

A solution containing 10 $g.l^{-1}$ gold, present as $[Au(CN)_2]^-$, was made up with 10 $mg.l^{-1}$ arsenic (III), 10^{-3} $mol.l^{-1}$ cyanide and 0.1 $mol.l^{-1}$ KNO_3 adjusted to pH 3 with citric acid. A cyclic voltammogram was again run to establish whether the gold would interfere with the arsenic and also to ensure that the gold (I) cyanide complex had not broken up at this pH. Figure 7.9 reveals that the gold (I) cyanide complex is still intact and that a 1000-fold more gold than arsenic did not interfere with the arsenic determination at all. There was also scope to increase the gold to arsenic concentration ratio without any difficulties being experienced.

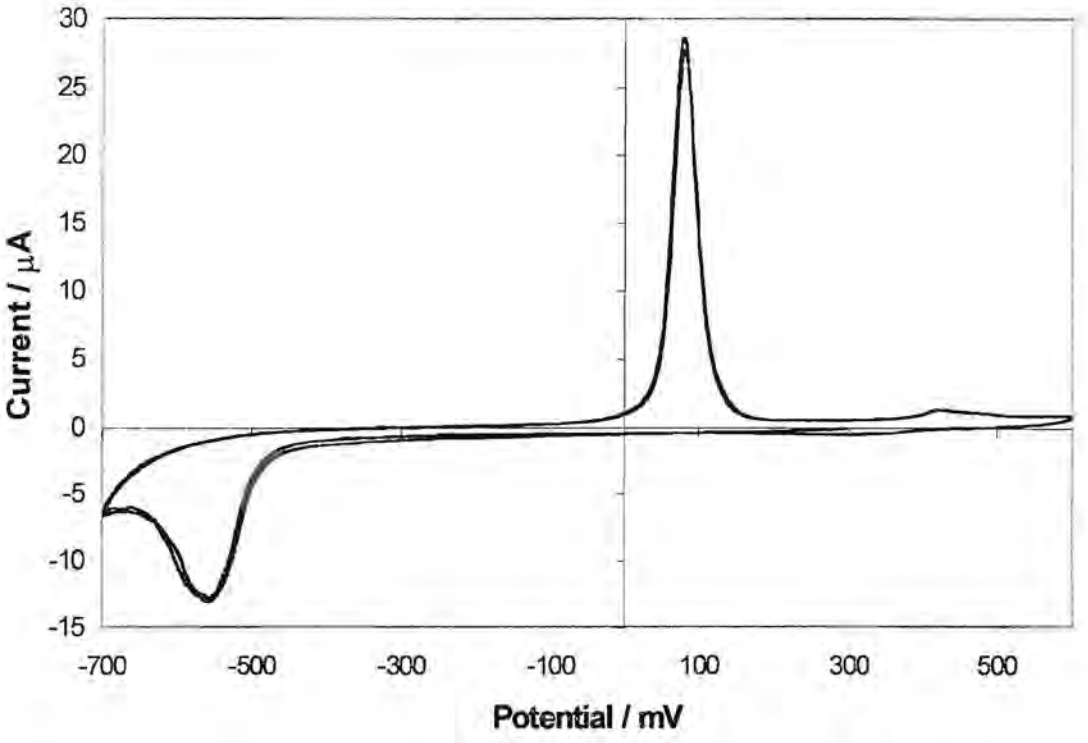

Figure 7.9: Cyclic voltammogram for 10 $g.l^{-1}$ gold (as $[Au(CN)_2]^-$) + 10 $mg.l^{-1}$ arsenic(III) + 10^{-3} $mol.l^{-1}$ cyanide at pH 3

Other important information could also be gained from the cyclic voltammograms [36]. The system that was to be studied further, displayed in figure 7.9, was looked at in more detail. For a chemically and electrochemically reversible couple,

$$\Delta E_p = E_{pa} - E_{pc} \approx \frac{0.058}{n}$$

In this case the arsenic redox reaction was a three electron process, therefore:

$$\Delta E_p \approx 0.019\,V$$

However, when looking at the peak separations,

$$\Delta E_p = 0.08 - (-0.58)$$

$$\Delta E_p = 0.59\,V$$

This implied that the arsenic redox system was irreversible and that the electron transfer between the electrode and the arsenic was slow. Also, for a reversible couple with no kinetic complications,

$$i_{pa} \approx i_{pc}$$

This was not the case for either a quiescent or a stirred solution.

7.4.2) Deposition Potential

The optimum deposition potential for arsenic (III) in a solution at pH 3 was investigated. The gold (I) cyanide complex was omitted from most of the solutions, unless specified otherwise, due to the cost of the substance as it was already proven that it would not interfere with the arsenic determination. A 10 $mg.l^{-1}$ arsenic (III) solution was made up as before. LSSV was done at various deposition potentials in a stirred solution with a deposition time of 10 s and a scan rate of 20 $mV.s^{-1}$. The results displayed in figure 7.10 show that the optimum deposition potential was –650 mV. This potential was used from here onward.

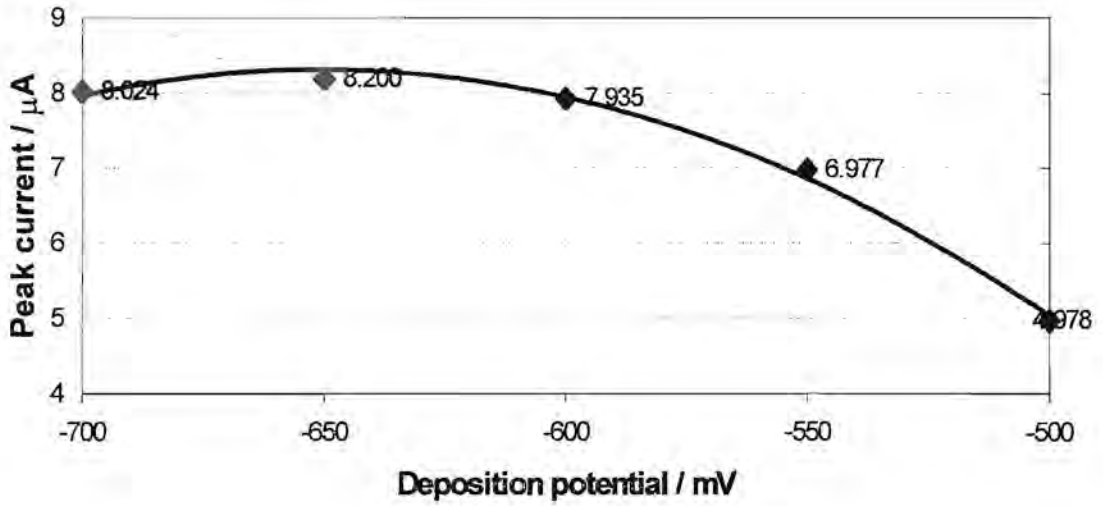

Figure 7.10: Graph of peak current versus deposition potential

7.4.3) Reproducibility

The reproducibility of the system was investigated by doing 10 runs of LSSV as above. This produced a RSD of 4.4%. This is acceptable, but there were some concerns. The peak current showed a definite increasing trend. This could be due to not all the arsenic being stripped from the electrode and hence a slow accumulation of arsenic. Also, the peak potential moved towards low values with successive runs. This seems to indicate that there is a slow change in the electrode surface.

7.4.4) Stripping Electrolytes

It was decided to look at a matrix exchange method to see whether it would be possible to reduce the gold film degradation. This would also help to improve the sensitivity of the determination and reduce interference. The flow system described in chapter 5 was used with deoxygenation taking place. iR compensation was always used.

7.4.4.1) Hydrochloric Acid

Hydrochloric acid was the first stripping electrolyte investigated as it was widely used and provided good sensitivity. The stripping peaks were also narrow which indicated that the charge-transfer reaction was fast and reversible [12,21,30]. It was found that when arsenic was determined in a hydrochloric acid matrix, chlorine was generated at the auxiliary electrode concurrent with arsenic deposition at the working electrode. The chlorine would then diffuse to the working electrode where it would readily oxidise the gold electrode surface, thereby making it inactive [27]. This was not a problem when using a WJE as only the solution from the jet reached the electrode surface, thus the chlorine could not diffuse to the working electrode and attack it. It has also been postulated that the gold film was oxidised in the presence of a high chloride concentration to the $[AuCl_4]^-$ complex. This would lead to the active gold surface area decreasing and hence poor reproducibility [12]. It was, however, suggested that hydrochloric acid concentrations greater than 7 $mol.l^{-1}$ be avoided as it could lead to the destruction of the glassy carbon substrate on prolonged exposure [29].

Various hydrochloric acid concentrations were considered and the corresponding peak currents were measured to determine which concentration gave the best sensitivity. This was done in the wall-jet flow cell using the FlowTEK procedure previously depicted in figure 5.26. The plating solution was a 1 $mg.l^{-1}$ arsenic (III) solution containing 10^{-3} $mol.l^{-1}$ cyanide and 0.1 $mol.l^{-1}$ KNO_3 adjusted to pH 3 using a citrate buffer. The citrate buffer was made up by mixing 0.1 $mol.l^{-1}$ disodium citrate with 0.1 $mol.l^{-1}$ hydrochloric acid in a ratio of 39.9 to 60.1. The disodium citrate was made up by adding

2.1014 g citric acid monohydrate to 20 ml 1 mol.l^{-1} sodium hydroxide and making it up to 100 ml. The buffer was then diluted 10 times when added to the sample. The buffer was used instead of just citric acid as it could control the pH more accurately. Data were collected using DPSV from –400 mV to 300 mV at a scan rate of 20 mV.s^{-1} after a 20 s deposition time at –650 mV. The other parameters were the default parameters of 50 mV pulse amplitude, 50 ms pulse width, 20 ms sample width, and 200 ms pulse period.

The results are displayed in figure 7.11. A 4 mol.l^{-1} hydrochloric acid concentration was used in further studies as it gave the best sensitivity. Higher hydrochloric acid solutions were not considered to prevent any degradation of the working electrode.

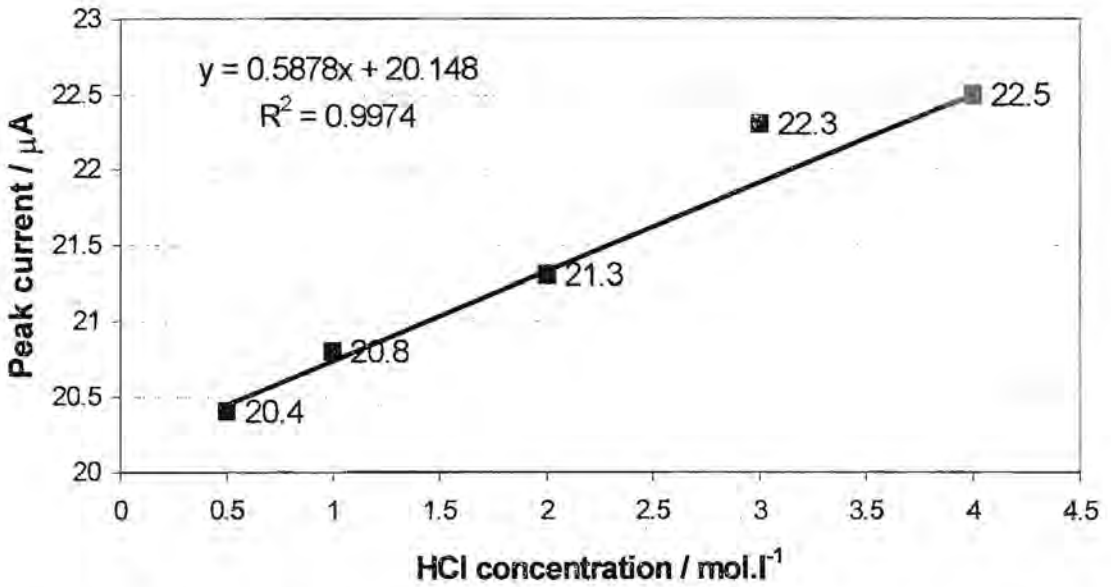

Figure 7.11: Graph of peak current versus hydrochloric acid concentration of the stripping electrolyte

A range of arsenic concentrations from 0.1 mg.l^{-1} to 1 mg.l^{-1} were studied to determine whether the relationship between arsenic concentration and peak current is linear. Data were collected using DPSV from –200 mV to 300 mV at a scan rate of 20 mV.s^{-1} after a 60 s deposition time at –650 mV. The other parameters were the default parameters as above. The FlowTEK method used was shown in figure 5.27.

Initially, instead of analysing the samples in an order of increasing concentration, the samples were mixed up and the 1 $mg.l^{-1}$ and 0.1 $mg.l^{-1}$ samples were transposed when analysed. The 1 $mg.l^{-1}$ arsenic solution was then analysed again. The findings are represented in figure 7.12. The peak current of 1.37 μA at 1 $mg.l^{-1}$ arsenic is the measurement taken again at the end of the analyses. This showed that the electrode definitely had some memory effects.

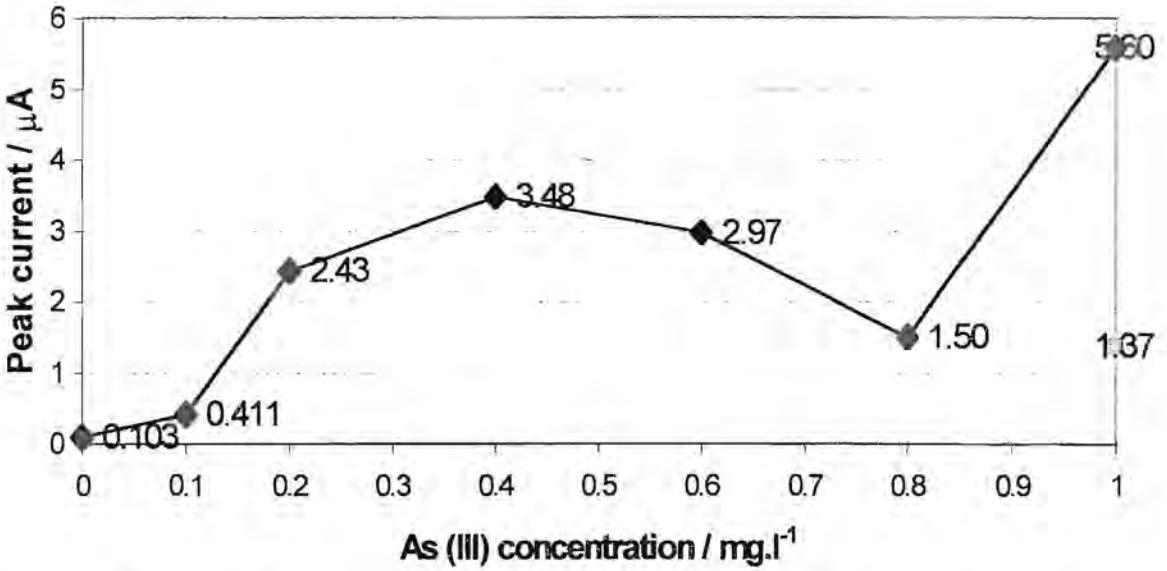

Figure 7.12: Graph of peak current versus arsenic (III) concentration where the order of analysis was not increasing in concentration

The experiment was repeated, but this time the samples were analysed in order of increasing concentration. The results are depicted in figure 7.13 and the voltammograms are shown in figure 7.14. The results were initially linear, but deviated from linearity after the 0.2 $mg.l^{-1}$ arsenic solution. This could have been due to the active surface area of the electrode being almost totally covered by arsenic (0). As elemental arsenic is a very poor conductor of electricity, only a monolayer of arsenic is deposited and therefore the peak current is limited [12,21,27,29,30]. A shorter accumulation time would solve this non-linearity at higher arsenic concentrations. Alternatively, it could have been that the gold film was degrading with time and the sensitivity started decreasing. This is quite possible as seen from the previous experiment

when the order of samples was confused, the gold film electrode was not very robust.

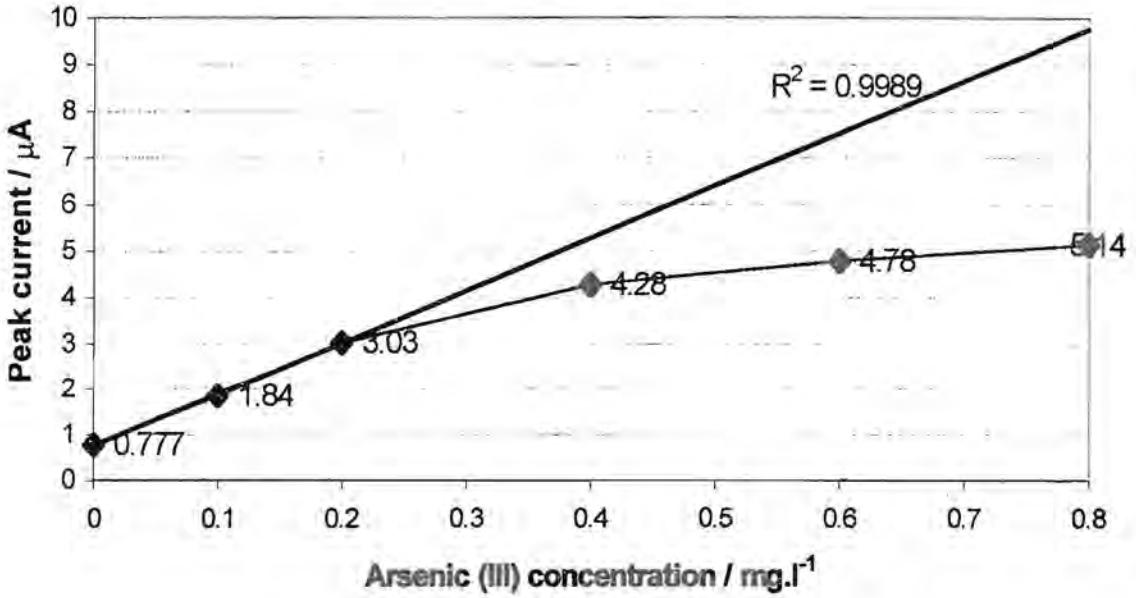

Figure 7.13: Graph of peak current versus arsenic (III) concentration where the order of analysis was increasing in concentration

It was therefore recommended that the samples should be read in order of increasing concentration. This would not be possible if data for a calibration graph were first collected and then the sample analysed, as the latter would probably give a deceptive lower current signal. Rather a method of standard addition could be used, which would not only make it possible to analyse in the concentration order required, but would also take the matrix effects into account.

The arsenic oxidation peaks were not symmetrical, particularly for the higher arsenic concentrations. There appeared to be a shoulder on the left side of the peaks. This could be due to the surface of the gold film changing with time, which supports the second postulate as to why the graph of arsenic concentration versus peak current deviated from linearity. It would be interesting to calculate the peak area and determine if it would yield more satisfactory results.

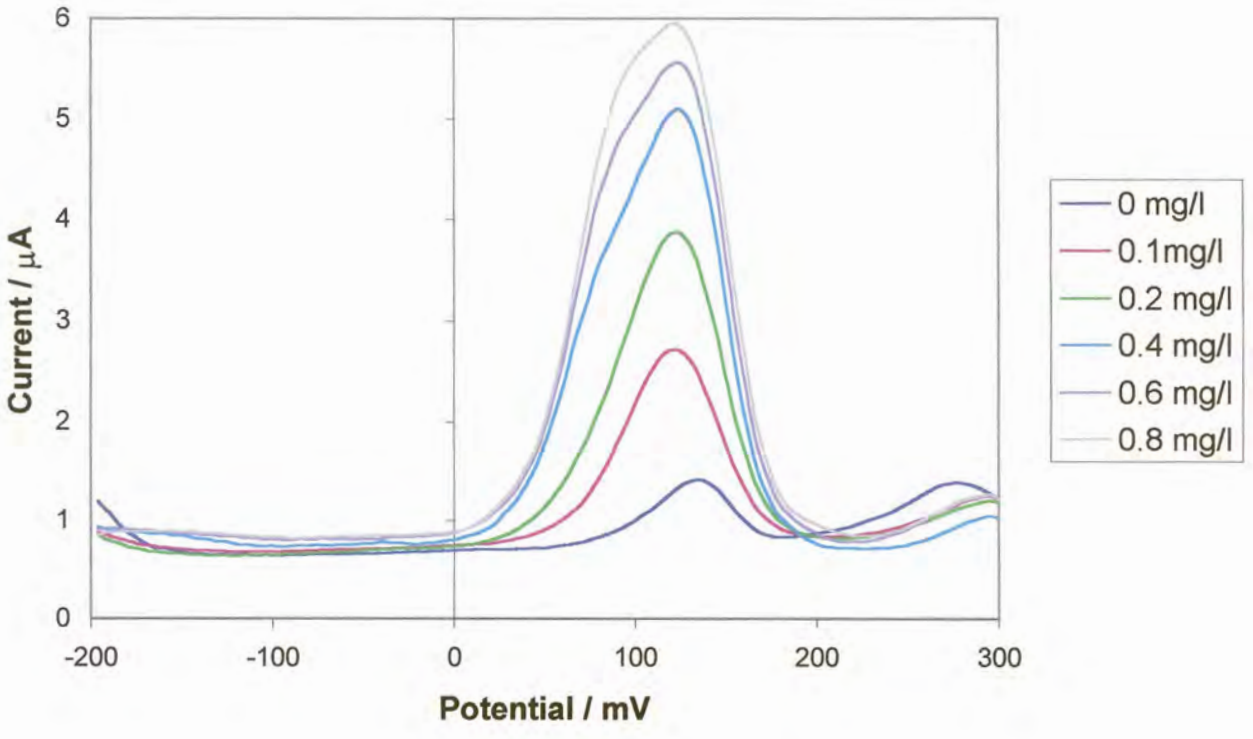

Figure 7.14: Voltammograms for increasing arsenic (III) concentration

7.4.4.2) Sulphuric and Hydrochloric Acid

Other stripping electrolytes were also investigated to find if the gold film electrode would degrade to a lesser extent.

At this point it was difficult to achieve a lustrous gold film of low resistance, so a step function was used to try and rejuvenate the glassy carbon electrode activity. The step function involved stepping from –1200 mV to 700 mV applying a pulse width of 250 ms for 1000 cycles in the gold plating solution. The gold film was then plated onto the GCE and it was found that this did improve the quality of the gold film.

A DPSV was collected for a 1 $mg.l^{-1}$ arsenic solution as before in the 4 $mol.l^{-1}$ hydrochloric acid solution. The voltammogram yielded a shoulder at about 180 mV that was not present before the electrochemical electrode treatment, as shown in figure 7.15. The shoulder decreased on successive runs while the main peak increased slightly. The origin of this shoulder is unknown. However, it could have been that with the electrochemical electrode

treatment, the electrode was activated to a greater degree which made conditions favourable for impurities to plate to a greater extent on the electrode. With successive runs, the impurity was stripped from the gold film which led to the reduction of the shoulder height. The arsenic peak could have increased in height as the impurity was stripped because a greater surface area of the electrode was now covered by gold.

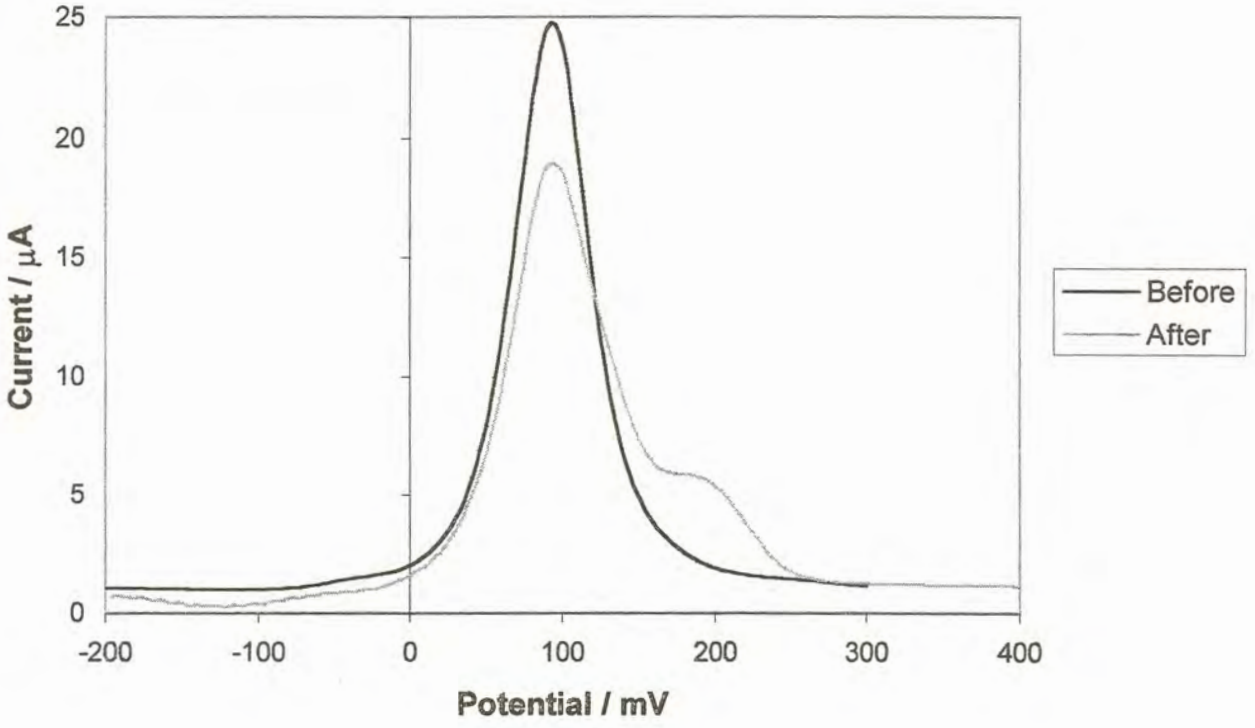

Figure 7.15: Voltammograms for 1 mg.l^{-1} arsenic with a 4 mol.l^{-1} HCl stripping electrolyte before and after electrochemical electrode treatment

Sulphuric acid as a stripping electrolyte was investigated. A 1 mol.l^{-1} solution produced a broad insensitive peak as shown in figure 7.16. 0.1 mol.l^{-1} hydrochloric acid was then added to this and it gave a sharper more sensitive peak. The shoulder that appears in the hydrochloric acid solution was resolved from the arsenic peak in the sulphuric acid-hydrochloric acid mixture. However the hydrochloric acid solution still yielded the most sensitive peak.

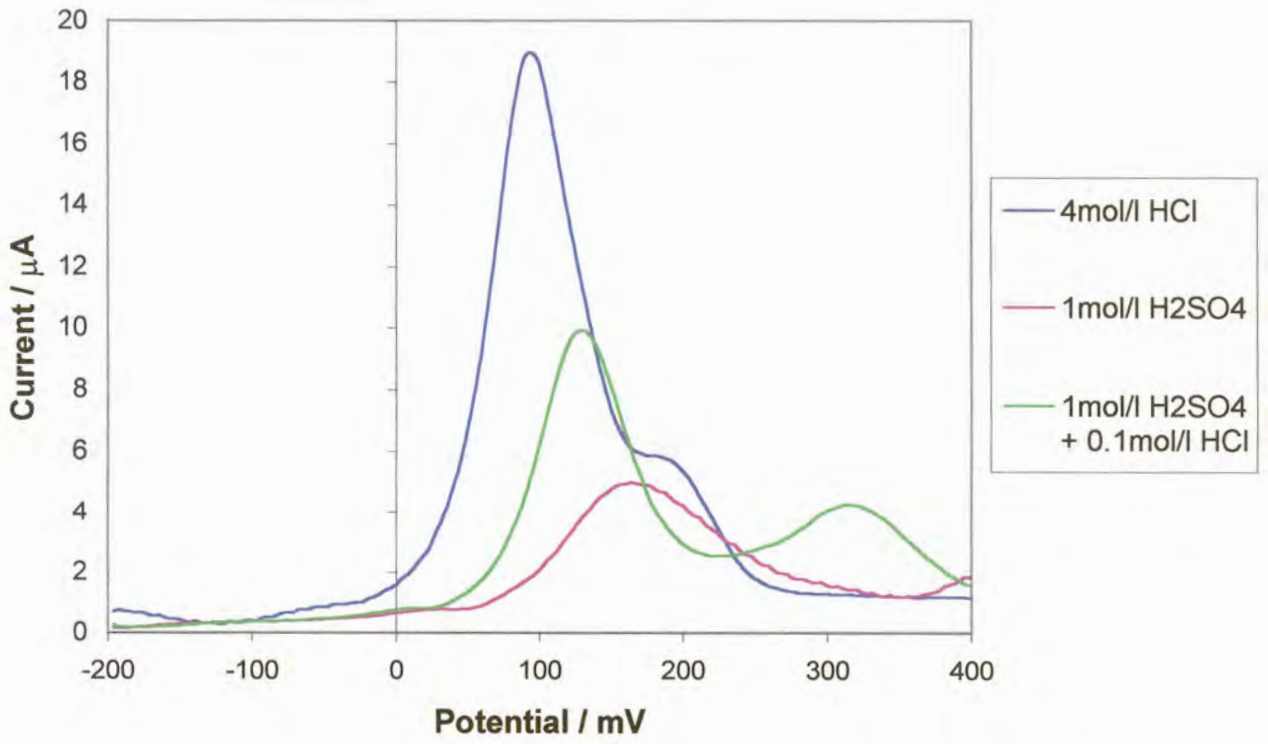

Figure 7.16: Voltammograms for 1 mg.l^{-1} arsenic with stripping electrolytes of 4 mol.l^{-1} HCl, 1 mol.l^{-1} H_2SO_4 and a mixture of 1 mol.l^{-1} H_2SO_4 + 0.1 mol.l^{-1} HCl

The sulphuric acid concentration was increased and the resultant voltammograms are presented in figure 7.17. The arsenic peaks were sharper and more sensitive for the 2 mol.l^{-1} sulphuric acid solutions containing hydrochloric acid than that for the 1 mol.l^{-1} solution. Increasing the amount of hydrochloric acid in the mixture also increases the peak height. Looking at even higher sulphuric acid concentrations did not alter the sensitivity significantly.

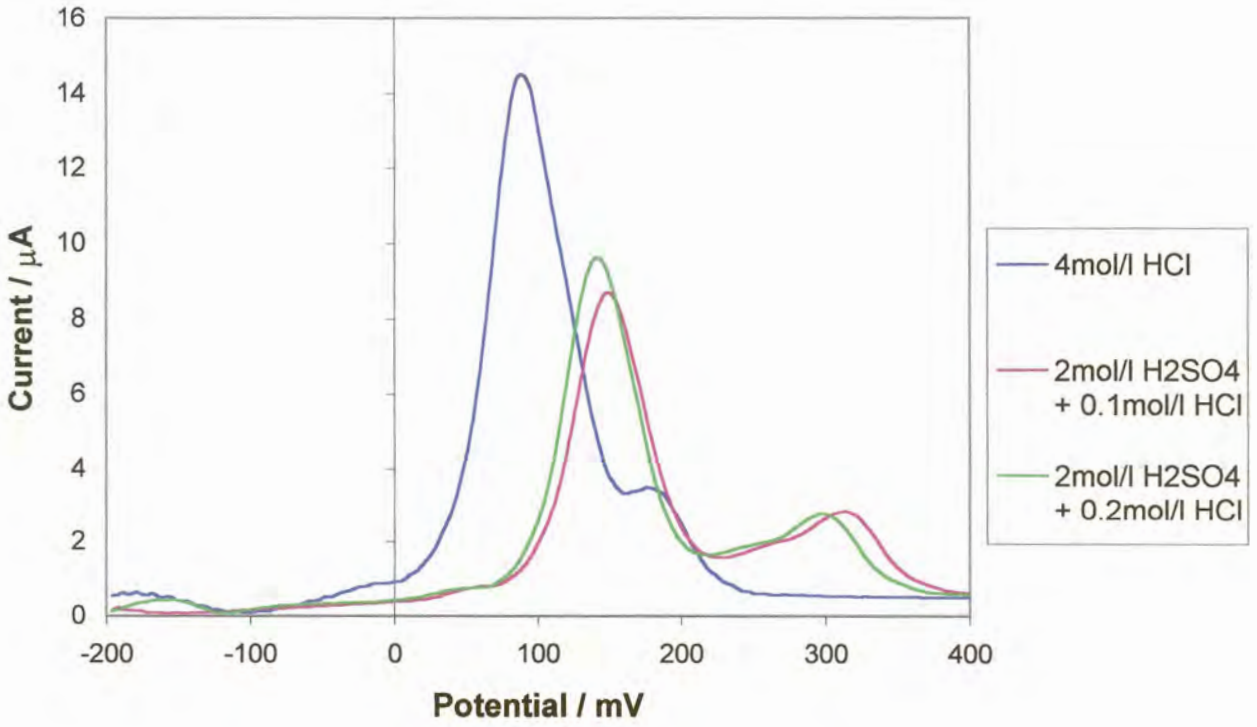

Figure 7.17: Voltammograms for 1 mg.l^{-1} arsenic with stripping electrolytes of 4 mol.l^{-1} HCl, 2 mol.l^{-1} H_2SO_4 + 0.1 mol.l^{-1} HCl and 2 mol.l^{-1} H_2SO_4 + 0.2 mol.l^{-1} HCl

The reproducibility for the two stripping electrolytes, that is 4 mol.l^{-1} hydrochloric acid and 2 mol.l^{-1} sulphuric acid + 0.2 mol.l^{-1} hydrochloric acid, was investigated. A 0.5 mg.l^{-1} arsenic solution was accumulated for 20 s at a potential of –650 mV. DPSV was performed between –200 mV and 400 mV at 20 mV.s^{-1}, with the other parameters being the default settings. The average peak height for the hydrochloric acid solution was 6.28 µA and the RSD was 3.2% for 20 runs. For the acid mixture, the average peak height was 3.30 µA with a RSD of 3.3%. The problem with the hydrochloric acid solution is that the position of the baseline had to be manually defined. This was due to the shoulder initially being well-defined and the baseline was drawn from the start of the peak to the start of the shoulder. With time the definition reduced and the baseline was then drawn from the start of the peak to the end of the shoulder.

The range of arsenic concentrations was again looked at using the 2 mol.l^{-1} sulphuric acid + 0.2 mol.l^{-1} hydrochloric acid stripping electrolyte. DPSV was applied from –200 mV to 400 mV at a scan rate of 20 mV.s^{-1} after a 60 s deposition time at –650 mV. The default settings were used for the other parameters. The results are depicted in figure 7.19 and the voltammograms are shown in figure 7.18. The correlation coefficient for the straight line was 0.9952 which shows greater linearity than that when using the 4 mol.l^{-1} hydrochloric acid as stripping electrolyte. This could be due to the reduced sensitivity when using the acid mixture. However, the polynomial fit to the calibration showed that there was a slight deviation from linearity.

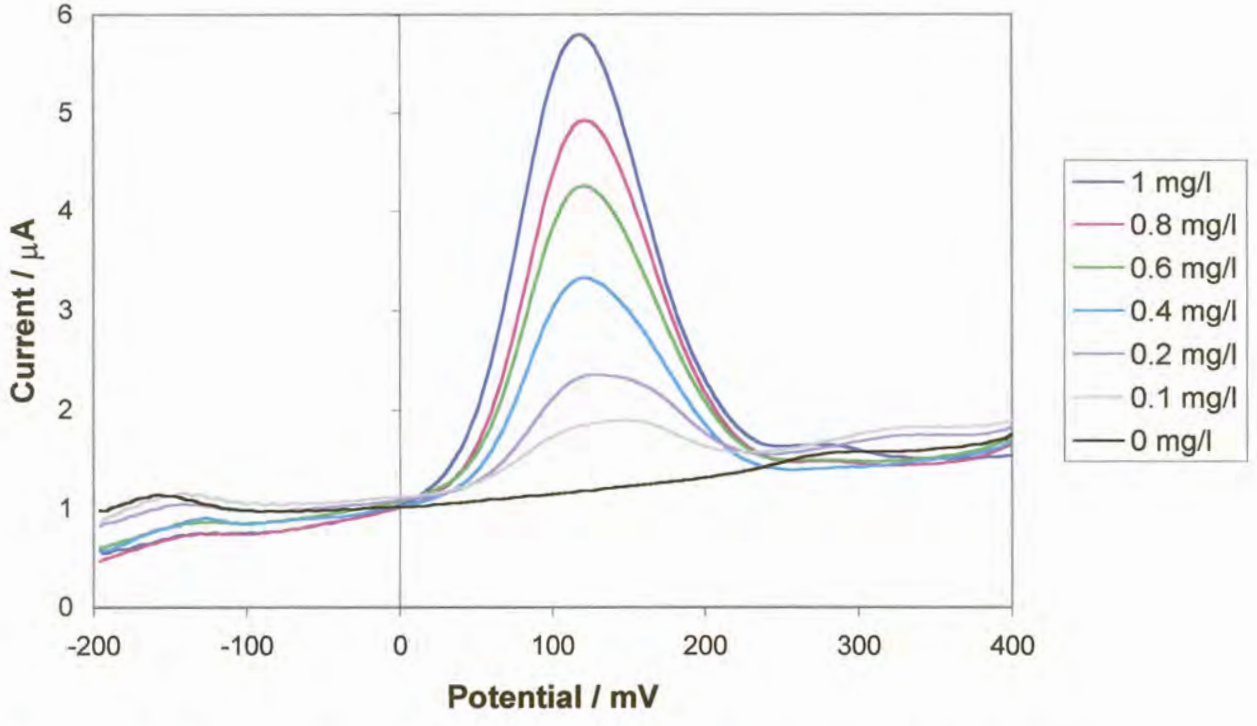

Figure 7.18: Voltammograms for increasing arsenic (III) concentration when using a 2 mol.l^{-1} H_2SO_4 + 0.2 mol.l^{-1} HCl stripping electrolyte

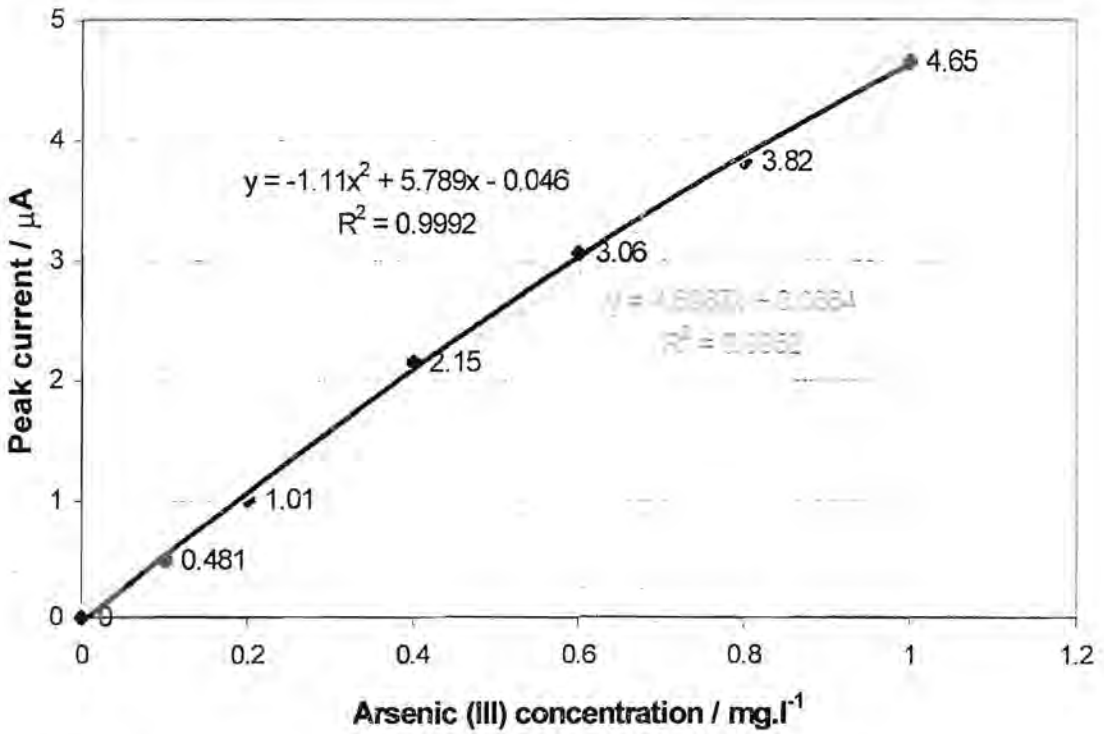

Figure 7.19: Graph of peak current versus arsenic (III) concentration when using a 2 mol.l^{-1} H_2SO_4 + 0.2 mol.l^{-1} HCl stripping electrolyte

It still remains difficult to say which stripping electrolyte is better to use, the 4 mol.l^{-1} hydrochloric acid solution or the 2 mol.l^{-1} sulphuric acid + 0.2 mol.l^{-1} hydrochloric acid solution. That would need to be assessed according to the requirements of the experiment.

7.4.3) Interferences

A list of impurites and their approximate concentrations in high purity gold was given in table 1.1. These impurities could also be possible interfents in the arsenic determination. In particular, copper, mercury, antimony, silver, selenium, bismuth and so on have been mentioned [12,13,16,29,31,35,36]. In this study, cobalt, silver and copper as interferences were investigated.

7.4.5.1) Cobalt

A 0.5 mg.l^{-1} arsenic solution was made up and data were collected as before, using a 20 s deposition time. The 2 mol.l^{-1} sulphuric acid + 0.2 mol.l^{-1} hydrochloric acid stripping electrolyte was used. Cobalt nitrate was added

such that the cobalt concentration was 0.5, 5 and 50 $mg.l^{-1}$ in the various solutions. The peak current for arsenic was monitored and compared to that with no cobalt present. The cobalt, at any of the concentrations, did not have an effect on the arsenic peak. Thus in the gold matrix that is being consider, cobalt should not present any problems.

7.4.5.2) Silver

Silver was added to the arsenic solutions as silver nitrate and was examined in the same manner as for the cobalt. At silver concentrations up to 5 $mg.l^{-1}$ there was no effect on the arsenic peak, but at 50 $mg.l^{-1}$ silver, the peak current for arsenic decreased. Interference at this level should not affect the analysis of arsenic in high purity gold due to the relatively low concentration of silver present in these samples.

7.4.5.3) Copper

The last interferent studied was copper. Once again it was added as its nitrate salt and analysed in a similar manner. However, the concentration range looked at was 0.2, 0.5, 1 and 5 $mg.l^{-1}$ copper. The voltammograms produced are given in figure 7.20. These show that concentrations above 0.2 $mg.l^{-1}$ seriously affect the arsenic peak due to the close proximity of these peaks to each other. By a 10 times excess of copper, the arsenic peak merely becomes a shoulder on the copper peak. This situation is not acceptable for the determination of arsenic in high purity gold as there is a good chance of there being at least double the amount of copper than arsenic present. Ways of preventing copper interference would have to be considered.

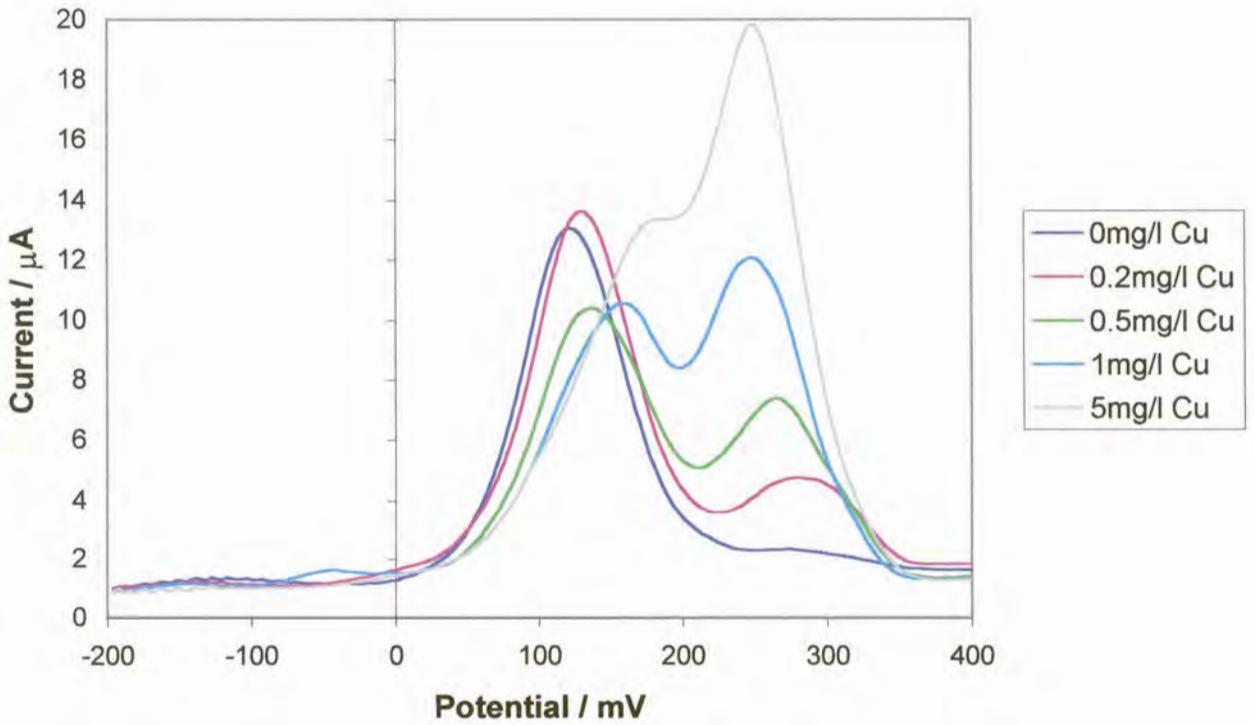

Figure 7.20: Voltammograms showing the effect of copper on the arsenic (III) peak

Interestingly, the copper peak does not seem to be affected by the arsenic present as the graph in figure 7.21 reveals. A linear graph is formed for concentrations up to 1 $mg.l^{-1}$ with a correlation coefficient of 0.9895.

It was not surprising that copper interfered with the arsenic determination. Apart from the oxidation peaks existing close together and overlapping, copper and arsenic combine strongly even in the presence of even a slight excess of copper and greatly reduces the arsenic response [13,29]. The fact that copper and arsenic form intermetallic compounds has been used to determine arsenic at a mercury electrode in the presence of copper [18].

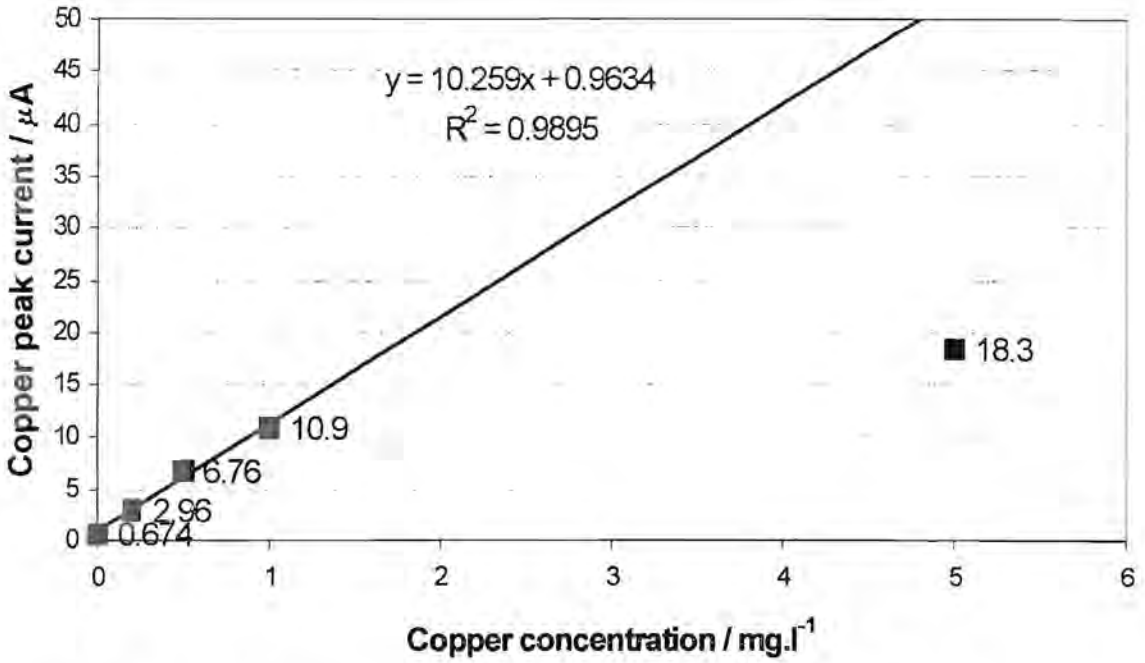

Figure 7.21: Graph of copper peak current versus copper concentration

7.5) DISCUSSION

The high purity gold could be dissolved in an alkaline cyanide solution in the presence of oxygen to form the gold (I) cyanide complex. This was to prevent the gold from depositing on the electrode simultaneously with the arsenic. Also, since cyanide is a reducing agent, arsenic would be present as arsenic (III) and thus a reduction step could be avoided.

It was found that using an alkaline solution produced interference from gold (I) cyanide and also lead to the passivation of the gold film electrode. Thus the sample solutions were adjusted to a pH of 3. Decomposition of the gold (I) cyanide complex was avoided by not using lower pH values. The optimum deposition potential was also found to be –650 mV, which produced sufficient reproducibility.

Matrix exchange was investigated in order to provide more sensitive arsenic determinations. Hydrochloric acid as a stripping electrolyte, of which a 4 $mol.l^{-1}$ solution was suggested, produced sensitive and reproducible results, but the linear range was fairly small. Sulphuric acid alone as a stripping

electrolyte yielded very poor sensitivity, but the addition of a small amount of hydrochloric acid appreciably improved the sensitivity. A larger linear range was obtained with the acid mixture when compared to that using hydrochloric acid alone. A composition of 2 $mol.l^{-1}$ sulphuric acid and 0.2 $mol.l^{-1}$ hydrochloric acid was recommended. Deciding which stripping electrolyte is best for the analysis would depend on the concentration of arsenic in the solution. If the arsenic concentration is low, hydrochloric acid would be the best to use due to the greater sensitivity. At higher arsenic concentrations, the sulphuric-hydrochloric acid mixture would be more suitable because of the greater linear range. A method of standard addition was required to reduce the memory effect displayed by the gold electrode and the samples had to be analysed in the order of increasing concentration.

Arsenic concentrations down to 0.1 $mg.l^{-1}$ could readily be detected using a 20 s deposition time for the hydrochloric acid stripping electrolyte or 60 s for the sulphuric-hydrochloric acid mixture. Lower concentrations were looked at, but insufficient sensitivity was obtained and increasing deposition times led to high background currents. In looking at the detection limit of the method, consider that 0.2 g gold was dissolved and the volume was made up to 20 ml. Assuming arsenic is present at 0.2 $mg.g^{-1}$ [37] in the gold sample, then 2.0 $\mu g.l^{-1}$ arsenic needs to be detected. Alternatively, an arsenic concentration of 10 $\mu g.g^{-1}$ in the gold sample can be detected if 0.2 g sample is dissolved in 20 ml of solution. The detection limit was not as low as that achieved by ICP-MS, which was 5 $\mu g.g^{-1}$ for arsenic [38], but was still sufficient to provide a valuable information for the typical arsenic concentrations in high purity gold up to 99.99% gold.

Cobalt, silver and copper were looked at as likely interferences. Cobalt and silver did not interfere when present at the concentration ratios likely to be found in high purity gold. Copper, however, interfered strongly due to the formation of intermetallic copper and arsenic [13,29]. The best way to curb this problem would be to complex the copper with a ligand that is stable and selective for copper, such as DMG. This would prevent intermetallic formation

and hence reduce interference. Cyanide forms a complex with copper, $[Cu(CN)4]^{2-}$, but it is not very stable (log β_4 = 31.3) [39] and it did not appear to affect the copper and arsenic interactions. As copper is present in high purity gold at concentrations which would lead to interference, the analysis of real samples was prevented as this interference would first have to be overcome.

7.6) REFERENCES

1) M.C. Sneed, J.L. Maynard and R.C. Brasted, Comprehensive Inorganic Chemistry, Volume II, D. von Nostrand company, USA, 1954
2) E. Guindy, Precious Metals, 6th International Conference, Pergamon Press, Toronto, Canada, 1983
3) D.W. Kirk, F.R. Foulkes and W.F. Graydon, J. Electrochem. Soc., 125 (1978) 1436
4) C.P. Thurgood, D.W. Kirk, F.R. Foulkes and W.F. Graydon, J. Electrochem. Soc., 128 (1981) 1680
5) D.W. Kirk, F.R. Foulkes and W.F. Graydon, J. Electrochem. Soc., 126 (1979) 2287
6) D.M. MacArthur, J. Electrochem. Soc., 119 (1972) 672
7) D.W. Kirk and F.R. Foulkes, J. Electrochem. Soc., 127 (1980) 1993
8) K.J. Cathro and D.F.A. Koch, J. Electrochem. Soc., 111 (1964) 1416
9) G.N. Gansinger, United States Patent No. 3989800, 1976
10) J.W. Mellor, A Comprehensive Treatise of Inorganic and Theoretical Chemistry, Volume II, Longmans, Green and Co., 1941
11) Gold Metallurgy in South Africa, Chamber of Mines of SA, Johannesburg, 1972
12) Y.-C. Sun, J. Mierzwa and M.-H. Yang, Talanta, 44 (1997) 1379
13) G. Forsberg, J.W. O'Laughlin, R.G. Megargle and S.R. Koirtyohann, Anal. Chem., 47 (1975) 1586
14) F.G. Bodewig, P. Valenta and H.W. Nurnberg, Fresenius Z. Anal. Chem., 311 (1982) 187
15) F.T. Henry and T.M. Thorpe, Anal. Chem., 52 (1980) 80

16) T.W. Hamilton, J. Ellis and T.M. Florence, Anal. Chim. Acta, 119 (1980) 225
17) F.T. Henry, T.O. Kirch and T.M. Thorpe, Anal. Chem., 51 (1979) 215
18) M. Kopanica and L. Novotny, Anal. Chim. Acta, 368 (1998) 211
19) I. Eguiarte, R.M. Alonso and R.M. Jimenez, Analyst, 121 (1996) 1835
20) D. Sancho, M. Vega, I. Deban, R. Pardo and G. Gonzalez, Analyst, 123 (1998) 743
21) P.H. Davis, G.R. Dulude, R.M. Griffin, W.R. Matson and E.W. Zink, Anal. Chem., 50 (1978) 137
22) S. Nielsen and E.H. Hansen, Anal. Chim. Acta, 343 (1997) 5
23) A.R.K. Dapaah and A. Ayame, Anal. Chim. Acta, 360 (1998) 43
24) S.B. Adeloju, T.M. Young, D. Jagner and G.E. Batley, Anal. Chim. Acta, 381 (1999) 207
25) P. Grundler and G.-U. Flechsig, Electrochim. Acta, 43 (1998) 3451
26) G. Henze, W. Wagner and S. Sander, Fresenius J. Anal. Chem, 358 (1997) 741
27) J.H. Aldstadt and A.F. Martin, Analyst, 121 (1996) 1387
28) A.J. Bard, Encyclopaedia of Electrochemistry of the Elements, Volume II, Marcel Dekker Inc., 1974
29) D. Jagner, M. Josefson and S. Westerlund, Anal. Chem., 53 (1981) 2144
30) J. Wang and B. Greene, J. Electroanal. Chem., 154 (1983) 261
31) T.M. Florence and G.E. Batley, Crit. Rev. in Anal. Chem., 9 (1980) 219
32) M. Lintern, A. Mann and D. Longman, Anal. Chim. Acta, 209 (1988) 193
33) F.R. Schlodder, H.H. Beyer and W.G. Zilske, Gold 100 Vol. 3, Proceedings of the Symposium on the Industrial uses of Gold, Johannesburg, SAIMM, 1986
34) P. Wilkinson, Gold Bulletin, 19 (1986) 75
35) G. Brauer, Handbook of Preparative Inorganic Chemistry, Volume 2, 2nd Edition, Academic Press, 1965
36) P.T. Kissinger and W.R. Heineman, Laboratory Techniques in Electroanalytical Chemistry, 2nd Edition, Marcel Dekker Inc, New York, 1996
37) E. Ivanova, N. Jordanov, I. Havesoz, M. Stoimenove and S. Kadieva, Fresenius J. Anal. Chem., 336 (1990) 501

38) S.M. Graham and R.V.D. Robert, Talanta, 41 (1994) 1369

39) B. Jamoussi, M. Zajzouf and B. Ben Hassine, Fresenius J. Anal. Chem., 356 (1996) 331

CHAPTER 8

CONCLUSION

The initial question of whether electroanalytical techniques would be suitable to determine trace impurities in complex matrices will be addressed at the end of this chapter once the work done in the project is first be examined. A conclusion will then be drawn from these findings.

Matrix exchange was used in both cases due to the complex nature of the samples. This improved the selectivity and the sensitivity of the determination by reducing interference and optimising the conditions for stripping. This involved designing flow cells and building up flow systems. The flow systems also produced improved mass transfer, they were fairly easy to use, the analysis time was faster (particularly with on-line deoxygenation) and the system was automated to an extent. FlowTEK provided easy control of the peristaltic pump and the selection valve used and it would have been ideal if it could also control the BAS software somewhat.

Two different flow systems were employed, each with their own pros and cons. Each system, however, had it own requirements and thus it was impossible to incorporate only all the positive aspects into one flow system. A balance was thus sought after.

Both segmented and non-segmented flow were employed. The non-segmented system could be controlled more rigorously whereas the compressibility in the segmented system created problems even when a back pressure was applied.

Oxygen was removed from solutions to prevent interference. This was achieved by passing the solutions through the semi-permeable silicone tubing surrounded by nitrogen. Diffusion of the oxygen through the tubing into the nitrogen atmosphere occurred due to a concentration gradient. This proved to be highly efficient and could

readily be used in flow systems. The extent of oxygen removal depended on the flow rate and at higher flow rates it was supplemented by sparging the solutions with nitrogen first, but this depends on the specific requirements. It did, however, complicate matters due to the time delay between introducing the sample into the system and the sample reaching the flow cell. The use of square wave voltammetry has been shown to reduce oxygen interference without the need for deoxygenating the solutions. This would be worthwhile investigating to reduce the complexity of the flow system.

Two different electrodes were utilised, namely a SMDE and a gold film electrode. The SMDE was easy to use, reproducible and there were no problems with surface effects. A flow cell was designed with mercury flow perpendicular to that of the solution for enhanced sensitivity, but the mercury drop was unstable at high flow rates or in a pulsating flow. For the gold film electrode it was difficult to plate a uniform gold film of good quality. It was found that plating the film in the diffusion-activated potential region produced the best results. It was not easy to activate the glassy carbon substrate uniformly and the reproducibility of the electrode was poor. The use of polishing and electrochemical regeneration produced different surface effects and led to variations in the voltammograms obtained. The gold film also suffered from memory effects and passivation, and had to be replated regularly. It could however be used in a wall-jet cell where the hydrodynamics is well-defined. Overall, the SMDE was preferred due to the reproducibility and the ease of use when compared to the gold film electrode, and probably most other film or solid electrodes for the analysis of complex samples. It cannot, however, be used in all instances and legislation prohibiting the use of mercury necessitates the use of other electrodes.

The use of electrochemical techniques has obviated the need for preliminary separations in the samples investigated. In this project both ASV and AdSV, with optimised deposition potentials and accumulation times, provided sufficient selectivity and sensitivity when used in conjunction with matrix exchange. The compositions of both the supporting and the stripping electrolytes are vital to improve the sensitivity and selectivity of the determination. This includes the nature of the components, their

concentrations an the pH of the solutions. The use of complexing agents when analysing complex matrices by electrochemical means is invaluable. In this work the major components in the samples, namely zinc and gold, were complexed to prevent interference. Cobalt as an analyte was complexed with DMG to make its determination at a mercury electrode possible and also improved the sensitivity. The interference by copper in the determination of arsenic could also possibly be removed by complexing it with DMG for example, so that its reduction potential is shifted. Cyclic voltammetry was an important tool for obtaining an overview of the electrochemical system and the interaction of the various components under different conditions.

In this project, cobalt was successfully determined in a synthetic zinc electrolyte with a detection limit of 0.2 $mg.l^{-1}$ using a 20 s accumulation time. Arsenic in the presence of high gold concentrations was determined down to 20 $\mu g.g^{-1}$ for a 20 s deposition time using a hydrochloric acid stripping electrolyte, or a 60 s deposition time using a sulphuric-hydrochloric acid mixture stripping electrolyte.

Thus it has been demonstrated that it is possible to apply electrochemical techniques for trace determination in complex matrices. However, the methods are very complex and matrix specific. Both the major and the minor components in the matrix could have profound influences on the analyte determination as demonstrated. It is not always easy to obtain detection limits in the low $\mu g.l^{-1}$ range. Due to the major method development that is required for this type of analysis and the extreme matrix dependence, it is not recommended for use in a non-routine laboratory. However it is well suited to monitor on-going processes and in a routine environment.

APPENDIX

FLOWTEK SET-UP

1) Connecting the devices

A device is an analytical instrument or component that needs to be controlled by this software. A selection valve and a peristaltic pump were used in this work. These devices were connected to digital output points on the distribution board.

2) Programming the function keys

The function keys F3 to F9 were configured to send output to the digital output ports. This allows a way of switching the devices without having to define a method or manually controlling each device. In the "set-up" menu under the "function keys" option, the function key to be programmed is chosen and the number to be sent to the digital port is entered. This was done as shown in table 1.

Table 1

Function key	Number
F3	1
F4	2
F5	4
F6	8
F7	16
F8	32
F9	64

3) Testing connection of the devices

When a certain function key was pressed, it enabled a particular device to perform a certain action. The findings are shown in table 2.

Table 2

Function key	**Device**	**Action**
F5	Selection valve (SV)	Home (H)
F6	Selection valve	Advance (A)
F7	Peristaltic pump (PP)	Off (O)
F8	Peristaltic pump	Forward (F)

This data then corresponded to the positions on the distribution board to which the devices had been connected as depicted in table 3. It was not necessary to pump in the reverse direction in the methods used, so this action was not specified.

Table 3

Number	1	2	4	8	16	32	64	128
Output port	1	2	3	4	5	6	7	8
Device			SV	SV	PP	PP		
Action			H	A	O	F		

4) Specify the devices

The type of devices and the digital output port to which it is connected were specified as in table 4.

Table 4

Type of device	SV	3
Digital output port	PP	5

5) Configuration of devices

The devices were configured as shown in table 5.

Table 5

Device number	7		8	
Device name	SV		PP	
Number of actions	2		2	
Narration of actions	H	A	O	F
Digital output of action	1	2	0	2
Hot key	H	A	O	F
Pulse length (0 for continuous)	0.1		0	

6) Building methods and procedures

The methods are built by specifying the duration of the method and then specifying a time during the method when a particular device must perform a certain action. Procedures can be built by running a number of methods after each other and/or by repeating a method or procedure a specified number of times.